A NEW FINITE TRANSMISSION ZERO GENERATION TECHNIQUE IN
EVANESCENT MODE WAVEGUIDE COMBLINE FILTERS

A THESIS SUBMITTED TO
THE GRADUATE SCHOOL OF NATURAL AND APPLIED SCIENCES
OF
MIDDLE EAST TECHNICAL UNIVERSITY

BY

ELİF İNAN

IN PARTIAL FULFILLMENT OF THE REQUIREMENTS
FOR
THE DEGREE OF MASTER OF SCIENCE
IN
ELECTRICAL AND ELECTRONICS ENGINEERING

JANUARY 2014

Approval of the thesis:

A NEW FINITE TRANSMISSION ZERO GENERATION TECHNIQUE IN EVANESCENT MODE WAVEGUIDE COMBLINE FILTERS

submitted by **ELİF İNAN** in partial fulfillment of the requirements for the degree of **Master of Science in Electrical and Electronics Engineering Department, Middle East Technical University** by,

Prof. Dr. Canan Özgen _____
Dean, Graduate School of **Natural and Applied Sciences**

Prof. Dr. Gönül Turhan Sayan _____
Head of Department, **Electrical and Electronics Engineering**

Prof. Dr. Nevzat Yıldırım _____
Supervisor, **Electrical and Electronics Eng. Dept., METU**

Examining Committee Members:

Prof. Dr. Canan Toker _____
Electrical and Electronics Engineering Dept., METU

Prof. Dr. Nevzat Yıldırım _____
Electrical and Electronics Engineering Dept., METU

Prof. Dr. Gülbin Dural _____
Electrical and Electronics Engineering Dept., METU

Prof. Dr. Şimşek Demir _____
Electrical and Electronics Engineering Dept., METU

Dr. Bülent Alıcıoğlu _____
Microwave Component Technologies Division, ASELSAN

Date: <u>20/01/2014</u>

I hereby declare that all information in this document has been obtained and presented in accordance with academic rules and ethical conduct. I also declare that, as required by these rules and conduct, I have fully cited and referenced all material and results that are not original to this work.

Name, Last name : ELİF İNAN

Signature :

ABSTRACT

A NEW FINITE TRANSMISSION ZERO GENERATION TECHNIQUE IN EVANESCENT MODE WAVEGUIDE COMBLINE FILTERS

İnan, Elif

M.Sc., Department of Electrical and Electronics Engineering

Supervisor: Prof. Dr. Nevzat Yıldırım

January 2014, 99 pages

With the recent development of the RF and microwave technology, sizes of the microwave filters become more of an issue. In this thesis, evanescent mode waveguide combline bandpass filters operating at 16.6-17 GHz frequency band suitable for miniaturized RF & microwave modules have been developed. In order to accomplish compact filter sizes, evanescent mode waveguide (EWG) and combline filter designs are incorporated. By using a filter design software Filpro and 3-D electromagnetic (EM) simulation software (CST) a 4-resonator EWG combline bandpass filter is designed. The size of the aforementioned filter design is then further decreased by incorporating Finite Transmission Zero(s) (FTZ). The method to realize the FTZ(s) in the EM simulator is a novel technique where dielectric material is placed in between two adjacent resonator rods creating a series capacitive reactance. This capacitance appears to be in parallel with the inherent series inductive reactance of the waveguide piece between adjacent rods, thus forming a parallel LC resonator in series arm, stopping signal flow at its resonance frequency, thus forming a FTZ. The tuning of the FTZ(s) is achieved by adjusting the height of

v

the corresponding dielectric material. The FTZ(s) can be placed on either sides of the passband, improving the selectivity of the filter while also reducing the length of the filter appreciably. Approximately 15% and 27% size reduction is observed after inserting one FTZ and two FTZs, respectively.

Keywords: Cavity Resonator, Microwave Filter, Evanescent Mode Waveguide Filter, Combline Filter, Finite Transmission Zero

ÖZ

SÖNÜMLENEN MOD TARAK FİLTRELERDE YENİ BİR İLETİM SIFIRI OLUŞTURMA TEKNİĞİ

İnan, Elif

Yüksek Lisans, Elektrik Elektronik Mühendisliği Bölümü

Tez Yöneticisi: Prof. Dr. Nevzat Yıldırım

Ocak 2014, 99 sayfa

Son zamanlarda gelişen RF ve mikrodalga teknolojisi ile birlikte mikrodalga filtrelerin boyutları da önem kazanmıştır. Bu tezde, 16,6-17 GHz frekans bandında çalışan, küçültülmüş boyutlardaki RF ve mikrodalga modüllerde kullanmaya uygun, sönümlenen mod dalga kılavuzu tarak tipi bant geçiren filtreler geliştirilmiştir. Kompakt filtre yapısı elde etmek için sönümlenen mod dalga kılavuzu ve tarak filtre yapıları birleştirilmiştir. Devre tasarım yazılımı Filpro ve 3 boyutlu elektromanyetik simülasyon ortamı CST kullanılarak 4 rezonatörlü sönümlenen mod tarak tipi bant geçiren filtre tasarlanmıştır. Söz konusu filtrenin boyutları, iletim sıfır(lar)ı eklenerek küçültülmüştür. İletim sıfır(lar)ını elektromanyetik simülasyon ortamında gerçeklemek için kullanılan özgün teknik, iletim sıfırlarını dielektrik materyal ile temsil etmektir. İletim sıfırının ayarlanması, ona karşılık gelen dielektrik materyalin boyunun ayarlanması ile sağlanmıştır. İletim sıfır(lar)ı kullanılarak filtrelerin bastırmaları iyileştirilmiş ve bir iletim sıfırı ile boyutta yaklaşık %15 küçülme, iki iletim sıfırı kullanılarak yaklaşık %27 küçülme elde edilmiştir.

Anahtar Kelimeler: Kavite Rezonatör, Mikrodalga Filtre, Sönümlenen Mod Dalga Kılavuzu Filtre, Tarak Filtre, İletim Sıfırı

To my family

ACKNOWLEDGEMENTS

TABLE OF CONTENTS

LIST OF FIGURES

FIGURES

xiii

xiv

LIST OF TABLES

CHAPTER 1

INTRODUCTION

1.1 Literature Survey on Microwave Filter Design and Combline Filters

Microwave filters play very important role in electronic systems, satellite communications, radars and wireless networks. These components are widely used in these systems in order to distinguish the wanted signals from unwanted ones. There are numerous applications for RF and microwave filters which require many different design approaches in communications. However, the first microwave filters were built for military purposes.

The basic of transmission line theory was first introduced by Oliver Heaviside around the late 19th century. [1] He considered that in order to guide an electromagnetic wave there are two metallic conductors are needed, even if there is single one, and then the other has to be an earth connection of something equivalent. Furthermore he considered propagation among a hollow guide where he came up with that the propagation is impossible without an inner conductor. Later, J. Larmor investigated the theory of resonant components, which became the basics for current resonance theory approaches. [1] Afterwards, Lord Rayleigh figured out that there is a possibility for electromagnetic waves to propagate in hollow guides, where he defined the theory of propagation of transverse electric and magnetic waves. He found out that the propagation of the waves inside a hollow waveguide depends on the cut-off frequency as well as the cross-sectional dimensions of the guide. [1]

After 1930s, the scientists at Bell Laboratories and the MIT (Massachusetts Institute of Technology) got involved in the waveguides and their transmission characteristics, which could be a good replacement for coaxial lines that are lossy compared to waveguides. [2]

The study on microwave filters also started around similar timeline. One of the first papers investigating the filter design focused on the ABCD parameters approach to derive the image impedance and phase and attenuation of various filter types. [3] During World War II, MIT Radiation laboratory focused on waveguide filters, Harvard Radio Research Laboratory dealt with various types of broad-band filters with coaxial resonators. During these days, the publication of Waveguide Handbook is achieved, which is the leading source for microwave electronics and still used today.

Afterwards, modern distributed circuit theory approach investigating capacitance-inductance- transmission line models has begun. K. Kuroda came up with a set of transformations has a name of himself as well, where a section of a transmission line with a parallel open-circuited stub can be converted into a series short-circuited stub or vice versa and then these identities started to be used in the literature. [3]

Initial theories on direct-coupled filters showed that the simple resonant cavities do not end up with better stopband characteristics, so the investigations lead to the use of chain of cavities that are directly coupled to each other. In order to obtain more satisfactory results, formulas were defined to use Butterworth and Chebyshev low-pass prototypes and look up tables were generated in order to decrease the cost of implementation where the use of the computers was not common as expected. A very good example of this is the book, Handbook of Filter Synthesis. [4]

Next, the idea of inter-cavity couplings by means of inverters was introduced. With this approach, the broader bandwidths with simpler equations for low-pass prototypes, lumped element filters, waveguide and stripline filters were presented. [5]

Parallel coupled filters were introduced in [6] and [7], which were also the building blocks for the interdigital and combline filters. In 1962 George Matthaei published the design procedure of an interdigital type bandpass filter where the resonator elements were placed between parallel ground planes. [8] His approach was started with lumped-element approach and the low-pass prototypes. Later on, he extended his study over combline filters. [9]

In the similar timeframe, waveguide filter design was challenged with the evanescent approach, which supports the waveguide propagation below cut-off frequency. [10] Since the design approach and the responses are similar for both evanescent mode and combline filters, merely the evanescent mode waveguide filters are argued to be the waveguide version of the combline filters. It was argued that both evanescent and combline filters have a number of axially spaced screws into the guide from the broad wall, which shows bandpass filter characteristics below cutoff frequency due to propagation of an evanescent form of TE10 mode and this could be in fact due to coupled TEM mode, supported by screws, perpendicular to the direction of propagation.

Combline and interdigital filters attracted lots of attention due to its ease to realize as well as electrical performances. Wenzel studied combline and capacitively loaded interdigital filters in [11]. In [12], detailed analysis with the coupling between two waveguides is presented. It has been shown that the coupling value depends on the resonant frequency of the screw tuned cavities, which is one of the most crucial remarks regarding to combline filter approach. He presented synthesis procedures and simple modification for using lumped capacitors. General equivalent circuits for the tapped-line narrow to moderate bandwidth combline filters were given in [13]. A new type of combline filters with superior steepness characteristics were introduced in [14], in which a practical design consideration operating at low microwave frequencies with a very compact design as well as a steep upper band was shown. Explicit expressions and design equations for combline and interdigital tapped-line input filter similar to the ones given in [9] and [13] are derived in [15]. In [16], a

3

technique to design microstrip tapped-line interdigital filters has been presented showing the superiority over conventional microstrip filters that the tapped-line filters were still realizable for moderate bandwidth. However it was also highlighted that the conventional microstrip filter was advantageous for high frequency and narrow band applications that the tap-point loading becomes comparable to wavelength and this loading may not be practical. Numerical analysis with finite difference method of a dielectric filled coaxial resonator filter with narrow air space in the medium between resonators and a higher unloaded Q and smaller in size compared to conventional dielectric filled coaxial resonator was demonstrated in [17]. Later, different dielectric-filled combline filters were designed and fabricated with the results illustrated in [18]. It was also shown that the wide stopband with weaker spurious signals can be realized by combining quarter-wavelength uniform impedance resonators with stepped impedance resonators. Another design of tapped combline filter was given in [19] where the composite effects of multiple quasi-TEM modes and non adjacent couplings were investigated. The reduction in cover height resulted in performance improvement in stopband, since the phase velocities of various quasi TEM modes were equalized with the corresponding cover height reduction. An inhomogeneous combline filter with metalized resonators and dielectric block with dielectric coupling holes in between the resonators together with its equivalent circuit was given in [20]. Design and fabrication of asymmetric broadside coupled coplanar waveguides for interdigital bandpass filters in order to achieve lighter weight, compact size, low insertion losses and very small fractional bandwidth were compared in [21] and good agreement were obtained. Similar deduction of the explicit expressions for combline and interdigital tapped-line input filter given in [9] and [13] was also done in [22]. It was derived that the approach in [13] fails to predict the insertion loss function for third order degree filter and true method to obtain the exact equivalent circuit was shown. Following this study, the bandwidth of the traditional combline filter was expressed in terms of a fraction of wavelength and ground-plane spacing and also showing the effect of on unloaded Q. [23] The increment achieved for unloaded Q of combline filter was shown to

4

resemble the higher Q of the evanescent mode waveguide filters. The ideas derived in [20] and [18] were revisited for non-dielectric case in [24] to improve the spurious performance of the combline filters. Stepped rod resonators of [18] and coupling slots similar to [20] were carefully combined to either shift to higher frequency or suppress the first spurious passband. The group delay approach to design the combline filters was demonstrated by Ness in [25] with examples. The theory of filter design from lowpass-to-bandpass transformations has been extended with the insertion of the group delay of the reflected signal. The equations relating the group delay to the coupling coefficients have been derived. By this way, precise tuning of the filter to succeed a specific bandpass response was demonstrated. Later in [26], less expensive and faster design and analysis approach for evanescent mode combline filters is given. The authors argue that the TEM analysis of combline filters is not enough. TEM field is being distorted at the open ends of the resonators yielding propagation of evanescent modes, explicitly affecting the couplings between the resonators and resulting in wider bandwidths. In [27], the authors introduced the design of various microwave filters. The lumped-element theory is given to simplify the crucial points to the beginners in this field. Furthermore the design methodology used for filter theory is expanded to the design of other passive microwave components. The design of ultra compact size cavity based combline filter for EMI filtering purposes is described in [28]. Later on, in [29], RF MEMS technology is used to tune the resonators of evanescent mode cavity filters. This approach is further extended in [30] with a novel method of changing the capacitive loading instead of mechanical movement of the screw by using RF MEMS switched capacitor banks.

Microwave circuits have been also modeled via various electromagnetic (EM) solvers based on numerical methods. After 1970s, the wide availability of computers increased attention to Computer Aided Design (CAD) tools. In 1990s, electromagnetic solvers began to spread over UNIX and personal computers (PCs). From that time, electromagnetic simulation has become important in engineering design approaches. 3D EM solvers as well as RF circuit design tools allowed to explore the effects of 3D discontinuities, interactions of the adjacent and non-

adjacent components in the circuit, resonances etc. Key EM tools can be counted as: CST Microwave Studio from Computer Simulation Technology, HFSS from Ansoft, Momentum from Agilent Technologies, Microwave Office from AWR Corporation, GENESYS from Eagleware etc. Any high frequency EM analysis can be handled with any of these tools.

Throughout this thesis, various combline type filter design and simulations were handled via Filpro and CST. The theoretical bandpass comb type filter designs are done via Filpro, which was developed by Prof. Dr. Nevzat Yildirim, METU, Turkey. Then the corresponding results are carried to CST for further tuning and realization.

1.2   Aim and Contributions of the Thesis

The modern RF and microwave module technology requires smaller elements, so the filters used in the modern modules should be as small as it can be. The aim of this thesis is to design a miniaturized combline filter that is convenient to use in modern type microwave modules, according to the specifications given in Table 1.1.

Table 1.1 Expected filter specifications

Passband corners	16600-17000 MHz
Return Loss	>15 dB
Length	<30 mm

It means that the filter should have smaller dimensions compared to the conventional combline bandpass filters. One way to implement the filter with smaller dimensions is to operate it in evanescent mode, namely below cutoff frequency. Hence, the combline filter structure will be incorporated with evanescent mode waveguide (EWG) structure. The dominant propagation mode for conventional rectangular waveguide filters is TE10 mode. The physical dimensions of the desired filter are set

by inspecting cutoff frequency of TE10 mode which is set by the width of the waveguide. The passband center (about 16.8 GHz) of the evanescent mode waveguide design should be well below cutoff frequency f_c to avoid degradation in response. After several iterations, the width and the height of the enclosure is selected as 6 mm and 4 mm, respectively. The cut-off frequency of the TE10 mode of the corresponding waveguide is 24.982 GHz. The length of the 4-resonator EWG combline filter accomplishing the above specifications is derived as 38.7 mm using the software CST.

In order to reduce the size more and increase the selectivity in lower stopband, a similar 4-resonator filter with a finite transmission zero (FTZ) added to the lower stopband of the filter (16000 MHz) is designed. The FTZ is implemented in the 3-D electromagnetic simulator software via a novel technique, where an adjustable-height dielectric block represents the FTZ. The selectivity of the bandpass filter for the lower frequency band is improved and the length is reduced to 33 mm leading to 15% reduction in size compared to EWG combline filter without FTZ.

Even more miniaturized version of this filter with sharper response in both upper and lower stopbands is designed with two FTZs. By following the aforementioned novel technique, i.e. replacing the FTZs with dielectric blocks, the length of the final EWG combline filter is reduced to 28 mm which means a further reduction of about 15% in size compared to one FTZ filter.

1.3   Overview of the Thesis

This document is structured into five chapters, the contents of which are outlined below.

Chapter 2 provides a brief summary of interdigital, combline and mixed digital filter structure with detailed explanation of the combline structure. Since the design is incorporated with EWG filter structure, EWG filter theory is also explained. In addition to the basic combline and EWG theory, group delay method that is used for

practical test and design of the combline filters is clarified. The last point indicated in this chapter is finite transmission zeros in EWG combline filters.

Chapter 3 discusses the definition of the problem as the reason of the design. In definition, the constraints on the design are extracted. After the description of the problem, the characterization of a resonator which is the building block of the filter is expressed. Chapter 3 also covers a 4-resonator EWG combline bandpass filter design in accordance with the recommendations given in Chapter 2.

In Chapter 4, the finite transmission zero(s) is(are) added to the filter designed in Chapter 3 via a novel technique. A detailed discussion of the technique is also included. Both the circuit-based design and physical realization using 3-D electromagnetic solvers are outlined.

The final chapter gives a conclusive discussion in accordance with the work outlined in the preceding chapters.

CHAPTER 2

BASIC THEORY BEHIND THE EVANESCENT MODE COMBLINE FILTER DESIGN

2.1 Interdigital, Combline and Mixed Digital Filters

Interdigital, capacitively loaded interdigital, combline and mixed digital filters are similar structures that they are formed by N-parallel coupled lines with each line (bar) being short circuited to ground at one end while the other end is either left open or terminated in a capacitive reactance. These filters are counted in the family of direct coupled resonator filters. The reason for this is that in the N-coupled line filters each line with the capacitive loading (if exists) form a shunt resonator. The difference between combline and interdigital filters can be seen in Figure 2.1 where in combline filters the short circuit (SC) ends of bars are on the same side (Figure 2.1.a) while in interdigital filters the SC ends alternate (Figure 2.1.b). Conventionally the name interdigital is used for filters without capacitive loadings. The name Capacitively Loaded Interdigital Filter with capacitive reactances is used in order to distinguish this type of filter from conventional interdigital filters. From here, it can be concluded that the classical interdigital filters are special cases of capacitively loaded interdigital filters obtained by setting capacitors to zero (Figure 2.1.c). However considering the fringing capacitors at the open ends, these filters can also be handled as capacitively loaded interdigital filters. Additionally, in Figure 2.1.d mixed digital structure where both comb and interdigital type couplings are also illustrated.
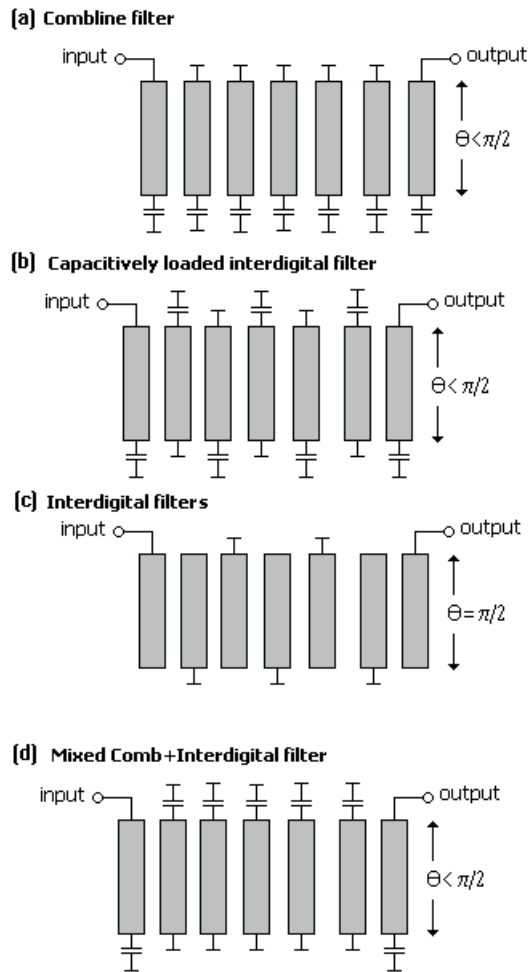
Figure 2.1 Combline and interdigital filter structures

Since the N-parallel coupled line part of this structure is the core sections of this filter, it needs special treatment to function properly. In general analysis of an N-parallel coupled conductor system need to be handled through electromagnetic simulation tools. The synthesis stage where developing a proper circuit model to be linked to the filter synthesis tools and then finding the physical dimensions from the element values of the circuit require a number of simplifying assumptions is given as follows:

- It will be assumed that only pure TEM or quasi-TEM modes of electromagnetic waves exist in the medium of operation. This assumption

leads to the usage of the commensurate length distributed element filter concepts to develop all-stub circuit models which can be linked easily to the filter synthesis tools.

- Another usual assumption is that the resonator bars are coupled to only the adjacent resonators. The rest of the all non-adjacent couplings are neglected. This assumption leads to a simple ladder type circuit model which can be converted into a direct coupled resonator form by simply adding the resonating capacitors.

In general these assumptions may hold to some degree in different realization structures, like slabline, stripline, microstrip, waveguide, etc. Fortunately, degradation in response because of such non-adjacent couplings and/or because of existence of non-TEM and evanescent wave modes can be corrected to a great extent by simply tuning or optimizing the design either at circuit theory level or during EM analysis and realization stages.

TEM wave assumption enables description of single and multiple coupled transmission lines in terms of static capacitance parameters of the system.

After a brief introduction about the comb type and interdigital filters, next, the theory behind the key concepts of combline structures are given.

2.2 Key Concepts on Combline Structures

In this section the key concepts related to combline filters will be summarized.

2.2.1 Characterization of Single TEM Mode Transmission Lines and SC Stubs

A single lossless transmission line operating in TEM mode (a two wire line) can be described by its characteristic impedance Z_0 (or admittance $Y_0=1/Z_0$) and its phase constant β which are defined as

$$Z_0 = 1/Y_0 = \sqrt{L/C} \tag{2.1}$$

$$\beta = \varpi \sqrt{LC} \tag{2.2}$$

where L and C are series inductance and shunt capacitance of the line per unit length as shown in Figure 2.2.
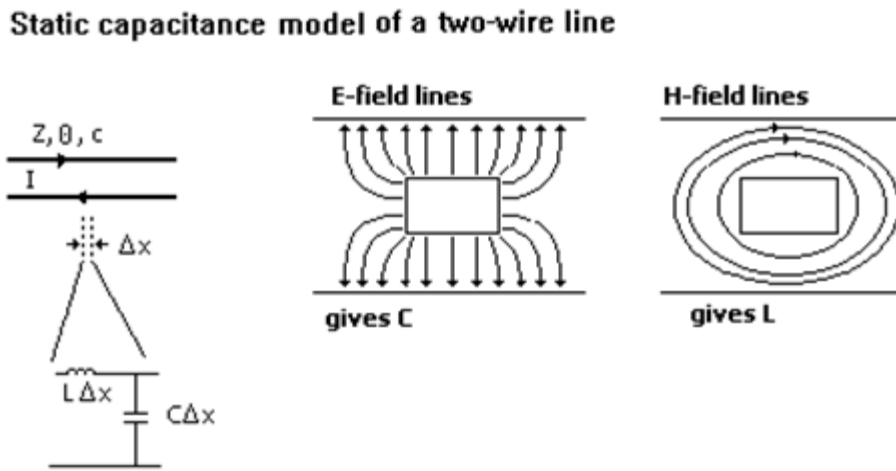
Figure 2.2 Static capacitance model of a TEM-mode transmission line

The transmission line is depicted as a two wire line with currents flowing in opposite directions as seen in the left illustration of Figure 2.2. An infinitesimal length Δx of the transmission line can be represented by its series inductance $L\Delta x$ and shunt capacitance $C\Delta x$. The electric and magnetic field lines of a slab type transmission line are also shown in the same figure. For transmission lines operating in TEM mode, the product of L and C are related through the electromagnetic parameters $\mu = \mu_r \mu_0$ and $\varepsilon = \varepsilon_r \varepsilon_0$ of the medium as

$$LC = \mu\varepsilon = \mu_0\mu_r\varepsilon_0\varepsilon_r = \mu_r\varepsilon_r / c^2 = 1/v^2 \qquad (2.3)$$

where c is the velocity of light, μ_r is relative permeability of the medium (unity for non-magnetic dielectrics), ε_r is the relative permittivity of the medium (dielectric constant) and

$$v = 1/\sqrt{\mu\varepsilon} = c/\sqrt{\mu_r\varepsilon_r} \qquad (2.4)$$

is the phase velocity of the wave. In a non-magnetic dielectric medium, by setting $\mu_r=1$, we have

$$v = c/\sqrt{\varepsilon_r} \qquad (2.5)$$

Thus, a TEM mode transmission line can be characterized when its capacitance C per unit length, inductance L per unit length and the dielectric constant of the medium, ε_r, are known. Since the calculation of the capacitance is usually easier for most structures, it is better to rearrange the definition of characteristic impedance and propagation constant as

$$Z_0 = 1/Y_0 = \sqrt{L/C} = 1/vC = \sqrt{\varepsilon_r}/cC \qquad (2.6)$$

$$\beta = \varpi\sqrt{LC} = \omega/v = \omega\sqrt{\varepsilon_r}/c = 2\pi f\sqrt{\varepsilon_r}/c \qquad (2.7)$$

By using the definition of guided wavelength λ,

$$\lambda = v/f = c/f\sqrt{\varepsilon_r} = \lambda_0/\sqrt{\varepsilon_r} \qquad (2.8)$$

where $\lambda_0 = c/f$ being the free space wavelength. The expression for the phase constant β may also be written in terms of wavelength as

$$\beta = 2\pi f\sqrt{\varepsilon_r}/c = 2\pi/\lambda = 2\pi\sqrt{\varepsilon_r}/\lambda_0 \qquad (2.9)$$

On the other hand, the capacitance parameter can also be calculated through the electrostatic field definition $Q=CV$ where Q is the total charge per unit length and V is the amplitude of the voltage wave travelling on an infinitely long conductor. This capacitance is commonly termed as the static capacitance of the transmission line,

because the electric field lines of the waves are the same as those in static electric field systems.

A transmission line piece of physical length d given in Figure 2.3.a can be characterized as follows:

The electrical length θ of a transmission line with physical length d is then defined as

$$\theta = \beta d = 2\pi d / \lambda = \omega d / v = \omega d \sqrt{\varepsilon_r} / c = 2\pi f d \sqrt{\varepsilon_r} / c \tag{2.10}$$

where λ is the wavelength at frequency f, in the medium with dielectric constant ε_r.

The frequency at which the physical length d becomes equal to quarter wavelength is termed as the quarter wave frequency f_q. Inserting $d=\lambda/4$ in (2.10), it is calculated that the electrical length is equal to $\pi/2$ at the quarter wave frequency:

$$\theta(f_q) = 2\pi d / \lambda = \pi / 2 \tag{2.11}$$

Using (2.11) we can get an expression for f_q in terms of the line length d as follows:

$$\theta(fq) = 2\pi f_q d \sqrt{\varepsilon_r} / c = \pi / 2 \tag{2.12}$$

$$f_q = c / 4d \sqrt{\varepsilon_r} \tag{2.13}$$

for the usual non-magnetic dielectric media.

The electrical length at any frequency f may also be written as

$$\theta(f) = (\pi / 2)(f / f_q) \tag{2.14}$$

When such a transmission line is used as a two-port element, it can be characterized in terms of its ABCD parameters as given in [31]:

A =	$\cos\theta$
B =	$jZ_0\sin\theta$
C =	$jY_0\sin\theta$
D =	$\cos\theta$

$$\tag{2.15}$$

14

An all-stub Pi and Tee models of such a transmission line are shown in Figure 2.3.b. The Pi-model consists of a parallel combination of a positive SC stub and a negative OC stub in series arm surrounded by two shunt OC stubs, all having half the length of transmission line. The Tee-model has a series combination of a negative SC stub and a positive OC stub in shunt arm surrounded by series SC stubs, all having halved lengths. The parallel and series combinations of SC and OC stubs, one having negative impedance indicates that these elements create a finite transmission zero on real (Σ) axis of $S=\Sigma+j\Phi$ domain. Figure 2.3.c shows all-lumped approximations of a transmission line that are available in Filpro.

(a) Characterization of a transmission line of length d

Z_o, θ, d
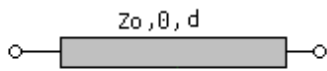
d= Physical length

$\beta = \omega / v = 2\pi / \lambda$: Phase constant

$\tau = \dfrac{d}{v}$: One way delay

$\theta(\omega) = \beta d = \dfrac{\omega d}{v} = \dfrac{\omega \sqrt{\varepsilon_r}\, d}{c} = \omega\tau$: Electrical length

$\theta(f) = \dfrac{\pi}{2} \dfrac{f}{fq}$: Electrical length

$fq = \dfrac{c}{4\sqrt{\varepsilon_r}\, d}$

$$\begin{bmatrix} A & B \\ C & D \end{bmatrix} = \begin{bmatrix} \cos\theta & jZo\sin\theta \\ j\sin\theta/Zo & \cos\theta \end{bmatrix}$$

(b) All-stub models of a transmission line:

$Zoc = -2Zo$

$Zsc = 2Zo$

$Zo \qquad Zo$

$Lng = d/2$

$Zo \qquad Zo$

$-Zo/2$

$Zo/2$

$Lng = d/2$

$Zo, Lng = d$

TL

Replace TLine By /
Pi-Model / All Stub
(Tee-model / All-Stub)
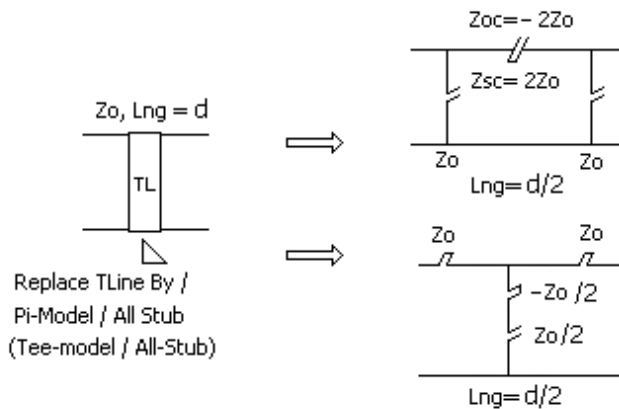
(c) Lumped element approximations of a transmission line for f<fq:

$Zo, Lng = d$

TL

Replace TLine By /
Pi-Model / All-Lumped)
(Tee-model / All-Lumped)
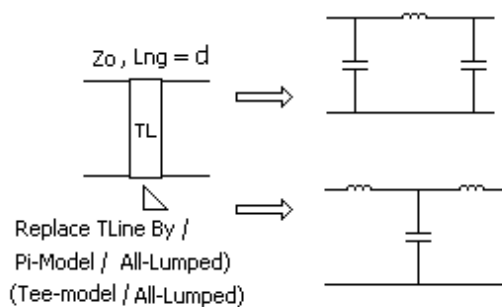
Figure 2.3 Characterization of a transmission line of length *d*

When a transmission line piece of length d is short circuited at one end it becomes a SC stub as illustrated in Figure 2.4.a and its input impedance is given by [31], [32]:

$$Zsc(f) = jZ_0 \tan \theta(f) = jZ_0 \tan(\pi f / 2f_q) \tag{2.16}$$

At the quarter wave frequency f_q, $\theta = \pi/2$, hence $\tan\theta = \infty$. So, at about $f = f_q$, a SC stub behaves like a parallel LC resonator. Therefore if a SC stub appears in series arm, it creates a finite transmission zero at $f_z = f_q$ and if it is connected in shunt arm then it acts as a shunt connected parallel resonator that can be used as resonator element of coupled resonator filters with passband center at $f_0 = f_q$ given in Figure 2.4.b.

For frequencies lower than f_q, a SC stub acts like an inductive reactance. Then, a resonator can be formed by connecting a capacitive reactance in parallel with it. Therefore a shunt SC stub in parallel with a capacitive reactance can be used as resonator element of coupled resonator filters with passband center $f_0 < f_q$ and a series arm SC stub in parallel with a capacitive reactance can be used to create a finite transmission zero at $f_z < f_q$ as seen in Figure 2.4.c.

Figure 2.4.d shows another circuit model for SC stubs. It is formed by paralleling a SC and an OC stub with doubled impedances and halved lengths. This exact identity can be used in manipulation of filters for finding different equivalent circuits.

(a)

Z_0, θ, d

$Zsc = j\, Z_0 \tan\theta$

shunt SC stub   Series SC stub

(b)   Shunt SC stub:

Z_0, θ, d

for $f \cong fq$ for $f < fq$

shunt resonator at f0=fq

Series SC stub

for $f \cong fq$ for $f < fq$

finite transmission zero at f=fq

(c)   Resonators for f<fq:

shunt parallel resonator for f<fq

finite transmission zero at f<fq

(d)   Half Length Stub Equivalent

Z_0, θ, d

$Zsc = Zoc = 2Z_0$
$Lng = d/2, \; \theta/2$

Z_0, θ, d

$Zsc = Zoc = 2Z_0$
$Lng = d/2, \; \theta/2$

Figure 2.4 Characterization of a SC stub

The standing wave patterns for voltage (electric field) and current (magnetic field) on a SC stub at different frequencies when it is excited at the other end are given in Figure 2.5. The electric field is zero (zero voltage) and the magnetic field is maximum (maximum current) at the SC end in all cases.

18

The case of $f=2f_q$ where the length d is equal to half wavelength is shown in Figure 2.5.a. One complete standing wave pattern appears along the 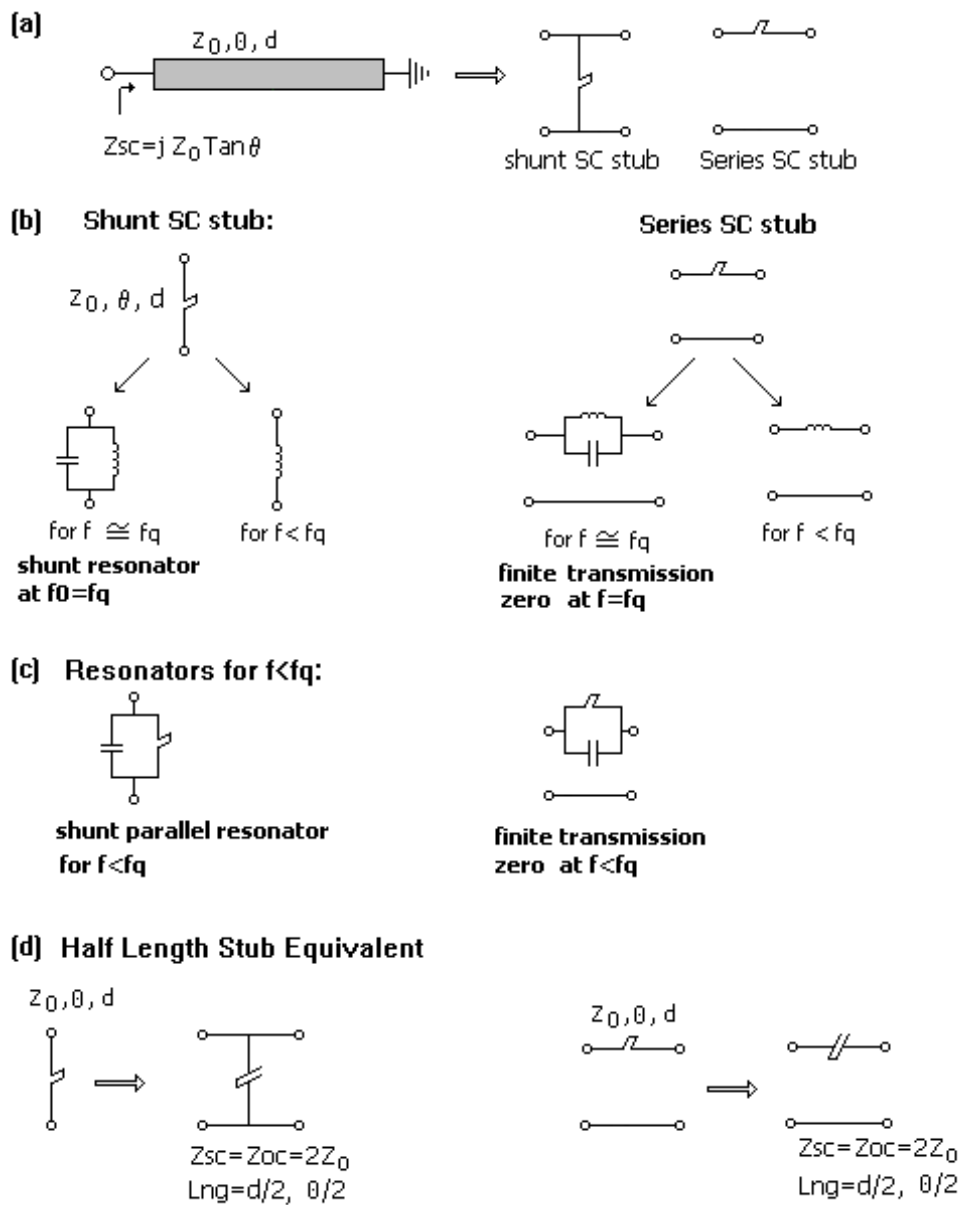line at this frequency. The magnitude of the electric field is zero at the SC end, and then increases and gets its maximum value at quarter wavelength away from the SC end. This point is the middle of the line and then starts to decrease and finally becomes zero again at the source end. The current (magnetic field) shows the opposite behaviour. That is it is maximum at the SC end, minimum in the middle of the line and again maximum but in the opposite direction at the source end. It should be noted that the direction of magnetic field reverses in the middle of the stub. The positions of maximum electric field is important because of the possibility of dielectric breakdown and the positions of maximum current is important because of excessive heating-melting in high power applications.

Figure 2.5.b shows the case for $f=f_q$ where the stub length becomes a quarter wavelength. Here the position of maximum electric field and minimum magnetic field shifts to the source end. This is a crucial pattern because many filters use quarter wavelength stubs. At this frequency the input impedance seen at the source end becomes infinite and the stub can be treated as a parallel resonator. The current is also maximum at the SC end with the direction of the magnetic field remains the same over the line. Since the electric field gets its maximum value at the source end in this case, the choice of the connector types in high power applications turns out to be important.

Figure 2.5.c and Figure 2.5.d show the cases where $f=f_q/2$ and $f<f_q/2$ respectively. Since the electrical length is less than a quarter wavelength for both cases, the first maximum of the electric field (minimum of magnetic field) cannot be reached over the line. Since the electrical length of the stub is short, little variation is observed in electric field and magnetic field. That is, electric field remains weak while magnetic field remains strong everywhere over the line. This idea is used to get magnetic (inductive) coupling between adjacent parallel coupled lines.
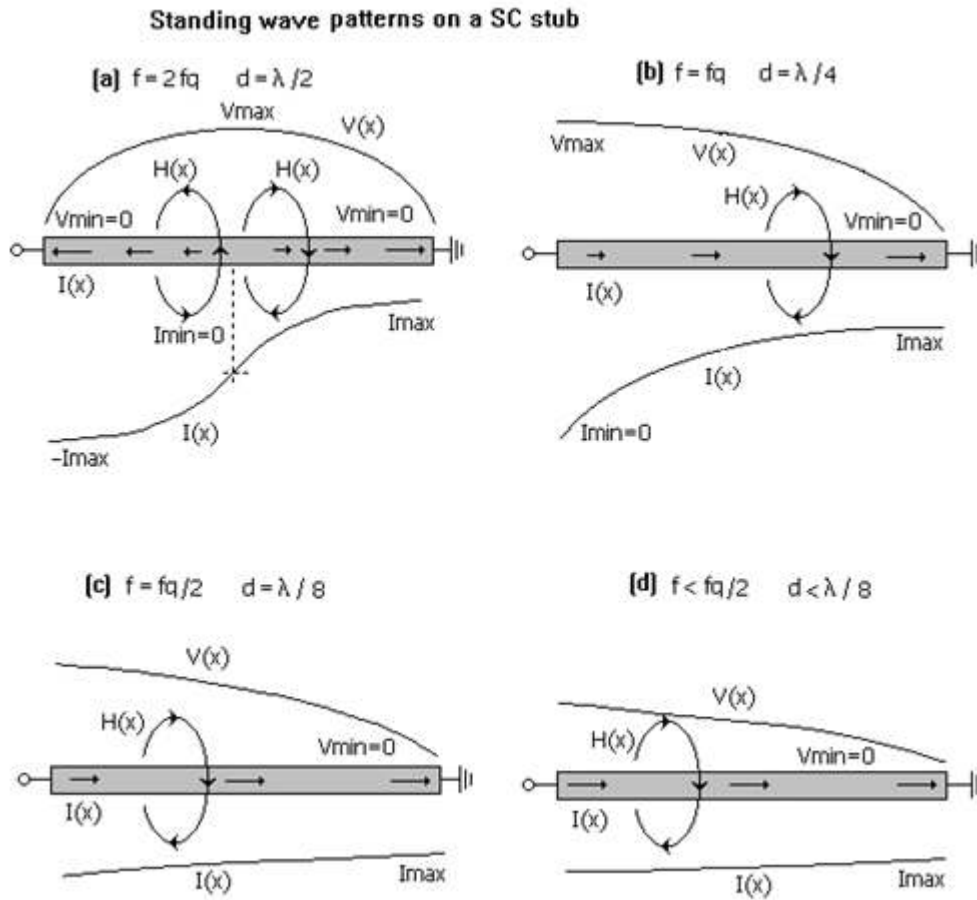
Figure 2.5 Standing wave patterns over a SC stub at different frequencies

In synthesis stage of a filter usually the impedances and lengths of stubs and transmission lines are determined. However in realization stage the physical dimensions of the filter, i.e. the width and the thickness of a line and spacings to ground planes, are going to be enough. If the medium is homogeneous then the parameters like the dielectric constant ε_r, the wavelength λ, the phase velocity v and the quarter wave frequency f_q are also known. Therefore the problem is determination of width-thickness-ground plane spacings. In order to figure out the corresponding spacings, first the capacitance C per unit length is found from the impedance Z_0 using (2.3) - (2.6) and then the physical dimensions are calculated by analytical formulations, graphs, charts or through electromagnetic simulation tools to

20

realize this capacitance. In an inhomogeneous medium where permittivity ε_r is different in different parts of the medium, an effective permittivity $\varepsilon_{r,eff}$ is needed to be calculated first and then this value is used in the formulations of phase velocity, wavelength and quarter wavelength frequency and capacitance. In dispersive medium, the effective permittivity is a function of frequency. Therefore the effective permittivity also becomes an unknown. Furthermore, practical lines involve discontinuities of diverse kinds. Therefore in general iterative trials through electromagnetic simulation tools are usually needed until the desired capacitance and hence the desired characteristic impedance is obtained [26]-[48].

2.2.2 Comb Type Coupled Line Pair

Figure 2.6.a shows comb type coupling obtained by shorting node-1b and node-2b to ground. Line-1-0 becomes a shunt SC stub between node-1a and ground, the Line-2-0 becomes a shunt SC stub between node-2a and ground while Line-1-2 becomes a SC stub between node-1a and node-2a, as shown in the figure.

The relations $Y_{ij}=vC_{ij}$ and the static capacitance matrix parameters can be used for calculating the physical dimensions for realization of the admittances. It is always desirable to have identical resonator bars. That is impedances of the shunt SC stubs need be equated. Conventionally this is done by capacitance matrix transformations of Wenzel [8]. On Filpro, this is done by Pi-Tee-L transformations, where the command Pi-Tee-L / Pi-to-Sym Pi is applied. With this process, the impedances of the shunt SC stubs become equal and a transformer is being produced, as described in Figure 2.6.b.
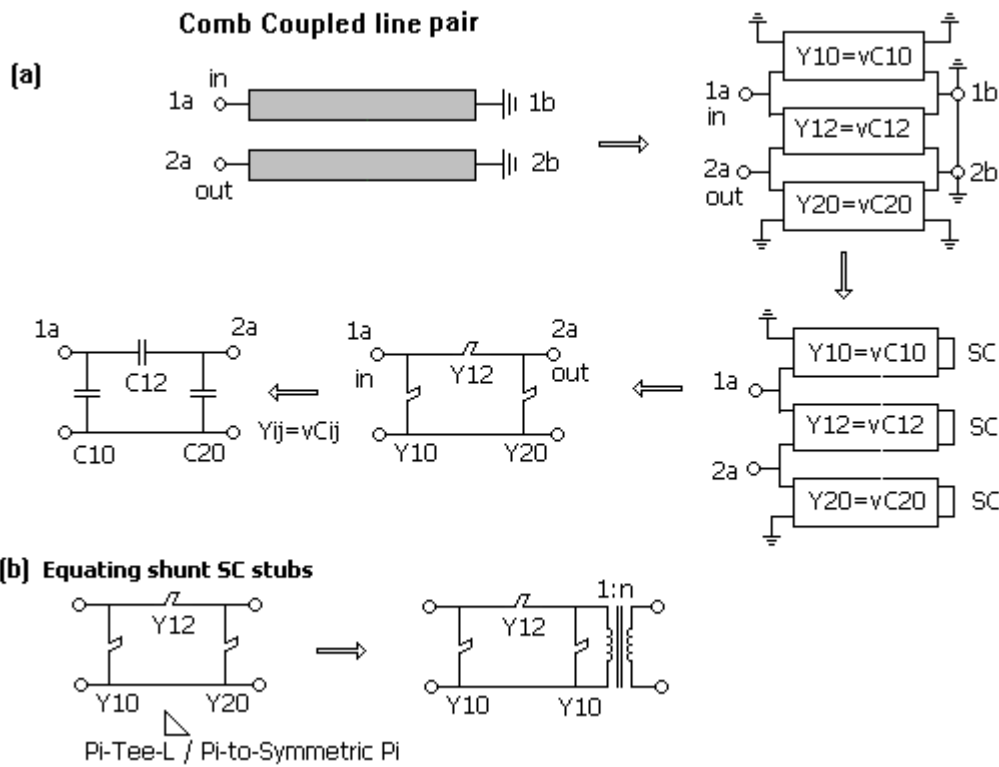
Figure 2.6 All-stub model of a comb type coupled line pair and Pi-Tee-L transformation for equating shunt SC stubs

In Figure 2.7, the coupling mechanism is described from different points of view. In Figure 2.7.a the two port network formed between Port-1a and Port-2a of the short circuited line pair which is indeed a comb coupled line pair is reconsidered. The shunt and series SC stubs can be converted into their half length equivalents which are paralleled OC and SC stubs of halved lengths and doubled impedance. The element coupling of the two shunt resonators is a paralleled OC+SC stub. The effect of paralleled SC and OC stubs shows itself as a finite transmission zero on $s=j\omega$ axis, at $\omega=\omega_q$ ($f=f_q$). At this frequency the positive and negative susceptances of OC and SC stubs cancel leading to zero coupling susceptance (infinite series reactance-parallel resonance), hence decoupling the two resonators. So, for comb type couplings, although the shunt resonators are open circuit, hence allow transmission

of signal from port-1a to port-2a, signal flow is stopped by the parallel resonator in series arm. Therefore in order to form a passband we have to use other mechanism. A passband can be formed by lowering the resonance frequency of the shunt arm elements by placing capacitive reactances in parallel with the shunt SC stubs which is given in Figure 2.7.b.

Figure 2.7 Coupling mechanisms in a comb coupled line pair

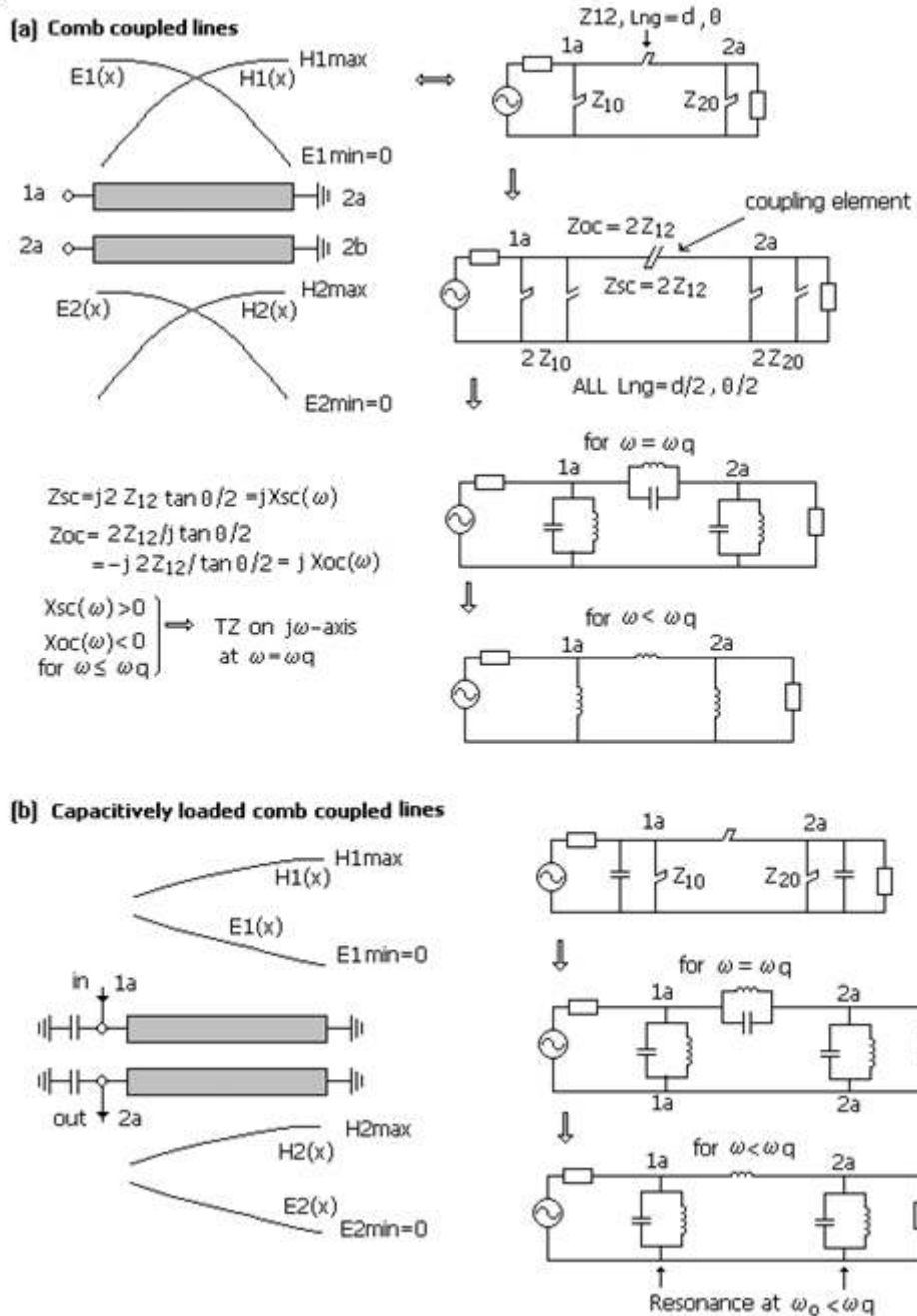From field theory perspective the coupling mechanism can be explained as follows: At frequencies about f_q, the lines are about quarter wave long. Therefore the electric and magnetic standing waves have maximum amplitude variation along the lines. At SC ends the E-field is zero and H-field is maximum while at the other ends E-field is maximum and H-field is minimum as also described detailed in Section 2.2.1. The magnetic field generates the inductive part of the coupling reactance while the electric field provides the capacitive part of the coupling reactance. In comb type structures electrically and magnetically coupled signals tend to cancel each other, as noticed in the stub model of the circuit. At frequency f_q, the cancellation of the coupling is complete, thus the power transfer between the lines is stopped. At frequencies $f<f_q$, the wavelength is longer compared to the wavelength at $f=f_q$, so the amplitude of the electric field standing wave remains small while the amplitude of magnetic field standing wave remains high due to the small electrical distance to the SC ends. Therefore the inductive (magnetic field) coupling becomes higher than the capacitive (electric field) coupling. So, the coupling reactance is inductive for $f<f_q$ with the shunt elements being inductive reactances. Therefore the circuit is made up of a ladder of series and shunt inductors as shown in the figure for $f<f_q$. The circuit can be made to possess a passband if the shunt inductors can be converted into parallel *LC* resonators by adding capacitive reactance in parallel with the shunt inductors as described before and shown in Figure 2.7.b. The circuit section can be treated as a series inductively coupled shunt resonator filter section.

In the above description of comb type coupling it is assumed that only TEM mode waves exist. However when a filter made up of N comb type coupled lines is placed in an enclosure; evanescent waves can propagate depending on the cross-sectional dimensions of the enclosure. These modes can create unaccounted coupling between resonators. In such cases the section of evanescent waveguide between adjacent resonator operating in TE10 mode can be approximated by a Pi-section of inductors. The shunt inductor of the Pi-section dominates the resonator impedances while the series inductor of the Pi-section acts as the coupling element. In order to approximate the TE10 mode, a lumped inductive reactance is added in parallel to the series SC

stub representing the TEM mode coupling. Since the filter response is very sensitive to coupling element variations in narrowband filters, the insertion of series inductor in parallel with the series SC stub widens the filter bandwidth. However, the degradation in the filter response can be corrected by small adjustments in coupling distances or by inserting tuning screws in between the resonators to disturb the coupling fields.

2.2.3 Nodal Resonance Frequency, Coupling Coefficients, The Quality Factor Concepts

In the old classical approaches where the direct coupled resonator filters were designed by mapping from ready lowpass (LP) prototype filters, the parameters Coupling Coefficient and External Q were sufficient to characterize the LP Prototype. Additionally, these parameters can be transformed to bandpass (BP) form through the same LP-to-BP frequency transformation function [33]. Thus, mostly the direct coupled resonator filters can be characterized through the BP transformed k-Q_{ext} parameters together with the Nodal Resonance Frequencies. This approach is more convenient in a sense that the design and realization by using LP prototype tables is simpler and after realization of the filter, the tuning and the testing to achieve the targeted insertion and return loss is faster. The parameters k-Q_{ext} are still useful for realization and testing/tuning stages of filters designed in Filpro where such filters are already synthesized directly as bandpass filters. Therefore the parameters k-Q_{ext} are not defined from the prototypes. Instead, after all element values are found, the aforementioned parameters are obtained by using their definitions given in the rest of this section in terms of element values of the filters.

Nodal Resonance Frequency

The direct coupled resonator lumped element filter is shown in Figure 2.8.a. The resonator elements are denoted by L_{10}-C_{10}, L_{20}-C_{20}, L_{30}-C_{30}, etc. The coupling elements are shown as L_{12}, C_{23}, L_{34}, etc. In filter design, the resonance frequencies of resonators are the easiest parameters to measure. The kth resonance frequency of the

26

isolated resonators is set by the elements L_{k0}-C_{k0}. However in filter measurements the coupling elements need to also be considered as well because the resonance frequency at a node is usually measured by grounding the other nodes which are coupled to this node. The resonance frequency measured by grounding the adjacent nodes is called as the Nodal Resonance Frequency of that node. The coupling elements will become shunt and will be added in parallel with the resonator elements of that node when the adjacent nodes are shorted to ground. Therefore Nodal Resonance Frequency is obtained via paralleling all the reactive elements connected at a node. In Figure 2.8.a the resonator elements of the nodes 1, 2 and 3 are shown. Their nodal resonance frequencies are given by

$$f_{0k} = 1/2\pi\sqrt{L_k C_k} \tag{2.17}$$

where L_k and C_k are now parallel combination of the node-to-ground elements L_{k0} and C_{k0} with the coupling elements $L_{k,k-1}$ and $L_{k,k+1}$ or $C_{k,k1-1}$ and $C_{k,k+1}$.
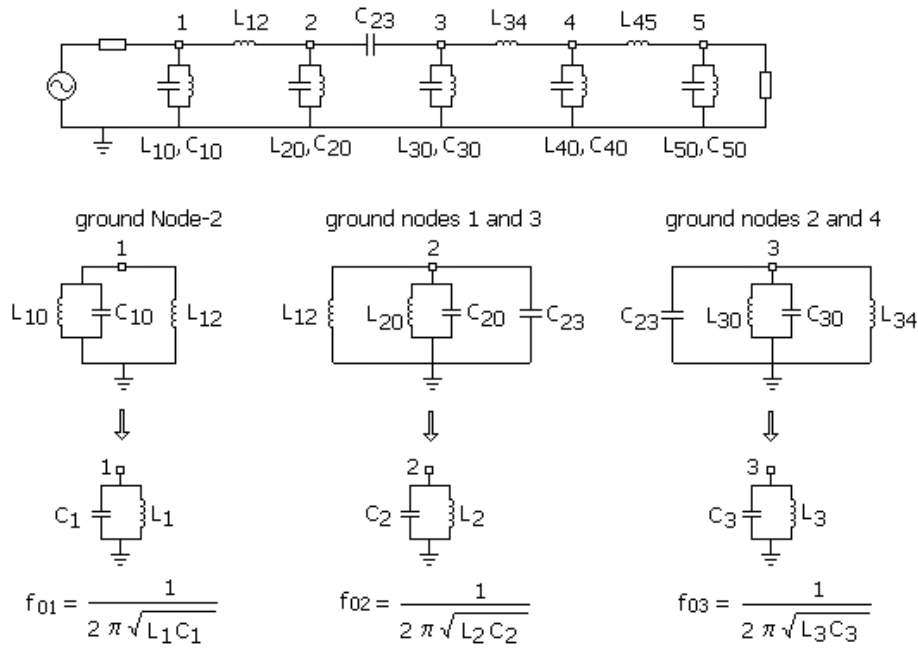
In combline filter circuits the resonators can be formed by a shunt SC stub in parallel with lumped capacitors or distributed capacitive reactances, like OC stubs. Figure 2.8.b shows the circuit of a combline filter with lumped capacitors. In the usual combline filters the coupling element is a series SC stub. If the coupling between resonators is of slot type then the coupling element needs to be modeled as a lumped inductor or other equivalent inductive reactances. When the adjacent nodes are grounded the total reactance at a node is obtained by paralleling all the elements connected to that node. Therefore in the circuit of Figure 2.8.b, the total shunt SC stub impedance is set by parallel combination of the node-to-ground SC stub and the SC stub connecting that node to the adjacent nodes. The nodal resonance frequency $f_{0k}=\omega_{0\kappa}/2\pi$ at node-k is found by equating the total susceptance of the node to zero:

$$\omega_{0k} C_k - 1/\left(Z_k Tan\left(\omega_{0k} d \sqrt{\varepsilon_r}/c\right)\right) = 0 \tag{2.18}$$

where Z_k is the total shunt SC stub impedance and d is the length of stub.

Nodal resonance frequencies

(a) Direct coupled LC-resonator filters

$$f_{01} = \frac{1}{2\pi\sqrt{L_1 C_1}}$$

$$f_{02} = \frac{1}{2\pi\sqrt{L_2 C_2}}$$

$$f_{03} = \frac{1}{2\pi\sqrt{L_3 C_3}}$$

(b) Combline filters

$$\omega_{0k} C_k - \frac{1}{Z_k \tan\theta(\omega_{0k})} = 0 \implies \text{SOLVE } \omega_{0k} \implies f_{0k}$$
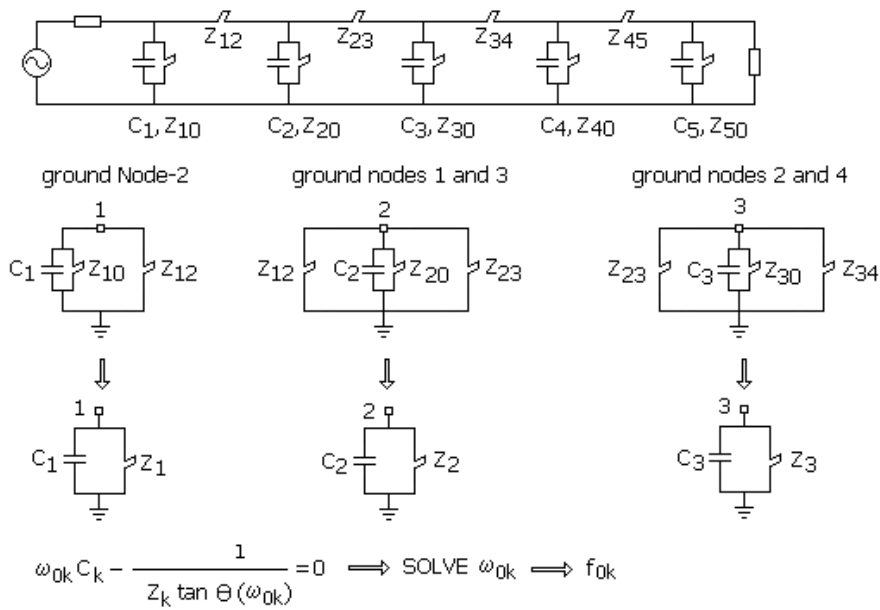
Figure 2.8 Determination of nodal resonance frequencies

28

Coupling Coefficients

Two circuits are said to be coupled when they are related in such a way that energy can interchange. More specifically the current exists in a circuit if and when the other circuit is energized. Since coupled circuits interact on one another, characteristics of one of the circuit are affected by the parameters of the other circuit to some extent depending on the degree of coupling. Therefore a measure of "degree of coupling" is a useful parameter. One measure of coupling between two circuits is the coupling coefficient defined in Figure 2.9, on a lumped element direct coupled LC resonator filter shown in Figure 2.9.a. When the nodes 1 and 2, are coupled inductively, after removal of the shunt capacitors at the nodes, a Pi-section of inductors is found as demonstrated in Figure 2.9.b. In order to find the coupling coefficient defined on this Pi-section, the circuit at node-1 is fed and node-2 is grounded leading to the circuit of Figure 2.9.c. In this circuit the total current I_1 entering node-1 is split into two components, I_{10} and I_{12}. The fractional part I_{12} of I_1, that is, I_{12}/I_1 is an index for the degree of coupling and calculated as

$$\frac{I_{12}}{I_1} = \frac{Y_{12}}{Y_{10} + Y_{12}} = \frac{1/L_{12}}{1/L_{10} + 1/L_{12}} \qquad (2.19)$$

Here, $Y10=1/j\omega L10$ and $Y12=1/j\omega L12$ are susceptances of L10 and L12 respectively. Similarly, feeding node-2 and grounding node-1 will end up with the circuit of Figure 2.9.d. In this circuit the fraction I_{21}/I_2 is also an index for the degree of coupling:

$$\frac{I_{21}}{I_2} = \frac{Y_{21}}{Y_{20} + Y_{21}} = \frac{1/L_{12}}{1/L_{20} + 1/L_{12}} \qquad (2.20)$$

In filter theory, the geometric mean of these two indices is defined as coupling coefficient k_{12} between the resonators of nodes 1 and 2 and found as

$$k_{12} = \sqrt{\left(\frac{I_{12}}{I_1}\right)\left(\frac{I_{21}}{I_2}\right)} = \frac{Y_{12}}{\sqrt{(Y_{10} + Y_{12})(Y_{20} + Y_{12})}}$$

$$= \frac{1/L_{12}}{\sqrt{(1/L_{10} + 1/L_{12})(1/L_{20} + 1/L_{12})}} = \frac{\sqrt{L_1 L_2}}{L_{12}} \tag{2.21}$$

where

$$1/L_1 = 1/L_{10} + 1/L_{12}, \quad 1/L_2 = 1/L_{20} + 1/L_{12} \tag{2.22}$$

are the total inductors connected at nodes 1 and 2 respectively.

From field theory point of view, coupling between two inductors is made through their magnetic fields. Therefore inductive couplings are also referred to as magnetic coupling coefficients, k_m.

Similarly a capacitive coupling coefficient is defined on a Pi-section of capacitors, as shown in Figure 2.9.e:

$$k_{23} = \frac{Y_{23}}{\sqrt{(Y_{20}+Y_{23})(Y_{23}+Y_{23})}} = \frac{C_{23}}{\sqrt{(C_{20}+C_{23})(C_{30}+C_{23})}} = \frac{C_{23}}{\sqrt{C_2 C_3}} \tag{2.23}$$

where $C_2=C_{20}+C_{23}$ and $C_3=C_{30}+C_{23}$ are total capacitors connected to nodes 2 and 3 respectively. Since the actual coupling is made through electric fields, capacitive couplings may also be called as electrical coupling, k_e.

In summary, coupling coefficient of any type, L or C, between two nodes is the ratio of the susceptance of the coupling element to the geometric mean of the total susceptance of the two nodes. If two shunt LC resonators are coupled through a series arm parallel LC resonator, then both electric and magnetic couplings are defined and the final coupling coefficient will be the difference of electric and magnetic coupling coefficients, k_e-k_m. Furthermore, the coupling coefficients for comb type couplings can be generalized as described in Figure 2.10 for $f < f_q$.
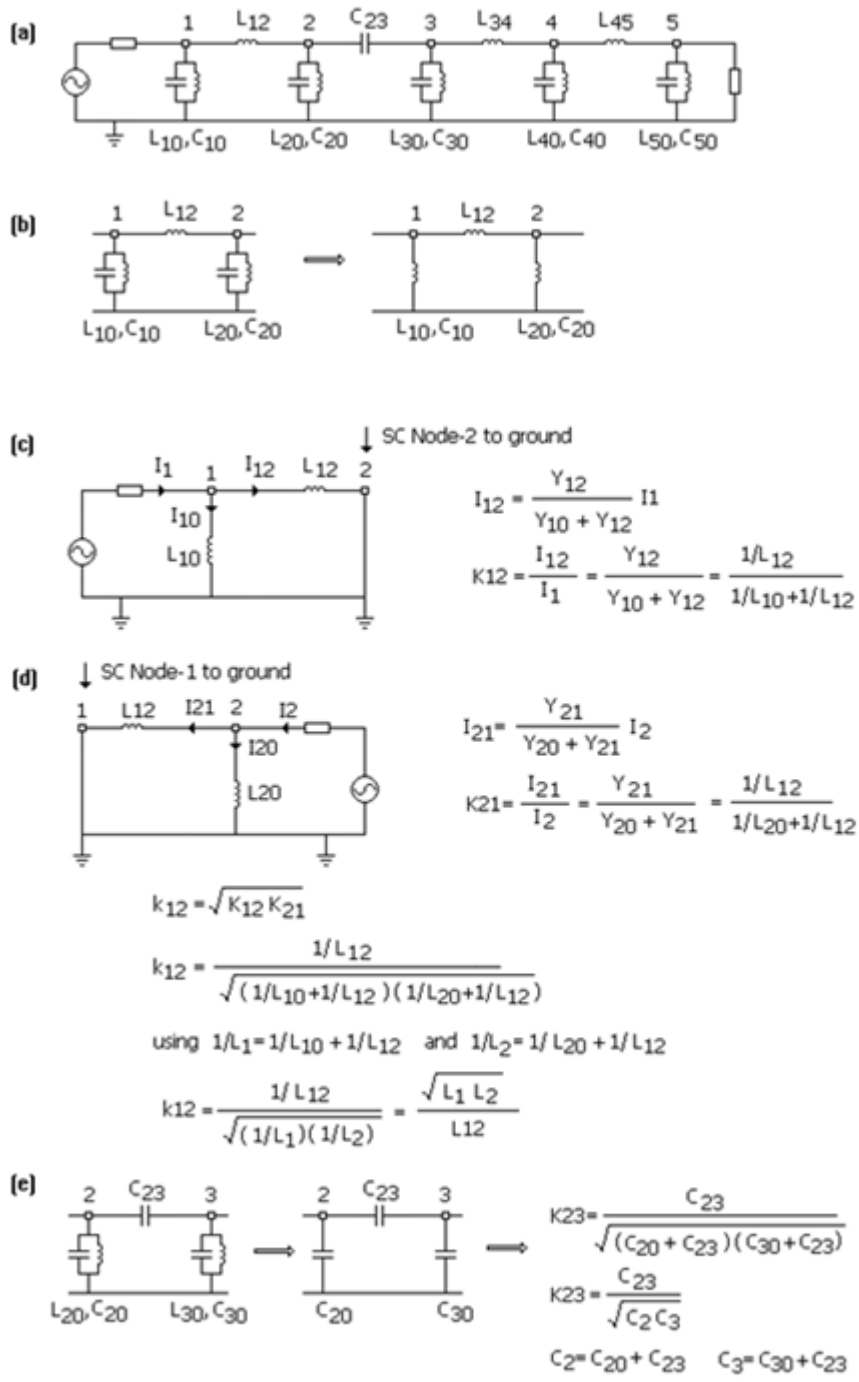
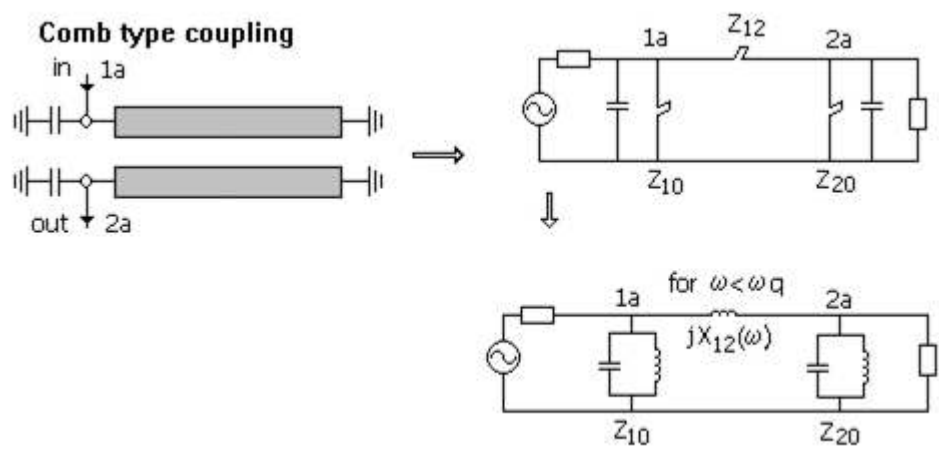**Figure 2.9** Coupling coefficients between lumped element resonators

Figure 2.10 Coupling coefficients for comb type coupling for $f < f_q$

Unloaded Q and External Q

The quality factor Q of an isolated RLC resonator is termed as Unloaded Q. For a series RLC resonator it is given in Figure 2.11.a and defined as follows:

$$Qu = \frac{1}{R_{sr}\omega_0 C_{sr}} = \frac{\omega_0 L_{sr}}{R_{sr}} \tag{2.24}$$

while for a shunt RLC resonator,

$$Qu = R_{sh}\omega_0 C_{sh} \tag{2.25}$$

In these equations R_{sr} and R_{sh} are equivalent resistors due to conductor and dielectric loss and ω_0 is the resonance frequency of resonator. These resistors are usually frequency dependent. However for narrowband filters they may be treated as constant. In practice R_{sr} is required to be as small as possible while R_{sh} is required to be very large to simulate ideal lossless LC resonators.

The quality factor of the resonators at source and load terminations is set by the source and load resistors, R_S and R_L, because these resistors have much more

32

influence than the loss resistors of the resonators. The loaded Q or External Q ($Qext$) of the filter is given in Figure 2.11.b. If a series LC resonator is adjacent to the source (load) resistor R_S, then its $Qext$ turns out to be

$$Qext = \frac{1}{R_s \omega_0 C_{sr}} = \frac{\omega_0 L_{sr}}{R_s}$$

(2.26)

and if a shunt LC resonator is adjacent to R_S, then its $Qext$ is given by

$$Qext = R_s \omega_0 C_{sh}$$

(2.27)

Usually some extra elements exist between the first resonator and R_s and the last resonator and R_L. For such cases the equivalent resistance and reactance seen when looking from the resonator to the source or load end is determined and then these resistive and reactive components are treated as integral parts of that resonator, and the above formulations are used to find $Qext$.
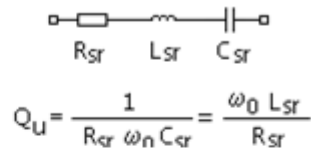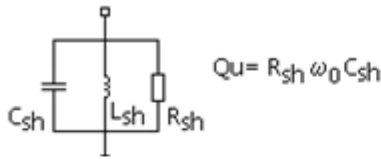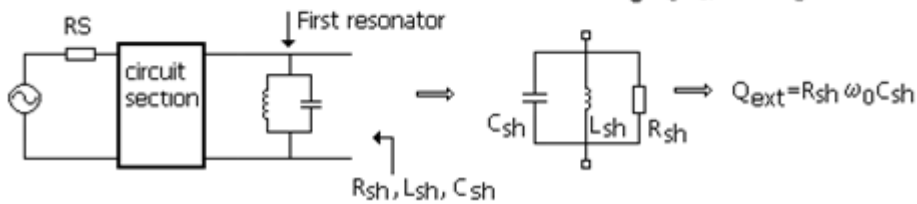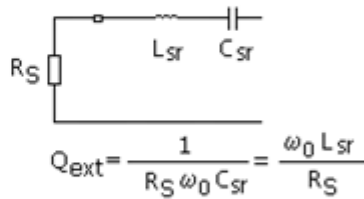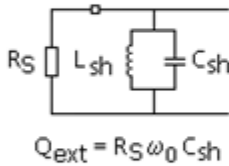
Figure 2.11 Unloaded Q and External Q of shunt and series resonators

To sum up, in the case of an inductor of inductance L, the series resonator R_{sr} represents the corresponding loss of the inductance. If R_{sr} is reduced, Q will increase as seen in (2.24). In a similar manner, parallel R_{sh} represents the losses of a capacitor. When R_{sh} increases, the Q also increases as seen in (2.25). In the case of quarter wave resonators or waveguide cavities, it is not easy to find out the losses due to aforementioned resistors. Because of this, Q, the quality factor, is taken into account. Q and loss are inversely related. On the other hand, Q can be considered as a measure of the energy stored in a resonator. For cavities or coaxial lines, bigger dimensions mean better energy storage capability, so bigger dimensions mean higher Q.

2.3 Group Delay Method for Combline Filter Tuning and Adjustment

Tuning of the parameters of direct coupled resonator filters, like width, thickness and spacings of resonators and capacitors is an extremely tedious process by inspection of only insertion loss and return loss parameters.

Bandpass filters can uniquely defined by their "Q" and external and internal couplings. In the case of tapped cavity coupled bandpass filters, the tapping point mostly defines the external coupling and the size and the proximity of the resonators define the internal couplings. Therefore, the analysis and the determination of the tapping points as well as the resonators will lead to the physical realization of the filter design faster. This means that the structures are to be modified during the development stage to obtain the correct coupling bandwidths or reflected group delays, which are directly related to each other and will be discussed in this section in detail. It is possible to measure the coupling bandwidths or reflected group delays to a high degree of accuracy, although it is mostly difficult to gain access to the resonators in the filter. For narrow bandpass filters, the finite "Q" is the limit for accuracy, however for the broader bandpass filters, the frequency dependency of the coupling networks in the filter design are dominating for accuracy. The Group Delay Approach is applicable to all types of bandpass filters, i.e., lumped element, cavity resonator, dielectric resonator, waveguide, microstrip etc. Hence this approach will also be used in fine tuning of the filters developed in this thesis.

The concept of coupling bandwidths has been used for filter designs since 1960s. Normalized coupling bandwidths are being calculated from the lowpass prototype g values. Furthermore, the inductive and capacitive elements in the lowpass prototype can be eliminated via admittance and impedance inverters. A better way to characterize a microwave bandpass filter is to consider the resonant elements as parallel L and C components and the couplings as admittance inverters consisting of inductive elements. If the coupling is being inductive, inductive element is used in the admittance inverter and if the coupling is being capacitive, capacitive element is used.

Adjustment of coupling coefficients of adjacent pairs of resonator is usually sufficient for tuning of the filter. However inspection of the frequencies of reflection zeros of the resulting filter and inspection of Delay of S11 when a resonator is shorted to ground will lead to better characterization of a microwave filter. [25] The idea behind this method is to short circuit the rest of the resonators which are not considered for the specific group delay in concern. The approach starts with short circuiting all resonators. Then one resonator is restored and tuned to find the group delay from the previously calculated coupling bandwidth via Filpro. Then two resonators are being restored and the group delay of two resonators is calculated. This process goes on until all the resonators have been restored and considered.

Coupling bandwidth, K_E, is used frequently in testing and adjustment stages of a filter. This parameter can be defined in terms of Q_{ext} and center frequency, f_0, of the filter as

$$K_E = \frac{f_0}{Q_{ext}}$$

(2.28)

For the first resonator, the coupling bandwidth K_E is given as [34]

$$K_E = 2/\pi t_{d1}$$

(2.29)

where t_{d1} is the measured group delay of s_{11} at f_0. This equation can be expressed as follows where the coupling bandwidth is expressed in terms of MHz and the time delay is in nanoseconds;

$$K_E(MHz) = 636.6/t_{d1}$$

(2.30)

By tuning the filter via the tuning screw, the corresponding coupling bandwidth as well as the group delay is achieved.

For the second resonator, two group delays are to be considered, only the first and second resonators are restored where the rest of the resonators are short circuited. The coupling bandwidth for this case is as follows:

$$K_{12}(MHz) = 636.6 / \sqrt{(t_{d1}t_{d2})} \tag{2.31}$$

For the third resonator, there resonators are restored and the equation to be used is

$$K_{23}(MHz) = 636.6 / \sqrt{(t_{d2}(t_{d3} - t_{d1}))} \tag{2.32}$$

This formula can be generalized for the *n*th resonator when *n* > 3 as,

$$K_{n-1n}(MHz) = 636.6 / \sqrt{(t_{d(n-1)} - t_{d(n-3)})(t_{dn} - t_{d(n-2)})} \tag{2.33}$$

where t_{dn} is the group delay of the *n*th resonator at f_0.

Since, the coupling coefficients and Q_{ext} values are calculated from the design in Filpro, the group delays of each resonator is calculated via (2.29) – (2.33) and then the spacing between the resonators and the tapping points are adjusted with respect to these group delay values.

2.4 Evanescent Mode Waveguide (EWG) Filters

By using conventional waveguides far below the cutoff frequency, f_c, of its dominant mode it is possible to realize miniaturized waveguide filters with similar or better performances.

At frequencies below the cutoff frequency, the propagation constant, β, becomes imaginary, and thus it turns into an attenuation constant as given in (2.35)

$$\beta = \frac{\omega\sqrt{\varepsilon_r}}{c}\sqrt{1 - (f_c / f)^2} = j\frac{\omega\sqrt{\varepsilon_r}}{c}\sqrt{(f_c / f)^2 - 1} = j\alpha \tag{2.34}$$

$$\alpha = \frac{\omega\sqrt{\varepsilon_r}}{c}\sqrt{(f_c / f)^2 - 1} = \frac{\omega_c\sqrt{\varepsilon_r}}{c}\sqrt{1 - (f / f_c)^2} \tag{2.35}$$

That is, the waves in all modes attenuate exponentially and the name Evanescent Mode Waveguide (EWG) comes from here. However, this attenuation is due to reflection of the waves, much like the attenuation in lossless filter elements in their stopbands and is different from the attenuation due to resistive loss.

On the other hand, in the cutoff region the characteristic impedance of the waveguide becomes purely imaginary. That is the waveguide acts as a reactive distributed element rather than a propagating transmission line. This reactive nature is exploited for realization of filters. Approximately equivalent circuit models of an EWG piece operating in TE10 mode are shown in Figure 2.12.
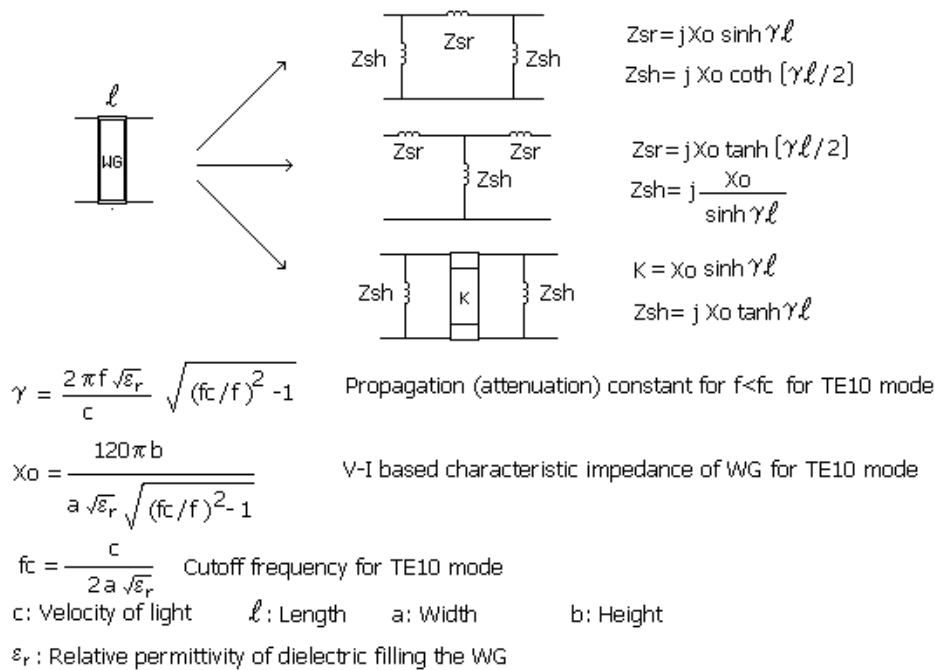

$$Z_{sr} = j X_o \sinh \gamma \ell$$
$$Z_{sh} = j X_o \coth [\gamma \ell / 2]$$

$$Z_{sr} = j X_o \tanh [\gamma \ell / 2]$$
$$Z_{sh} = j \frac{X_o}{\sinh \gamma \ell}$$

$$K = X_o \sinh \gamma \ell$$
$$Z_{sh} = j X_o \tanh \gamma \ell$$

$$\gamma = \frac{2 \pi f \sqrt{\varepsilon_r}}{c} \sqrt{(f_c / f)^2 - 1}$$ Propagation (attenuation) constant for f<fc for TE10 mode

$$X_o = \frac{120 \pi b}{a \sqrt{\varepsilon_r} \sqrt{(f_c / f)^2 - 1}}$$ V-I based characteristic impedance of WG for TE10 mode

$$f_c = \frac{c}{2 a \sqrt{\varepsilon_r}}$$ Cutoff frequency for TE10 mode

c: Velocity of light ℓ : Length   a: Width   b: Height

ε_r : Relative permittivity of dielectric filling the WG

Figure 2.12 Pi, Tee and inverter models of an evanescent mode waveguide piece operating in TE10 mode

Using the circuit models described in Figure 2.12, it is possible to convert the bandpass filter circuits shown in Figure 2.13 into an EWG filter. That is, an evanescent waveguide piece can be converted into a filter by shunt capacitive loadings at proper positions along the waveguide. The circuit of Figure 2.13 has a single transmission zero at f=0 and the rest at f=∞, the same as a combline filter. Therefore EWG filters have selectivities similar to combline filters.
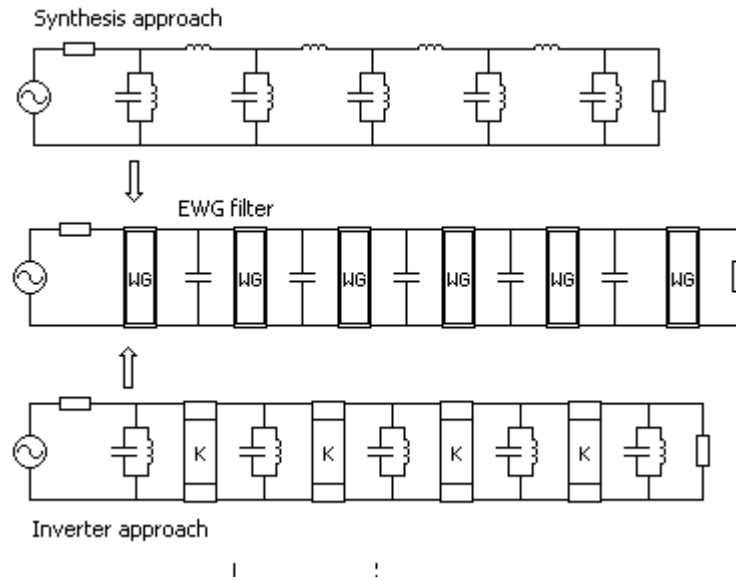
Figure 2.13 Lumped element bandpass filter prototypes that can be converted into EWG filters

Such filters can be designed in frequency ranges starting from VHF frequencies to millimeter wave frequencies, with bandwidths from 1-percent up to an octave or wider band and with wide stopbands. Actually the inductive reactances used in modeling EWG pieces are not lumped inductors. Compared to lumped inductors, they have higher rate of increase with frequency because the attenuation tends to zero as frequency approaches to the cutoff frequency, f_c. The effect of this approximation shows itself as a shrink in bandwidth. However at frequencies well below the cutoff frequency the shrinkage in bandwidth reduces considerably.

The lumped capacitors can be formed by capacitive posts such as shown in Figure 2.14. The posts have some inductive reactances which should be taken into consideration during the synthesis stage of the filter. That is, a good circuit model is necessary for the posts to be used during the synthesis. Since such inductances are geometry, frequency and mode dependent usually full EM modeling and simulation is needed for this purpose.
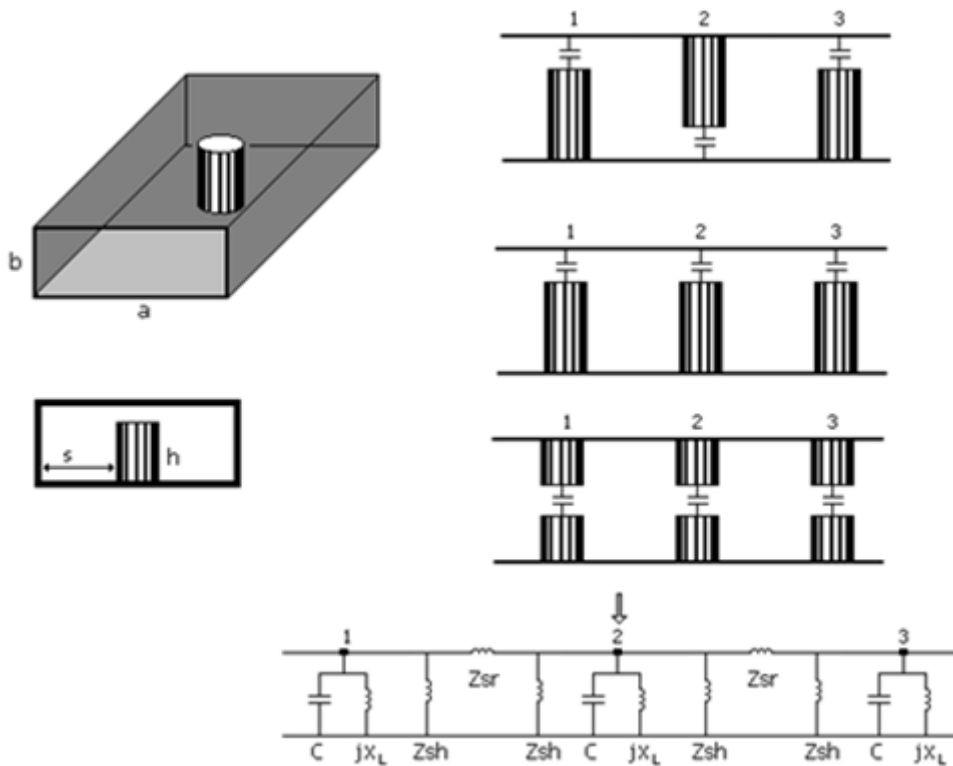
Figure 2.14 Capacitive posts in an EWG filter

Figure 2.15.a shows the electric field lines of TE10 mode and the surface currents on the walls of the guide. A vertical post of height h<b can be placed inside the guide to get a lumped capacitor effect as shown in Figure 2.15.b. The electric field of TE10 mode will induce charges and hence current along the post. The charges accumulated at the top end of the post create strong electric field between the end of post and top wall, creating the capacitive effect. However existence of the post presents a discontinuity and complicates the problem basically by leading to local mode conversions.

1) TEM waves along the posts:

The current along the post completes its path through the top and side walls down to the bottom wall as shown in Figure 2.15.b. The electric field lines extending from the post to the side walls of the guide suggest existence of TEM wave propagation along

the post, in much the same way as the TEM wave mode assumption along the fingers of combline or interdigital filters. In this respect the conducting post in between and parallel to the two side walls can be treated as a slab line with TEM mode characteristic impedance z_0 set by its radius and distances to side walls (s in the figure). Since one end of the post is connected to ground plane (bottom or top wall) it can be simulated as a SC stub of length h. Thus, a standing wave exists on the SC stub with zero voltage (maximum current) at SC end and maximum voltage (zero current) at the capacitor end. Given the parameters h and z_0, the reactance X_L of the post can be calculated as the input reactance of the SC stub as

$$X_L = Z_0 \tan\theta$$

where θ is the electrical length of the post. An equivalent lumped inductance can be derived as

$$L = (Z_0 \tan\theta) / \omega_0$$

where ω_0 is the passband center of the intended filter. Thus, we have an inductive reactance in series with the capacitor C, forming an LC type resonator. However, although the inductive and capacitive reactances seem to be in series, actually it is not a series LC resonator, but a parallel LC resonator simply because both ends of the LC element are connected to each other through the side walls of the guide. That, if the junction of SC stub and capacitor shown as node-A in the figure is taken as a node, the SC stub and capacitor are actually in parallel, extending from node-A to ground as shown in the circuit model of Figure 2.15.b. Thus, we actually have a parallel resonator similar to the resonators of combline and capacitively loaded interdigital filters.

The transversal TEM modes over the posts should decay in longitudinal direction of the guide. If they don't decay sufficiently at the position of the next post then the nature of coupling between adjacent posts will change. That is we may have both evanescent TE10 mode and TEM mode type couplings. If they decay sufficiently then we will have only Evanescent TE10 mode type coupling. This aspect of the
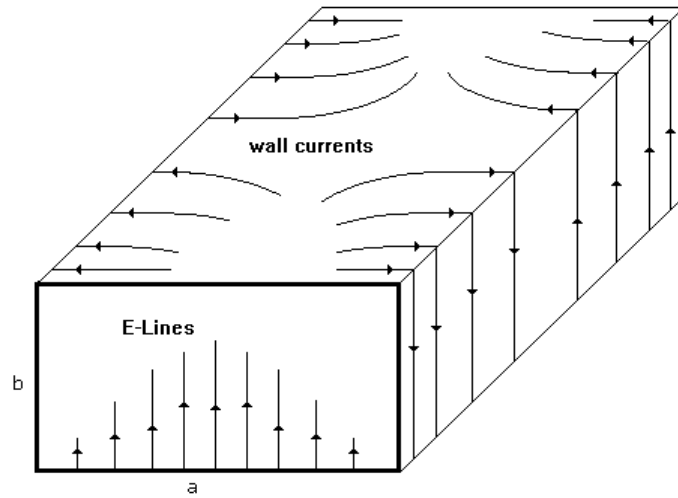
problem depends on the geometry and dimensions of guide and posts and needs modal EM analysis.
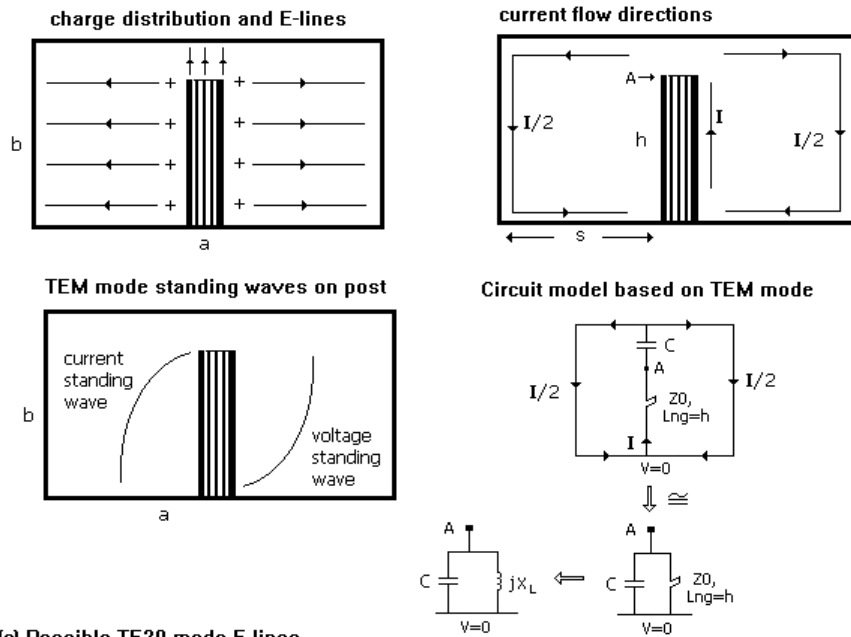
2) TE20 and higher order modes:

The side surface of the post forms a conducting wall which forces the electric field solutions to be zero on its surface. Such a boundary condition can be satisfied by higher order modes like TE20, TE40, etc. As an example the electric field lines of TE20 mode are shown in Figure 2.15.c. Since these modes decay at a higher rate than the fundamental TE10 mode, they may lead to only local energy storage which means that the reactance of the LC resonator may need trimming. However in cases where the adjacent resonator rods are close to each other (wideband filters), these higher order modes may also lead to extra (unaccounted) coupling between adjacent resonators.

In any case a good EM analysis will be helpful.

(a) Electric field lines and wall currents for TE10 mode

wall currents

E-Lines

b

a

(b) TEM-Line model of a post in a waveguide under TE10 mode excitation

charge distribution and E-lines

b

a

current flow directions

A→

I/2   h   I   I/2

s

TEM mode standing waves on post

current
standing
wave

voltage
standing
wave

b

a

Circuit model based on TEM mode

C
A

I/2   Z0,   I/2
        Lng=h

I

V=0

⇓ ≅

A   A

C ⊥ jX_L   ⟸   C ⊥   Z0,
                      Lng=h

V=0   V=0

(c) Possible TE20 mode E-lines

A→

b

a
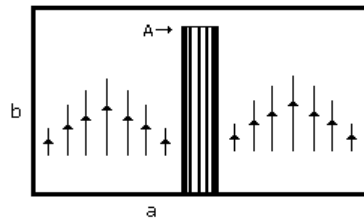
Figure 2.15 Field lines and TEM circuit model of a post in an EWG

43

2.5 EWG Filters and Combline Filters

There are similarities between combline filters and EWG filters. If a combline filter is built in an enclosure with rectangular cross-section then the enclosure may also be treated as a waveguide. When the enclosure cross-sectional dimensions allow only evanescent waveguide modes to travel in the longitudinal directions within the enclosure, corresponding combline filter will act like an EWG filter.

In the development of distributed element circuit models of combline filters, it is assumed that only TEM mode waves travel in the transversal directions, along the rods. The TEM wave travelling in between a rod and ground plane helps to define characteristic impedance Z_{k0} for rod-k defined by the distance between rod and ground and also by the radius (cross-sectional dimensions) of the rod together with the dielectric constant of the medium. The input excitation is coupled to the first rod to induce electric field/current along the rod which in turn creates the TEM waves between rods and ground and in between adjacent rods. One end of each rod is connected to a capacitor (C_k) and the other end is connected to the enclosure wall which is grounded. Thus, the rods can be modelled as SC stubs of impedance Z_{k0} between one port of the capacitor and ground. Since the other port of the capacitor is also grounded, the rod and capacitor forms a parallel resonator made up of a shunt SC stub and lumped element capacitor. The waves over each rod form standing waves with maximum of current at the grounded end and maximum of the voltage at the capacitively loaded end as depicted in Figure 2.16.a. Coupling between the adjacent rods of combline are provided by the odd mode TEM waves travelling in between the rods. For example, rods k and k+1 are assumed to form a two-wire-line of characteristic impedance $Z_{k,k+1}$. So, the medium between adjacent rods acts as a two-wire transmission line grounded at the same side ends, forming a SC stub. This SC stub represents the coupling element between adjacent resonators. In Figure 2.16.a two-resonator combline structure with the capacitors C_{10} and C_{20} and characteristic impedances of the shunt SC stubs denoted by Z_{10} and Z_{20} are given.

For frequencies f<f_q where f_q is the quarter wavelength frequency of the rods, the SC stubs can be approximated as lumped element inductors as shown in the figure.
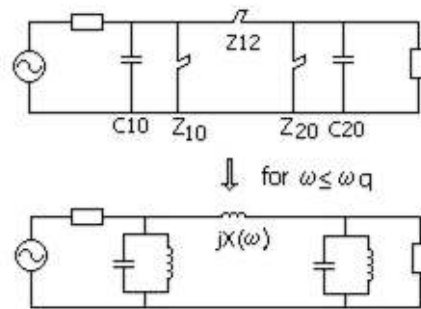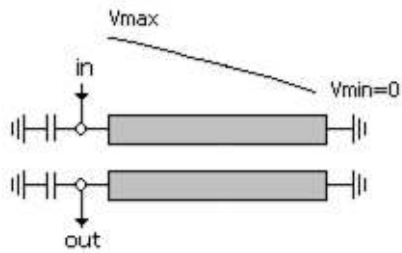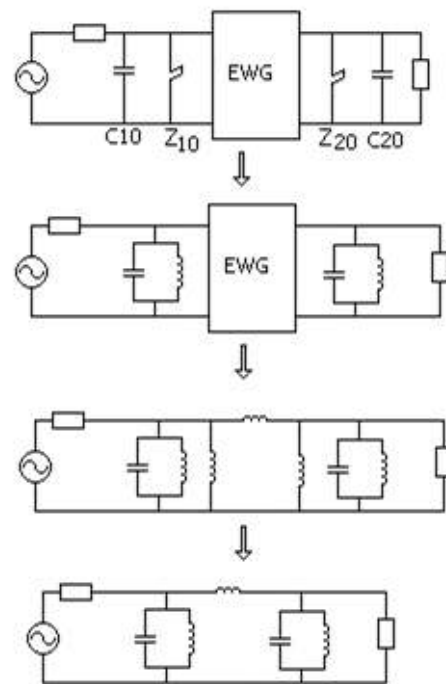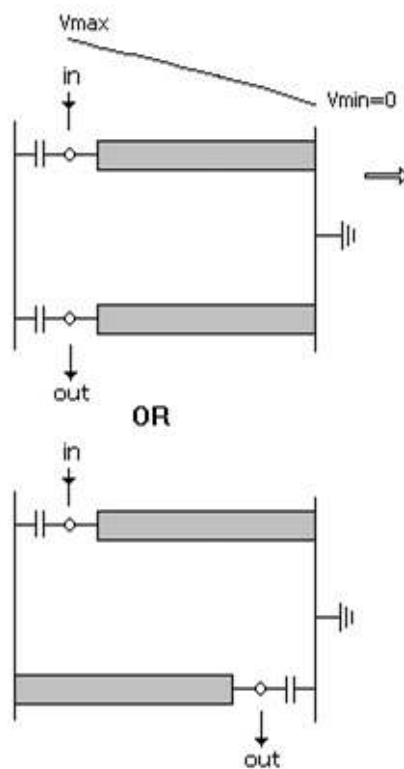

Figure 2.16 Circuit models of Combline and EWG filters

Figure 2.16.b shows the circuit model of a portion of EWG filter. The coupling between adjacent resonators will be provided only by the evanescent waves supported by the enclosure cross-sectional dimensions. If the inductive Pi-model is used for the EWG filter design, then the circuit model leads to the lumped element form as given on the right hand side of Figure 2.16.b where shunt parallel resonators made up of parallel connection of shunt inductor of the Pi-model of EWG and the parallel resonator model of the capacitive posts are formed. Since these shunt resonators are coupled to each other inductively (through the series inductor of the Pi-model of EWG), if the capacitors are placed at the same side ends of the rods then the same lumped element prototype as the Comb type filters will be formed as seen in the figure.

The main difference between combline and EWG lies in the interpretation of the coupling conditions. In combline, coupling is provided by the TEM waves travelling in between the adjacent rods, in the transversal plane of the housing. However, in EWG filters, coupling is provided by the evanescent waveguide pieces modelling the waves travelling in longitudinal direction. As stated earlier, if the housing of a combline allows only evanescent waveguide modes to travel in the longitudinal directions within the housing, then TEM waves in transversal direction and evanescent waves in longitudinal direction will exist which means that such filters may also be treated as EWG filters.

On the other hand, possible evanescent mode waves in longitudinal direction for the combline filters are usually assumed to be ineffective compared to the main TEM modes travelling along the coupled lines. However, as indicated in [35], this may not hold under every circumstance. That is the coupling between adjacent rods may get some interference from the longitudinal travelling evanescent modes that are unintentionally supported by the enclosure leading to mixed type couplings. For example in combline filters, besides the series SC stub a lumped inductor in parallel with the SC stub to simulate the EWG type coupling should be added. Experiments indicate that some of the evanescent modes may be suppressed by grounding the

46

alternate ends of adjacent rods, but in combline filters the same side ends of rods are grounded that more evanescent modes could be generated because of the asymmetry of the top and bottom halves of the structure. Effects of evanescent mode couplings result as bandwidth widening.

In conclusion, it is clear that in the most general circuit model of Comb-EWG structures couplings between adjacent resonators may be of combinations of TEM type and EWG type couplings which may also requires the incorporation of higher order EWG modes as well. Therefore a generally valid circuit model can only be developed after a detailed analysis of existing wave modes which requires the use of full wave EM simulations.

2.6 Finite Transmission Zeros in EWG Combline Filters

Circuit models of the combline filters involve inductive couplings between adjacent resonators, appearing as series arm SC stubs which displays inductive reactance for *f<fq* as described before. This series inductive reactance can be resonated by paralleling it with a capacitive reactance to create a finite transmission zero. This is possible by introducing a series lumped capacitor between open ends (capacitively loaded ends) of the adjacent lines [36]. The parallel capacitive reactance can be implemented easily in comb type coupled line sections by narrowing the gap between the ungrounded tips of adjacent lines. In this thesis an alternative novel approach is tested for realization of capacitive reactance by introducing a dielectric slab between adjacent rods.

Next chapter describes the complete design and realization of a comb type bandpass filter in detail starting with a characterization of a single resonator, which is the building block of the corresponding filter.

CHAPTER 3

DESIGN METHODOLOGY OF A EWG COMBLINE BANDPASS FILTER

In this chapter, the design stages of EWG combline filter are developed in detail. By using the theory given in Chapter 2, first of all the building blocks of this type of filter, the resonators, are investigated. The chapter begins with the characterization of a single resonator. Then a 4-resonator bandpass filter is designed by starting with the lumped element model of the filter in Filpro. After determining the circuit of the corresponding filter, the coupling coefficients, external Q, resonant frequencies and the group delays are extracted. By using these parameters, the physical dimensions of the filter are derived and the design is implemented in EM simulation software, CST. Various tests and trials are performed in order to achieve the expected filter specifications.

3.1   Characterization of a Resonator

The detailed theory about the resonators is given in Chapter 2. Here, the design methodology of the resonators is described. The crucial point to be derived is the dimensions of the resonators.

The characteristic impedance of a coaxial line is a function of the cross-sectional dimensions of the line as well as the dielectric constant of the dielectric located in between the conductors. When the inner conductor is assumed to be resonator and the outer conductor is assumed to be enclosure of the resonator, the cross section of a

single resonator inside an enclosure can be modeled like a coaxial line. For different cross sections and enclosures, the characteristic impedances of the resonators are approximated in Table 3.1. [37]

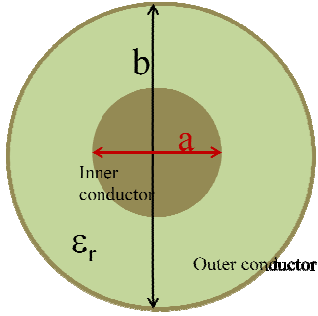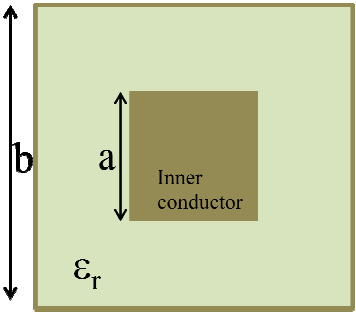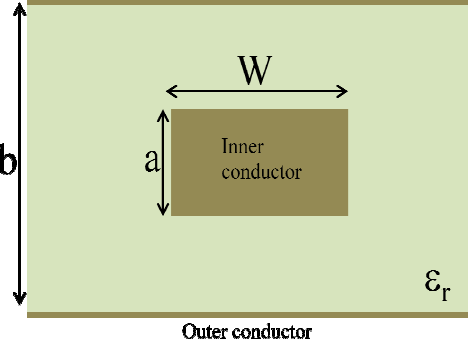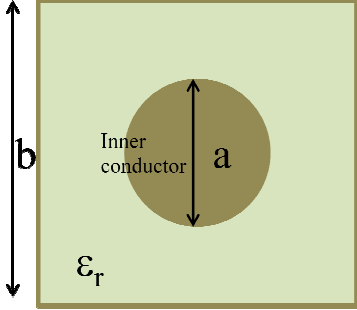**Table 3.1** Approximate characteristic impedances for various resonator types

Resonator type	Visualization	Approximate characteristic impedance equation (Ohm)
Inner conductor: Circle Outer conductor: Circle		$$Z_0 = \frac{59.952 \ln \frac{b}{a}}{\sqrt{\varepsilon_r}}$$
Inner conductor: Square Outer conductor: Square		$$Z_0 = \frac{136.7 \log_{10}\left(0.9259\frac{b}{a}\right)}{\sqrt{\varepsilon_r}}$$
Inner conductor: Rectangular Outer conductor: Rectangular		$$Z_0 = \frac{94.172}{x(W/b) + 1/x \ln F(x)}$$ where $$x = \frac{1}{1 - a/b}$$ $$F(x) = \frac{(x+1)^{x+1}}{(x-1)^{x-1}}$$

Table 3.1 (continued) Approximate characteristic impedances for various resonator types

Inner conductor: Circle Outer conductor: Square		$Z_0 = \dfrac{59.952\ln\left(1.0787\dfrac{b}{a}\right)}{\sqrt{\varepsilon_r}}$

When the above approximations for different resonator types are plotted for varying "a/b" ratio with the air to be assumed in between the conductors ($\varepsilon_r=1$), the characteristic impedances given in Figure 3.1 are achieved.
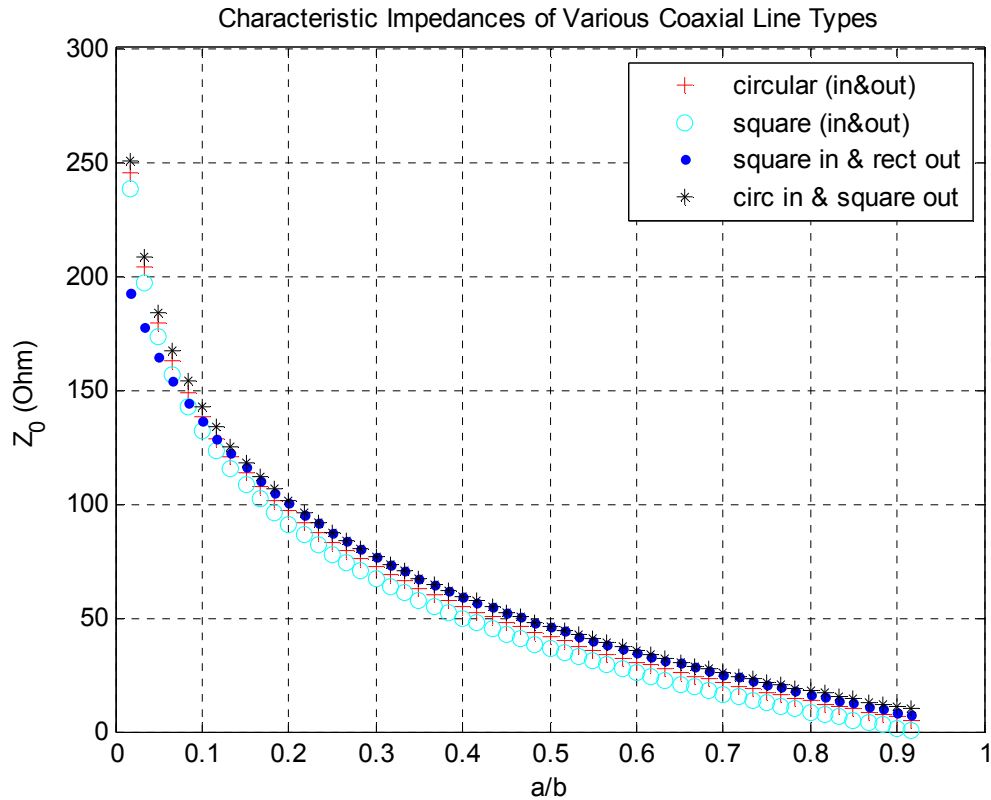
Figure 3.1 Characteristic impedances of various coaxial line types vs. a/b ratio

The characteristic impedances of the resonators slightly vary for different coaxial line types as illustrated in Figure 3.1, which is expected.

Throughout this thesis, square inner conductors are considered, since the realization of this type of conductor is more feasible and practical when a dielectric material is being added in between the resonators which will be discussed in Chapter 4.

Next, the quality factor of the square coaxial line will be demonstrated. The quality factor, Q, which explained earlier in Chapter 2, is being determined by the attenuation of the line and has to be high enough to have less attenuation.

The attenuation of a coaxial line is approximated as [38]

$$\alpha_c = 1.898 \times 10^{-4} \sqrt{\varepsilon_r} \sqrt{f(GHz)} \left(\frac{1+b/a}{b \ln b/a} \right) \text{(dB/unit length)} \qquad (3.1)$$

which is due the ohmic losses in conductors. In this case, again there is no dielectric is assumed in between the conductors. The Q factor of the coaxial line with the attenuation of (3.1) is given by [38]

$$Q_c = \frac{\pi \sqrt{\varepsilon_r}}{\lambda \alpha_c} \qquad (3.2)$$

The plot for the normalized unloaded Q factor is given below in Figure 3.2. The values are normalized with respect to the highest value for the sake of simplicity.
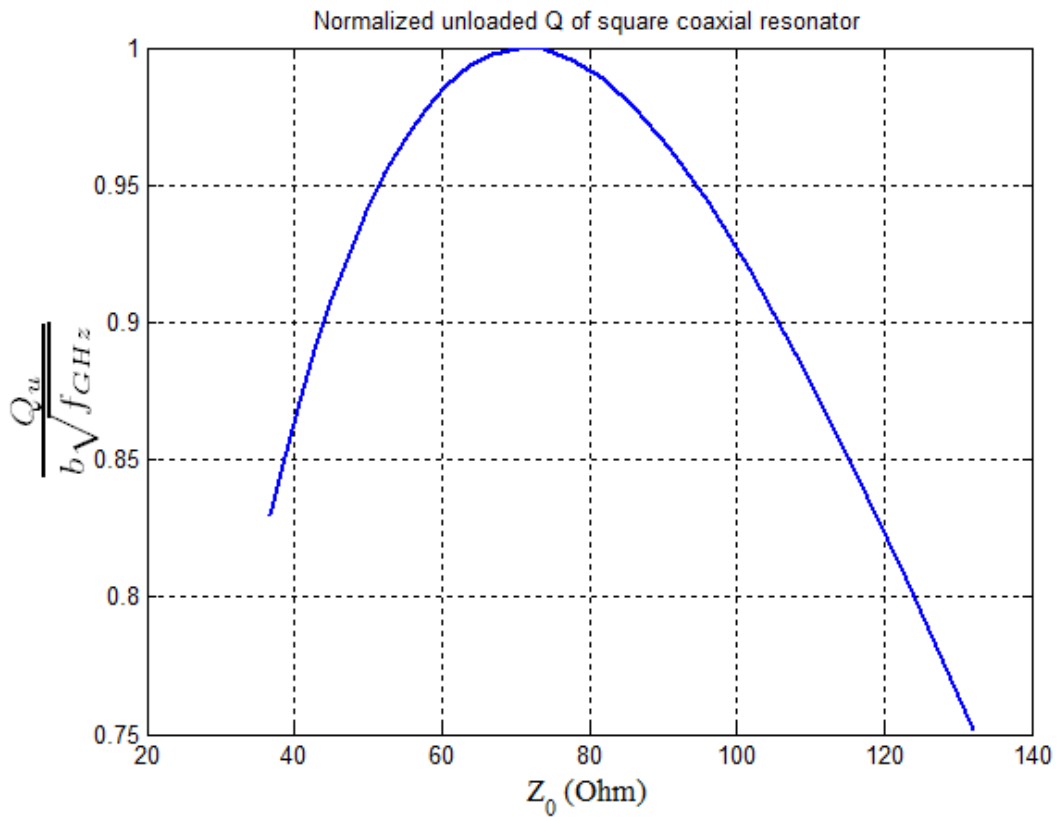
Figure 3.2 The normalized unloaded Q factor of a square transmission line vs. Characteristic impedance of the square coaxial resonator

The Q-factor of a coaxial line gets its highest value when the characteristic impedance is around 70 Ohm for a square coaxial line. In order to achieve the highest quality factor, the characteristic impedance of the square resonators is chosen to be 70 Ohm. Then, by considering Figure 3.1 again, the value of "a/b" which is the ratio of the thickness of the inner conductor to the width of the enclosure is determined as 0.33 where the characteristic impedance value for the square inner conductor & rectangular outer conductor resonator is 70 Ohm.

On the other hand, by using (2.35), the attenuation constant versus frequency normalized to cutoff frequency is depicted in Figure 3.3.
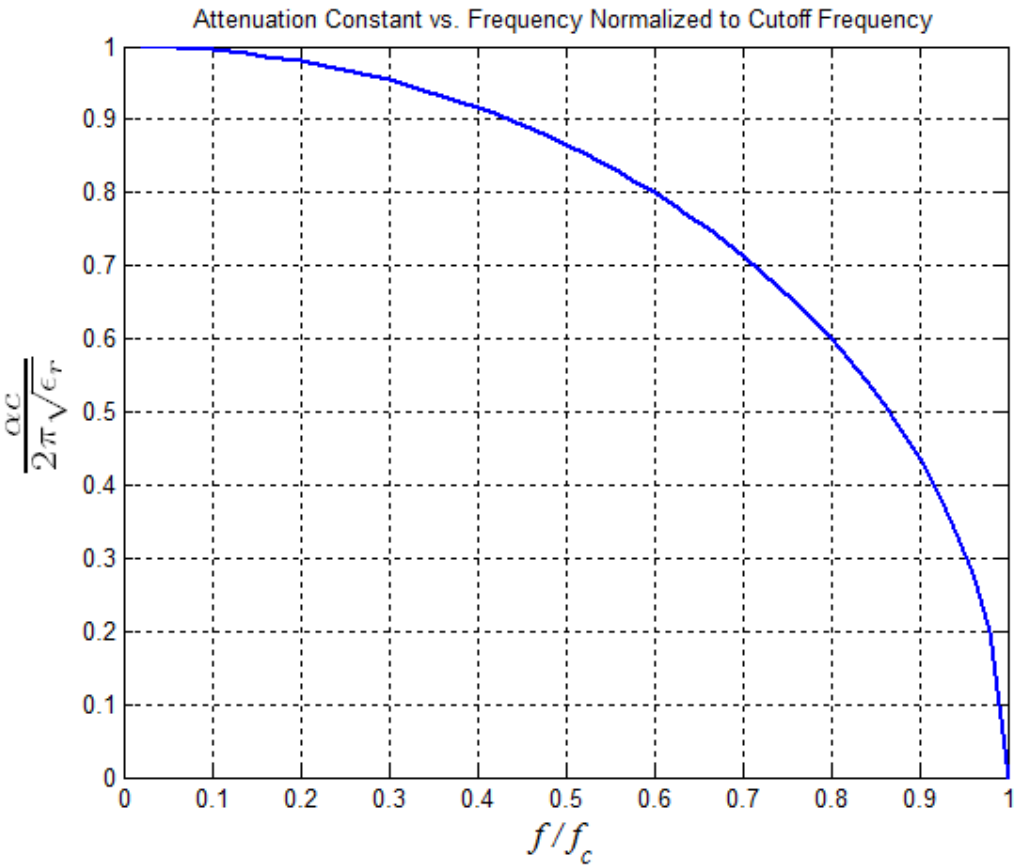
Figure 3.3 The attenuation constant vs. Frequency normalized to cutoff frequency for EWG filters

As seen from the graph, well below cut off frequency the attenuation becomes flatter. From this point of view, in order to achieve more flatness through the passband of the filter, the attenuation at the edges of the passband have to be similar, thus the width of the evanescent mode waveguide have to be chosen small enough in order to stay far enough from the original cut-off frequency of the waveguide.

Table 3.2 given below illustrates the cut off frequencies with respect to the width of the waveguide.

Table 3.2 Filter width vs. Cut off frequency

Width (mm)	Cut off Frequency (GHz)
8	18.737
7	21.413
6	24.982
5	29.979

From Table 3.2, it is seen that the smaller width of the enclosure will lead to higher cut-off frequency, so lower passband ripple.

After a good understanding of the effects of the resonator and the waveguide dimensions on filter design, next the characterization of an EWG combline filter via Filpro is investigated.

3.2 Characterization of an EWG Combline Filter

The initial circuit is formed according to the given specifications in table. The circuit is synthesized on Filpro with the given specifications is illustrated in Figure 3.4.
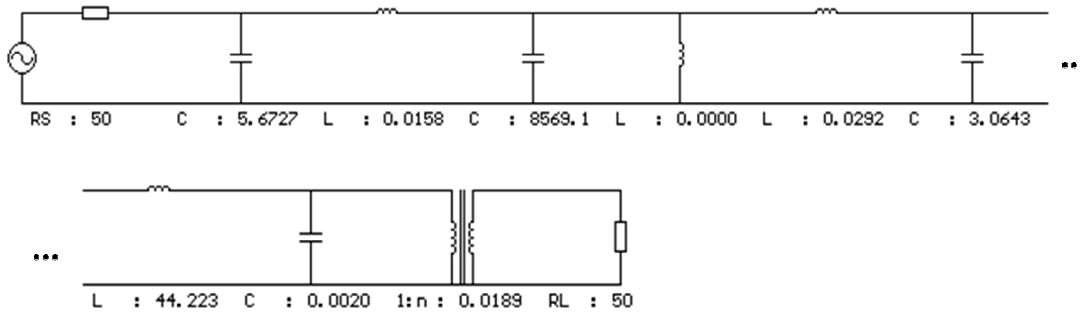

Figure 3.4 Initial Filpro circuit for EWG combline filter design

Next, the initial circuit is converted into the inductively coupled shunt LC resonator form as seen in Figure 3.5.
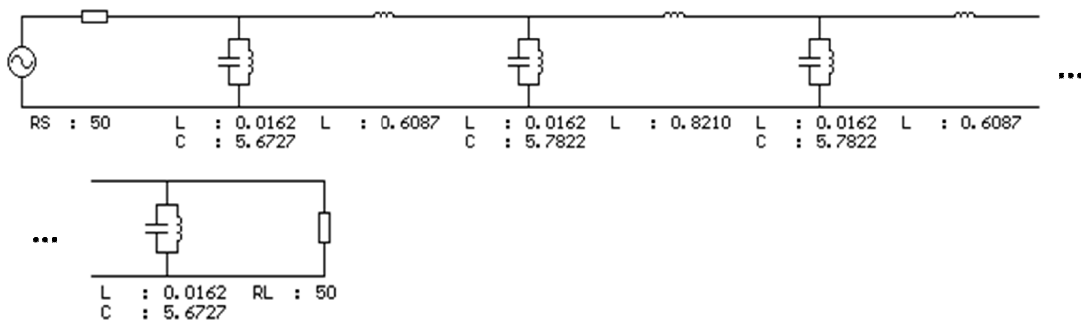

Figure 3.5 Inductively coupled shunt LC resonator form of the initial circuit

In order to proceed with the EWG design, the circuit is scaled up in impedance such that the Pi-sections of inductors of the circuit of Figure 3.5 will be equivalent to

waveguide pieces with desired cross sectional dimensions and proper lengths between resonator rods. The shunt capacitors will be realized at the open ends of rods which as gap capacitors. The desired waveguide parameters are given in Table 3.3.

Table 3.3 EWG parameters of the filter design inserted into Filpro

EWG parameters	
Width of EWG	6mm
Height of EWG	4mm
Dielectric constant	1
Passband center	16800 MHz
Characteristic impedance of the posts	70 Ohm
Height of the posts	< 4mm

The shunt LC resonators are actually formed by shunt legs of the Pi-models of EWG piece together with the inductance and capacitance of the resonator rods. There are some remarks regarding to Table 3.3. Since the passband center of the EWG filter is 16800 MHz, from Table 3.2, the choice of the EWG width of 6mm will lead to flatter attenuation through the passband. As detailed in the previous section, in order to achieve the characteristic impedance of 70 Ohm, the ratio of the width of the post to the width of the enclosure has to be 0.33. So, the width of the posts will be set to 2mm in the EM analysis. Also the height of posts must be less than the height b of the waveguide to allow for the capacitance gap. The corresponding circuit after setting EWG parameters is given in Figure 3.6.
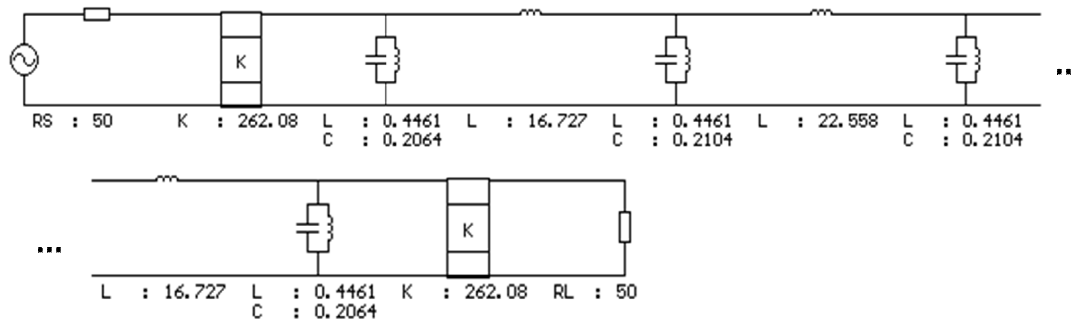
Figure 3.6 The circuit in Filpro after scaling the circuit for the selected EWG parameters

As described in Chapter 2, the EWG pieces can be represented as Pi sections of inductors. As seen in Figure 3.6, there are three symmetric Pi sections composed of inductors which are replaced by EWGs next and Filpro calculates the lengths of each EWG which are about 5.3 and 6 mm. These waveguide lengths will be considered as a starting point to set the separation between the resonators in the following designs. Figure 3.7 shows the circuit after replacing the inductive Pi-sections of Figure 3.6 by EWG pieces.
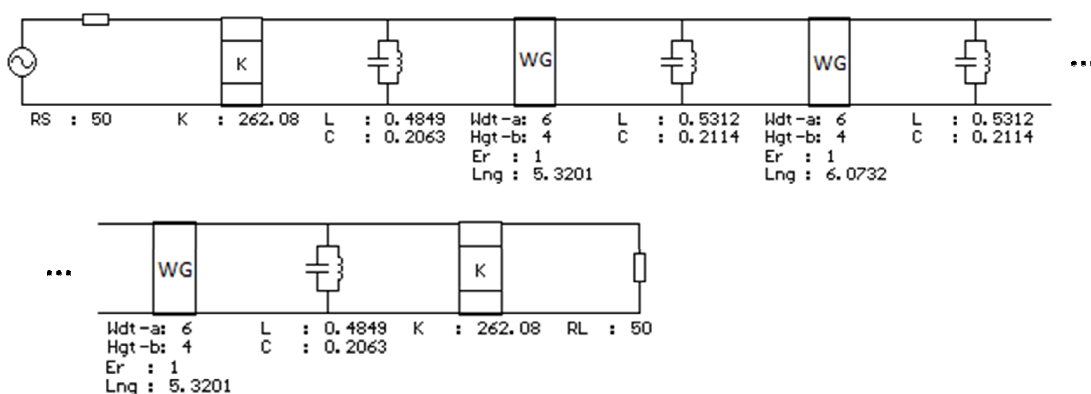
Figure 3.7 Filpro circuit after Pi-sections of inductors are replaced by EWGs

Then, the shunt LC resonators in between EWGs are converted into SC Stub+Capacitor forms given in Figure 3.8 to represent the posts, where one end of the post is connected to the ground forming an SC stub and there is a gap between the other end of the post and the enclosure forming a capacitance.
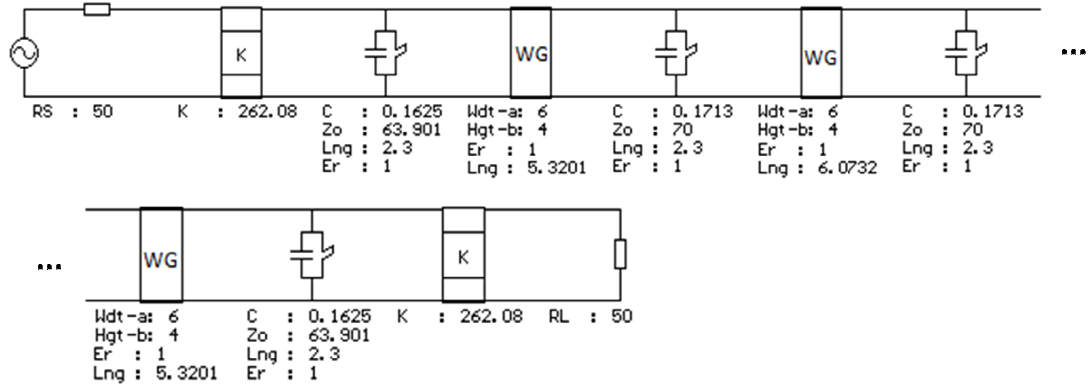
Figure 3.8 Filpro circuit after conversion of the LC resonators into SC Stub+Capacitor form

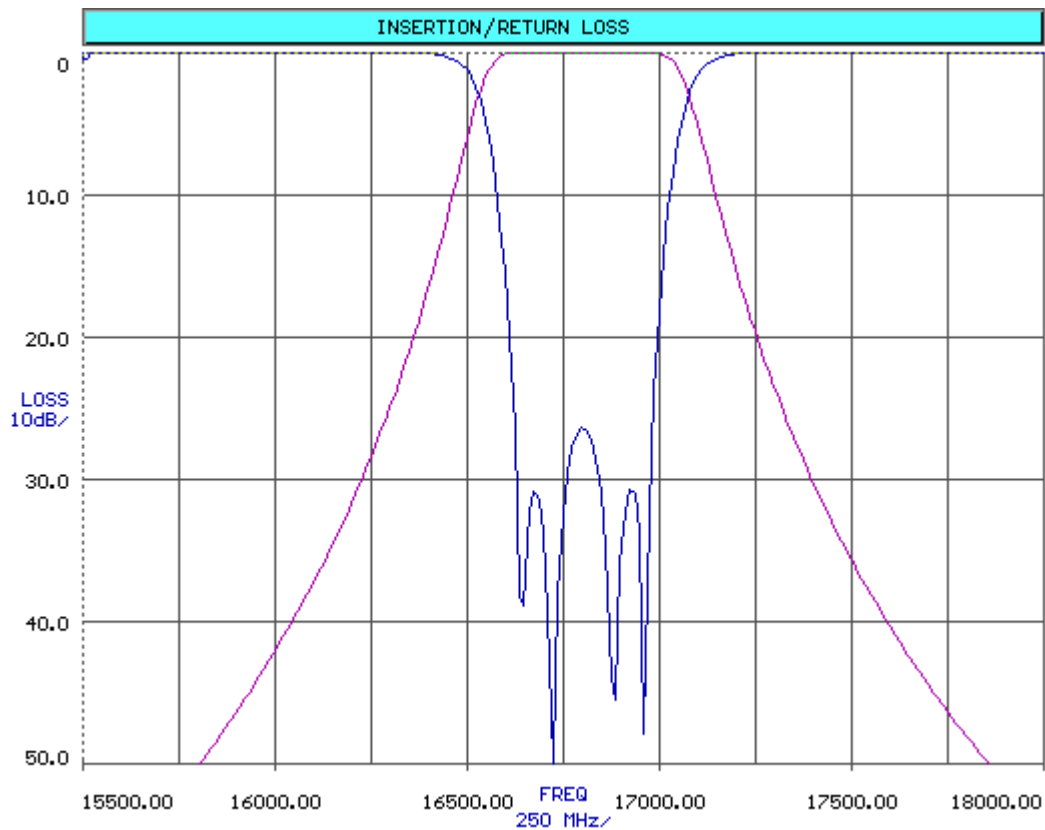The resulting S parameters of the circuit above are shown in Figure 3.9.

59

Figure 3.9 The response of the EWG filter calculated via Filpro

However, the circuit given in Figure 3.8 includes inverters at the input and output ports. These inverters should be converted to the tapped form in order to proceed with the realization of the design. So, the inverters with the parallel LC resonators next to them are replaced with the tapping points having the same the quarter wavelength frequency, f_q of the SC stubs of the resonators. The impedance of the tapping points is set to 70 Ohm which is the impedance of the resonators in the circuit as seen in Figure 3.10.
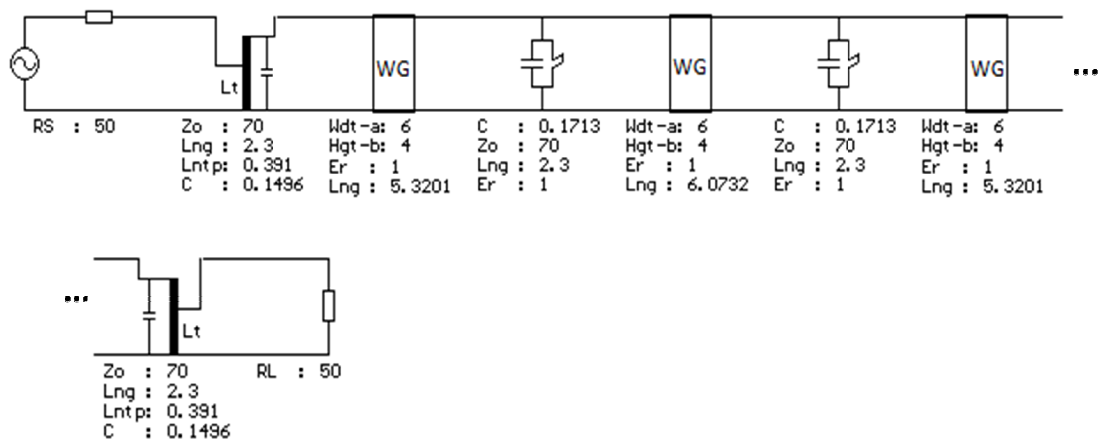
Figure 3.10 Filpro circuit after replacing the inverters with tapping points

After equating the impedances of the tapping points to the posts, some degradation in the final response occurs as seen in Figure 3.11.
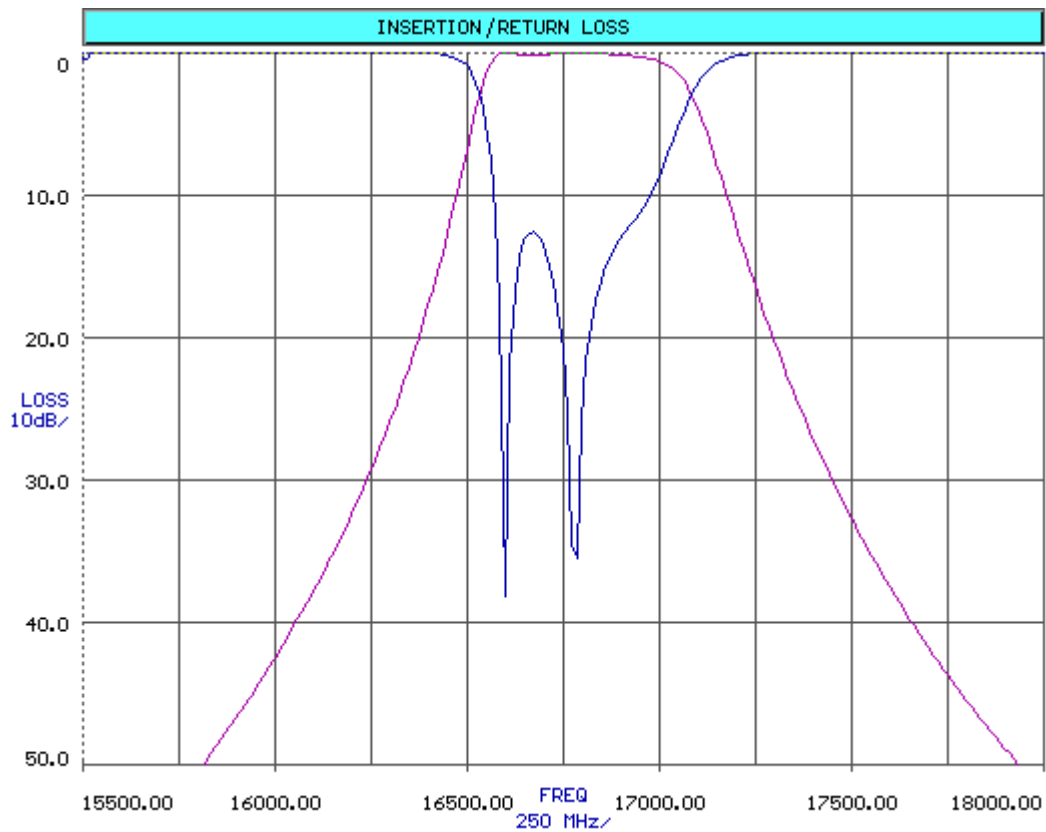
Figure 3.11 The response of the EWG filter after insertion of the tapping points

The lengths of waveguides and capacitances of the resonators are tuned to have better insertion loss, passband ripple as well as lower return loss, and the final Filpro circuit and the filter response are given in Figure 3.12 and Figure 3.13, respectively.
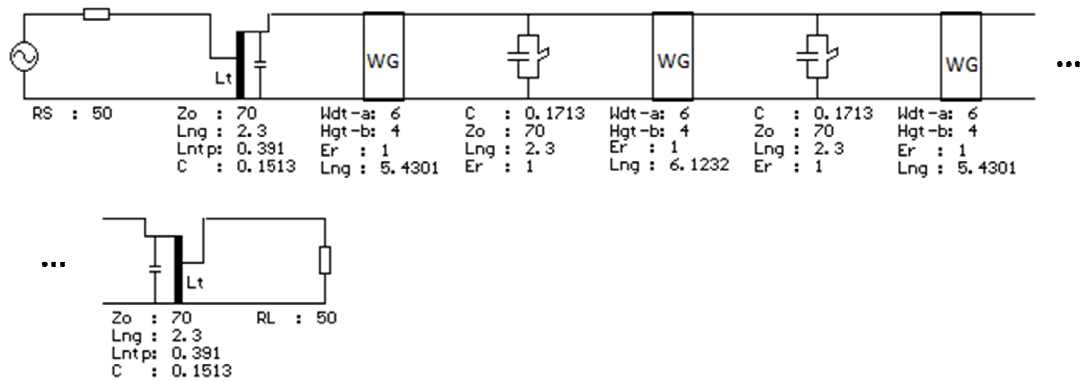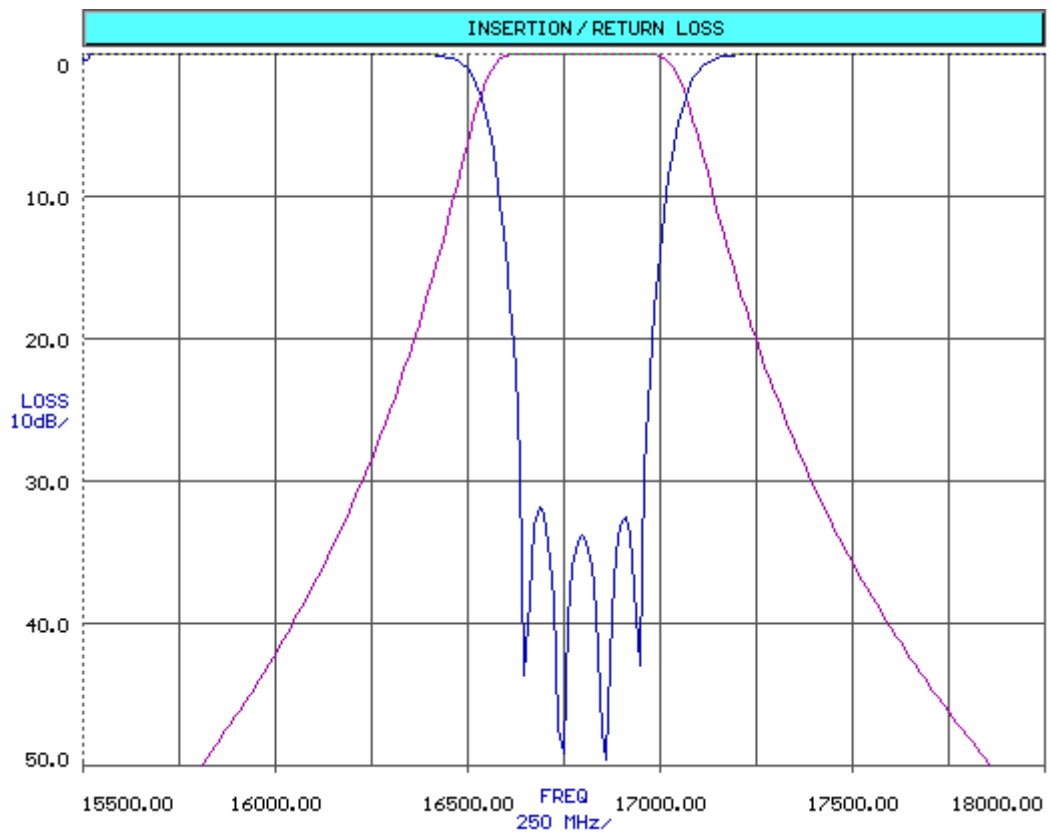
Figure 3.12 Final Filpro circuit after tuning

Figure 3.13 Final response of the filter derived via Filpro

After investigating the properties of the resonators and the design approach of the EWG type filters together with establishing a starting point regarding to the separation between the resonators, a complete EWG combline bandpass filter design via starting from Filpro and continuing in CST is described in the next section.

3.3 EWG Combline Filter Tuning by Group Delay Approach

In this section, a 4-resonator bandpass filter will be designed using group delay of S11. Design steps will be explained in detailed to understand the methodology lying behind.

First of all, the filter is designed in Filpro in order to calculate corresponding coupling coefficients of the bandpass filter. The filter specifications are given in Table 3.4.

Table 3.4 The expected filter specifications for 4-resonator filter design

By Prototype with Inverters	Shunt Caps + Inverters
Degree	4
Ripple (dB)	0.01
Filter Type	Lumped, BPF
Passband Corners (MHz)	16600-17000

After inserting the specifications of the filter to Filpro, the software automatically generates the circuit given in Figure 3.14.
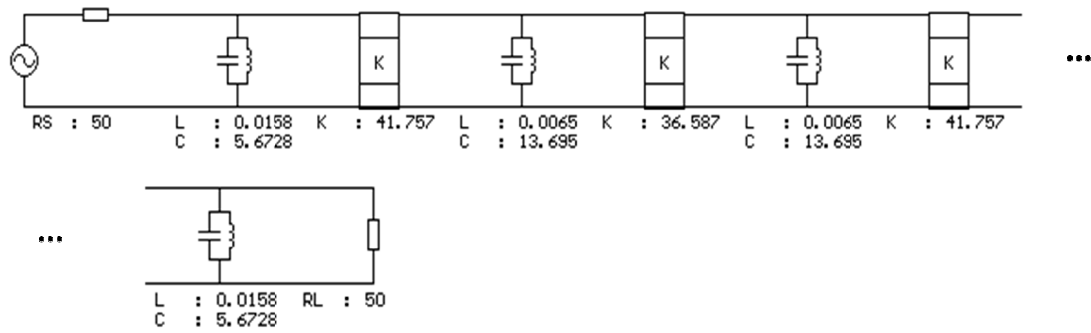
Figure 3.14 Initial Filpro circuit generated automatically for 4-resonator bandpass filter design

The software is capable of calculating the external Q and the coupling coefficient values, k for any built circuit. Here the corresponding parameters derived by Filpro are given in Table 3.5..

Table 3.5 External Q and the coupling coefficients of the 4-resonator bandpass filter design

Q external (source)	29.9404
Q external (load)	29.9404
k1,2	0.0257
k2,3	0.0189
k3,4	0.0257

Using the equations, (2.29) - (2.33), the group delays of S_{11} at f_0 for all the resonators are calculated. All group delays are demonstrated in Table 3.6.

Table 3.6 The group delays of 4-resonator bandpass filter

Resonator Order	Group Delay (ns)
First	1.13
Second	1.91
Third	1.91
Fourth	1.13

Since the filter is symmetric, the group delay values of first and fourth resonator and second and third resonator are the same as seen in Table 3.6.

As explained in Section 2.6, the group delay values derived will guide the rest of the design to find tapping point and proximity of resonators.

After calculation of the necessary parameters, the design is carried to CST in order to realize and tune to the expected filter specifications. In order to achieve high unloaded Q and low transmission line attenuation, the widths of the square resonators are chosen as 2mm with the filter width to be 6mm as derived in the previous section for $Z_0 = 70\Omega$. The height of the filter is set to 4mm and the heights of the resonators are set to 2.3mm as a starting point and will be tuned later. 4-resonator cavity filter drawn initially via CST is illustrated in Figure 3.15.
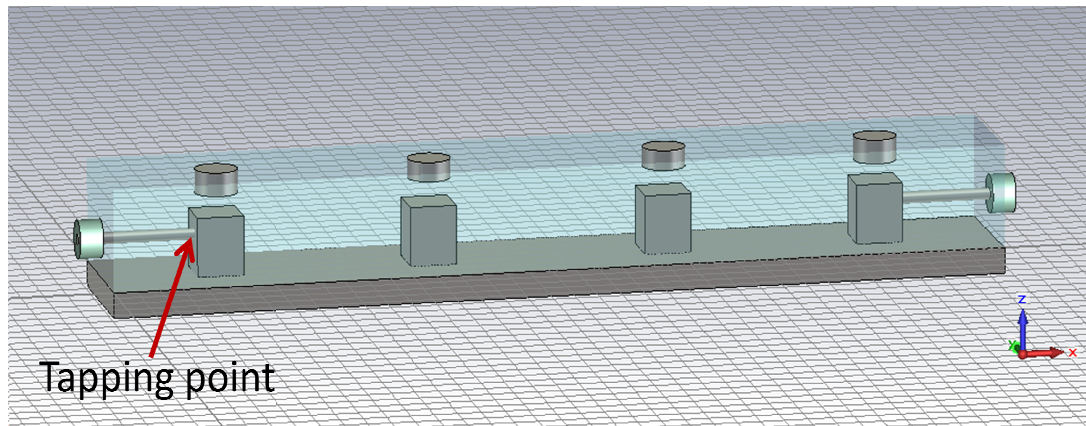
Figure 3.15 4-resonator cavity filter designed in CST

In order to proceed with the group delay method described in detail in Chapter 2, all of the resonators except the first one are shorted to ground. The visualization of this step is given in Figure 3.16 where the first resonator has a gap between the ground and the tapping point, while the rest are connected to ground plane by connecting the tap screws to the stubs as seen clearly.
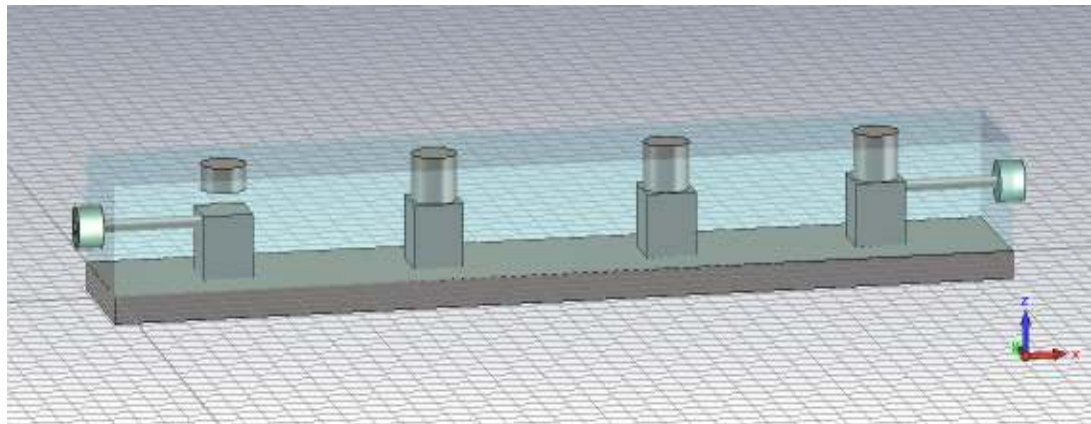

Figure 3.16 The filter drawing in CST when all of the resonators are shorted to ground except the first one.

The plot of the group delay versus frequency for 14-20 GHz frequency range is presented in Figure 3.17.
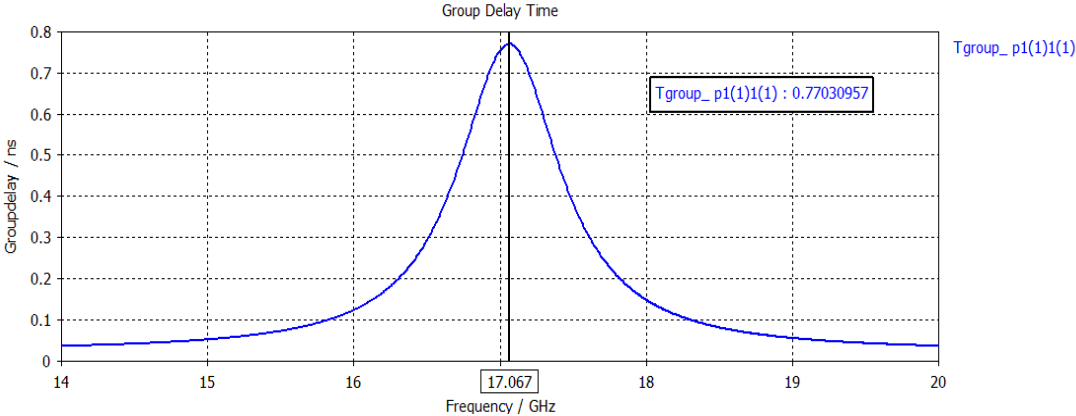

Figure 3.17 The simulated group delay when only first resonator is restored

The first group delay value of the design in Figure 3.16 is 0.77 ns at about 17 GHz which is highlighted in Figure 3.17. However as given in Table 3.6, the first group delay value has to be 1.13 ns at f_0 = 16.8 GHz. In order to adjust the group delay value to 1.13 ns, the spacing between the tapping point and the ground plane is adjusted. Also in order to set the center frequency, capacitance is adjusted by tuning the screw. After a few trials, first group delay is settled as shown in Figure 3.18.
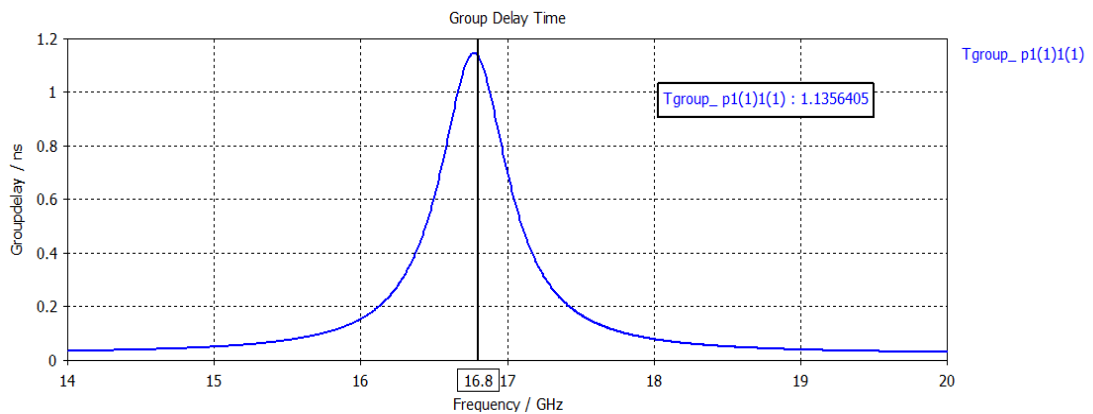
Figure 3.18 First group delay value after necessary tuning

Next the group delay of the first and second resonators will be adjusted. In order to proceed, first two resonators are being restored with keeping the rest grounded as illustrated in Figure 3.19.
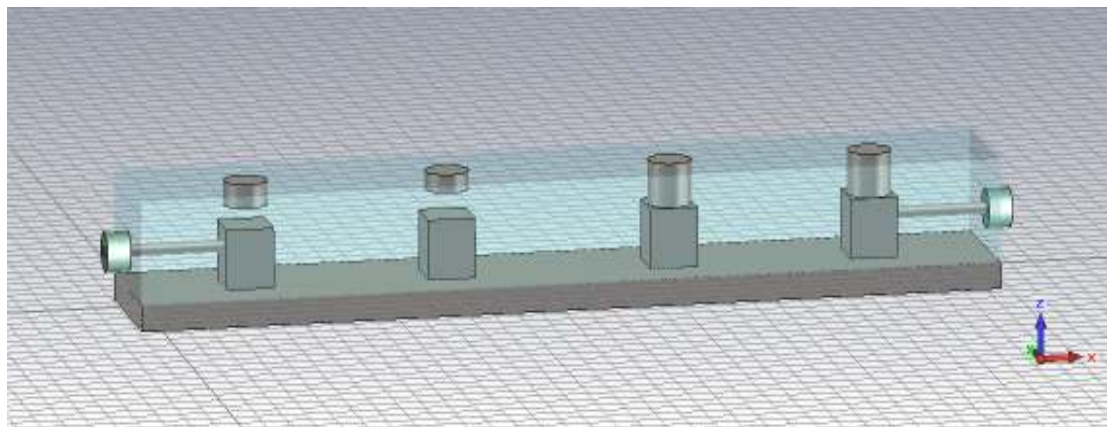

Figure 3.19 The drawing of the filter when first 2 resonators are restored in order to calculate the second group delay

In order to achieve the expected second group delay value given in Table 3.6, necessary tuning is accomplished via adjusting the spacing between first and second

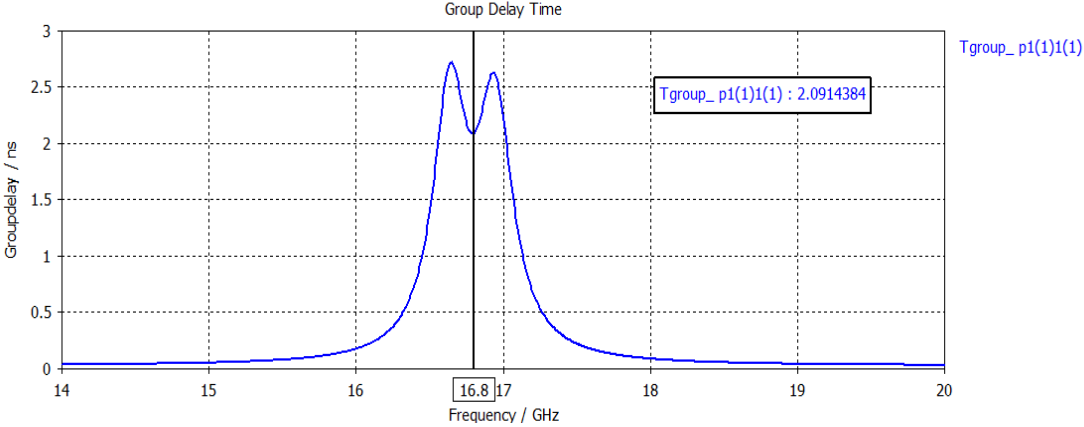resonator and tuning the second screw to adjust the capacitance as depicted in Figure 3.20.

Figure 3.20 The value and the frequency of the second group delay when 2 resonators are restored.

Since the filter is symmetric, the positions of the screws for the third and fourth resonator have already been derived while adjusting the first and second group delays. Again the tapping point for the output port will be the same as the input. The final drawing of the filter after restoring all of the resonators by proper adjustment of the rest of the resonators' parameters from first 2 resonators is presented in Figure 3.21. Until now, the only parameter which has not yet been considered is the spacing between the second and third resonator. This value can be tuned while trying to achieve the final S-parameters regarding to initial design specifications given in Table 3.4.
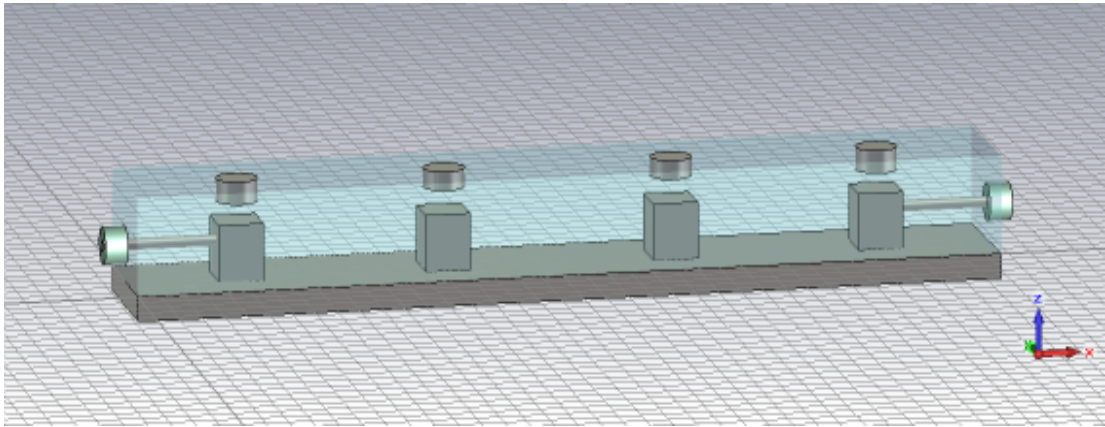
Figure 3.21 The drawing of the filter when all resonators are restored

The spacing between the second and third resonators is further tuned and final response of the bandpass filter including the insertion and return losses is illustrated in Figure 3.22.
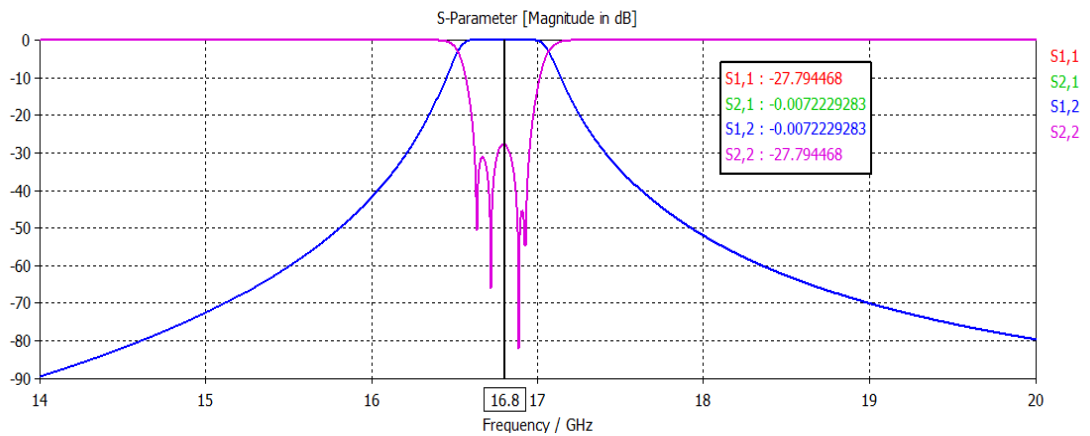

Figure 3.22 The final response of the combline bandpass filter

The total length of the filter is 38.7 mm. Main design stages are completed. For implementation of the filter, losses should be incorporated and design steps should be repeated.

71

Next chapter is describing a novel approach to decrease the filter size by inserting finite transmission zeros to the design and implementing this theory by adding dielectric material in between the resonators.

CHAPTER 4

DESIGN AND IMPLEMENTATION OF EWG COMBLINE FILTERS WITH FINITE TRANSMISSION ZEROS (FTZS)

The selectivity of the EWG combline filters can be further improved by adding transmission zeros created by coupling resonator lines to the resonators. Circuit models of the combline filters involve inductive couplings between adjacent resonators, appearing as series arm SC stubs. If these inductive coupling elements are resonated by paralleling with capacitive reactances, it is possible to form finite transmission zero sections. The parallel capacitive reactance can be implemented easily in comb type coupled line sections by narrowing the gap between the ungrounded tips of adjacent lines.

As explained in Chapter 2, SC stub is added to the series arm in order to form a transmission zero at the finite frequency. If more SC stubs are added, then more FTZs are formed. Both cases will be investigated in detail next.

First of all, one finite zero will be added below the passband, and then two zeros will be added on each side of the passband. More FTZs can be added to both side of the passband depending on the given insertion and return loss specifications and degree of the filter.

4.1   4-Resonator Filter with 1-FTZ

In this section, 4-Resonator filter with one FTZ is designed and realized. The circuit will be synthesized in Filpro as distributed element bandpass filter. As the first trial

one FTZ is placed in the lower stopband. Given the following specifications in Table 4.1, the circuit is defined in Filpro.

Table 4.1 4-resonator 1-FTZ filter specifications

By Synthesis	Distributed, BPF, EquiRipple
Ripple (dB)	0.01
Passband Corners (MHz)	16600-17000
Transmission Zeros	1 Nzero, 5 Ninf, 1 FTZ (@16000 MHz)
Degree	4
Quarter Wave Frequency (f_q) (MHz)	25200

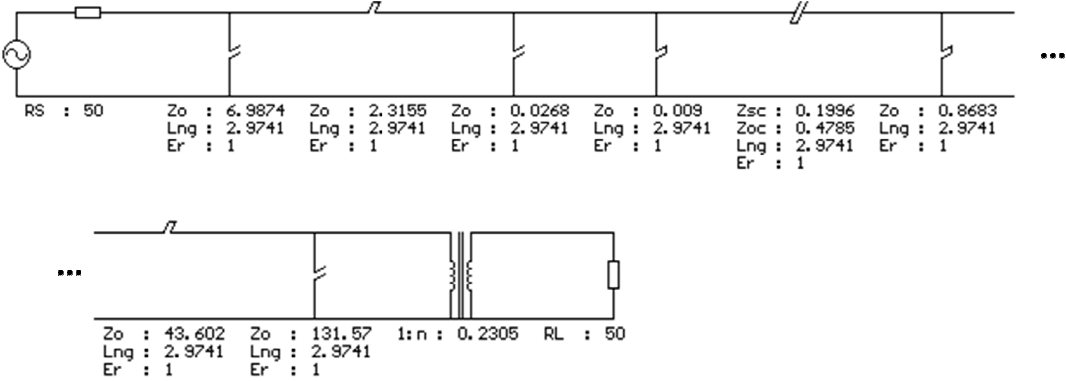The synthesized circuit is depicted in Figure 4.1.

Figure 4.1 Initial 4-resonator 1-FTZ circuit built in Filpro

Next, the shunt SC stubs are distributed into the circuit using Pi-Tee-L transformations such that each shunt OC stub in between the transmission lines will have a SC stub in parallel, with equal impedances as seen in Figure 4.2. The parallel

OC and SC stub pairs form the shunt resonators, similar to the shunt LC resonators of lumped BP filters. By this way, all the resonators will have equal impedances and sizes for convenient design and manufacturing.
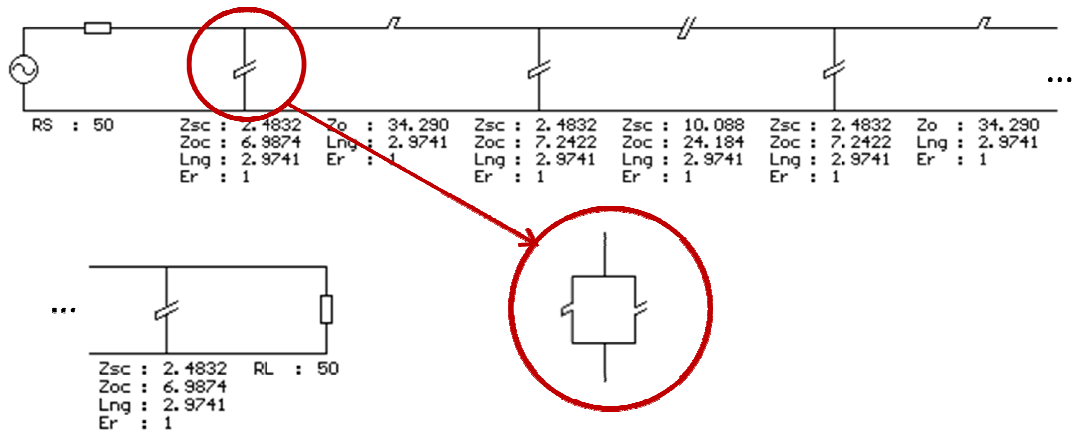

Figure 4.2 The circuit that the shunt OC stubs are distributed into circuit

Then the OC stub components of the OC+SC Stub resonators are converted into equivalent lumped capacitors as seen in Figure 4.3.
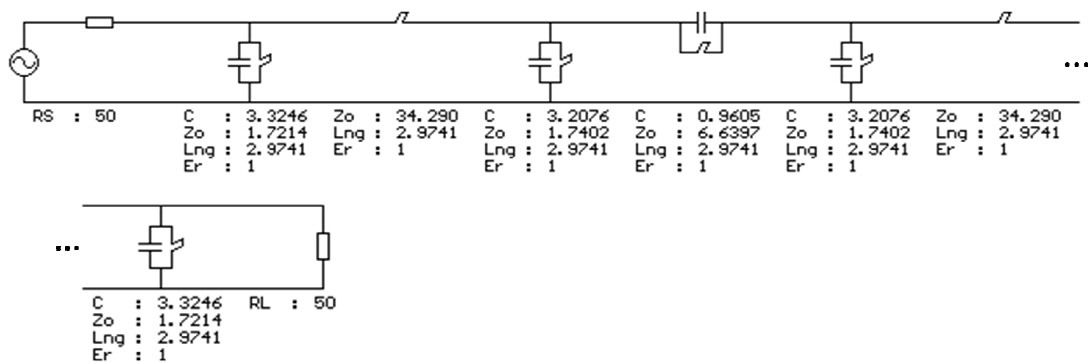

Figure 4.3 The circuit that the OC stub components of the OC+SC Stub elements are converted into lumped capacitors

The frequency response of return loss, S11, and insertion loss, S21, of the circuit shown in Figure 4.3 is plotted in Figure 4.4. The FTZ is located at about 16000 MHz in the lower stopband as expected.
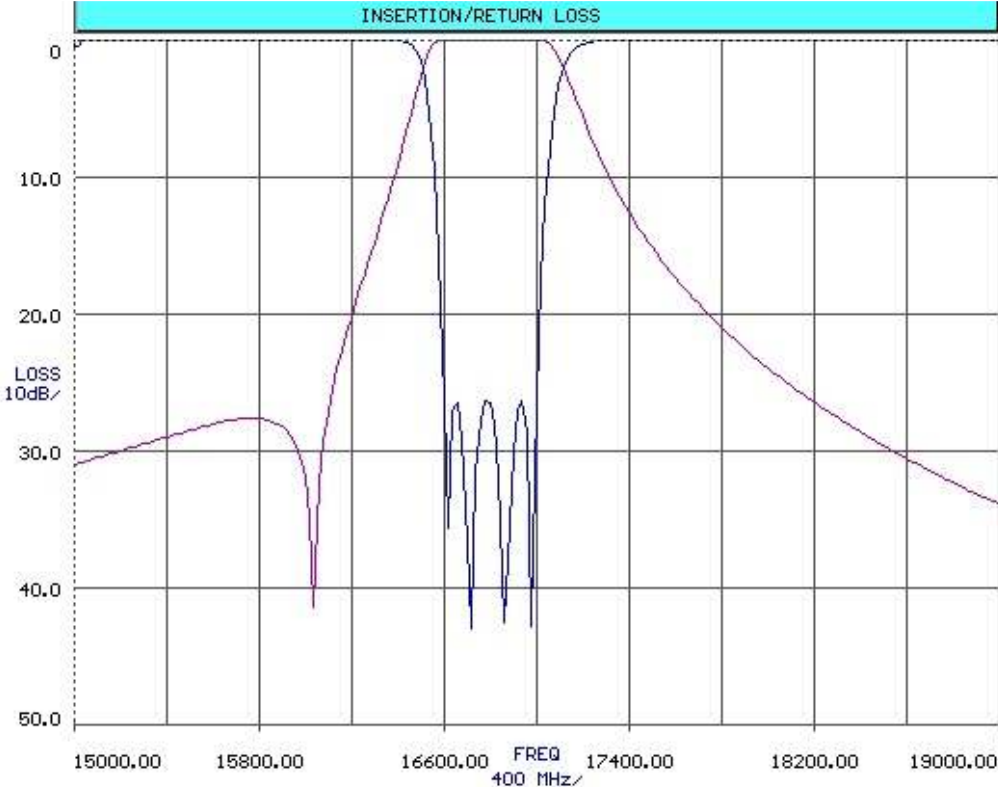

Figure 4.4 The insertion and return losses of the filter after insertion of FTZ

Since the calculation of the group delay values as given in Chapter 3 does not hold when FTZ exists in the design, the plot for the group delay versus frequency generated via Filpro will be used during tuning stages. As explained in Chapter 3, in order to simulate first resonator's group delay all the resonators are short circuited by setting the capacitance values large enough except the first one. Then the group delay of the first resonator is found as 1.137 ns at 16830 MHz as depicted in Figure 4.5.
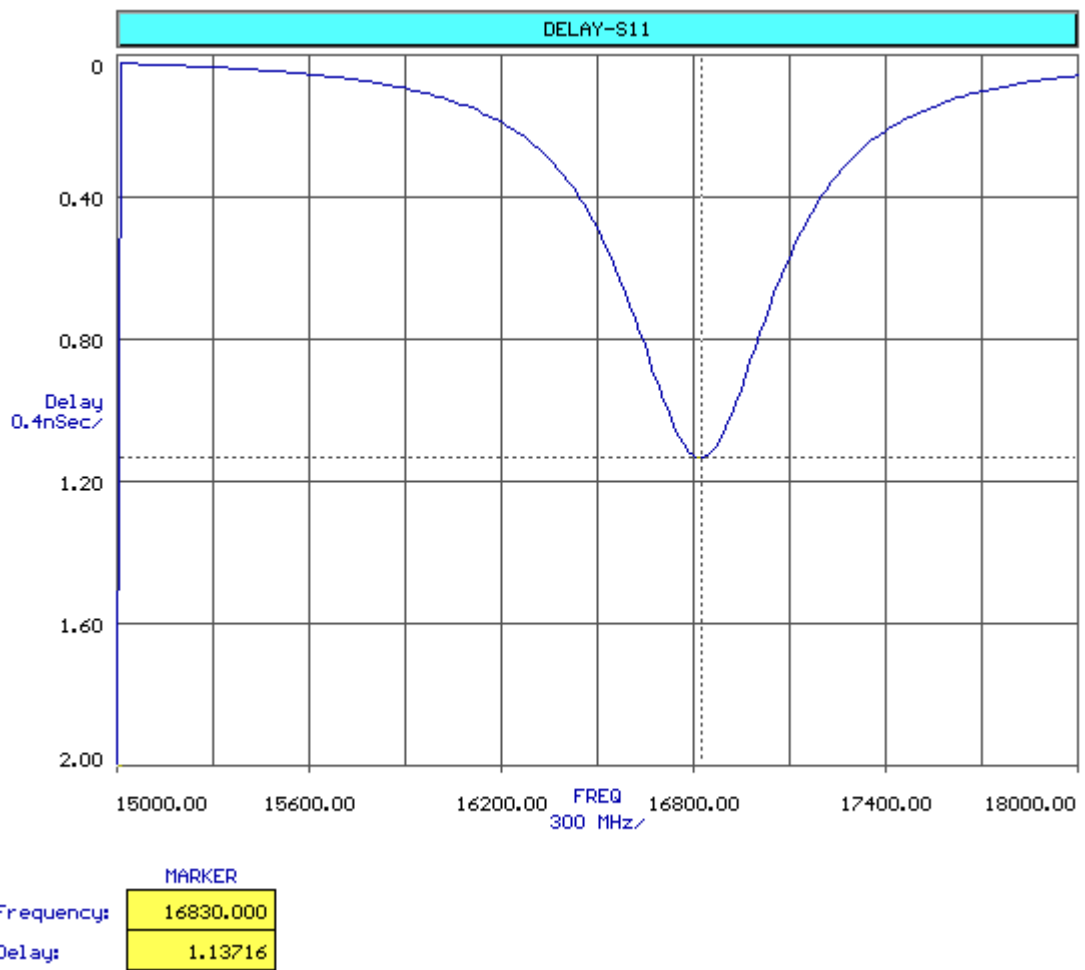
Figure 4.5 First group delay vs. Frequency simulated in Filpro

Next, the second group delay is found by restoring first and second resonators. The same procedure is followed. The group delay of the circuit is plotted in Figure 4.6.
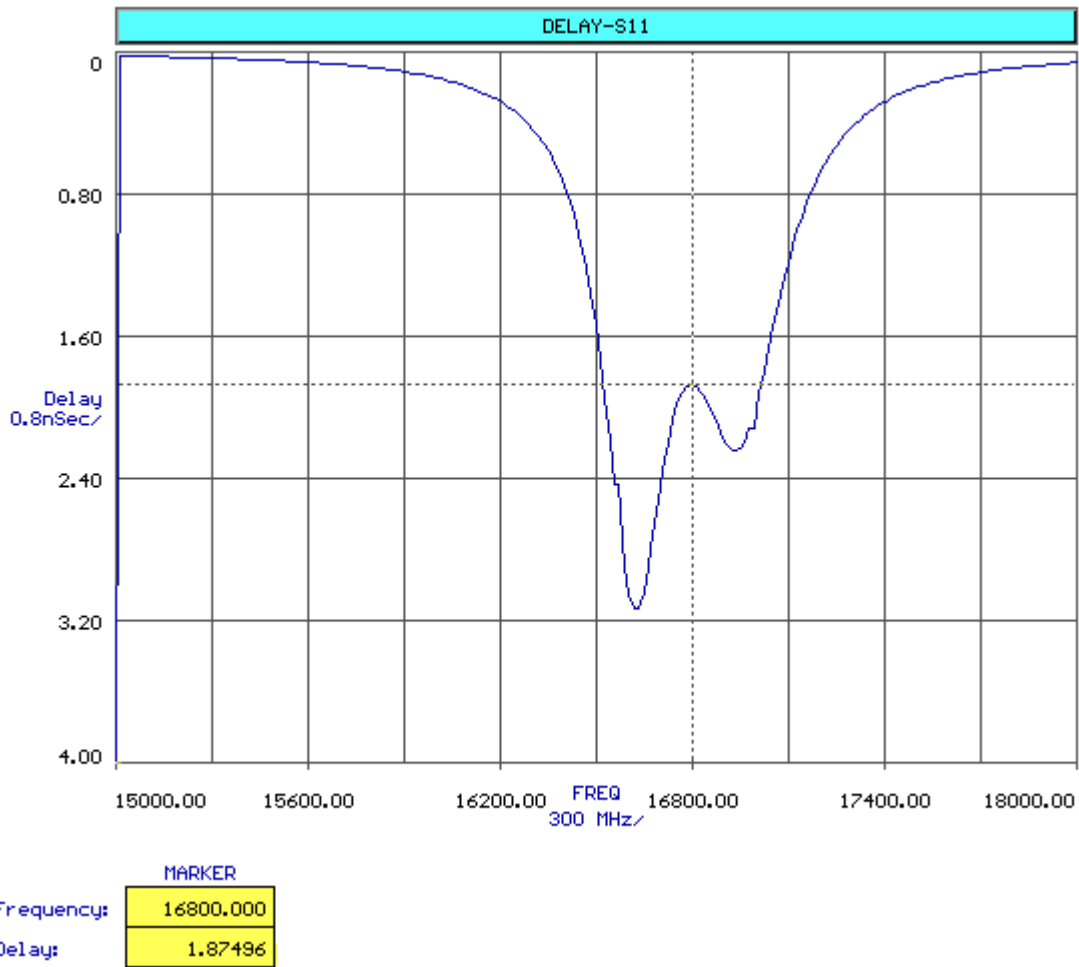
Figure 4.6 Second group delay vs. Frequency simulated in Filpro

Since the circuit is symmetric, there is no need to observe the rest of group delay values.

After collecting the expected group delay plots, the circuit is drawn in CST EM simulator software and differential ports are added as shown in Figure 4.7. First and second ports reflect the input and output of the filter, respectively.
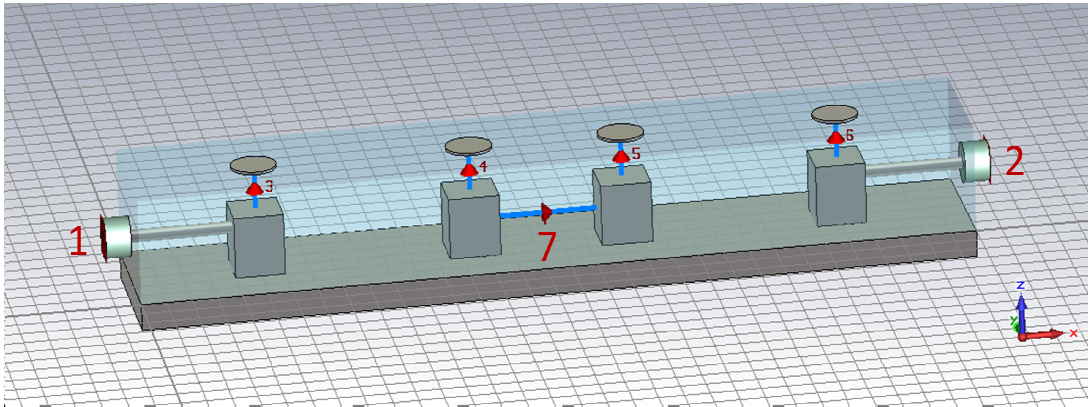
78

Figure 4.7 4-resonator 1-FTZ filter designed in CST

External lumped capacitor elements are added to the differential ports as depicted in Figure 4.8 to create the FTZ. The capacitances of the corresponding capacitors in Port 3, 4, 5 and 6 will be adjusted by tuning of the screws and could be realized by turning the screws, changing the spacing between the resonator and the screw, itself. The last port, 7, which is between second and third resonator will simulate the FTZ value and will be investigated in detail, later in this section.
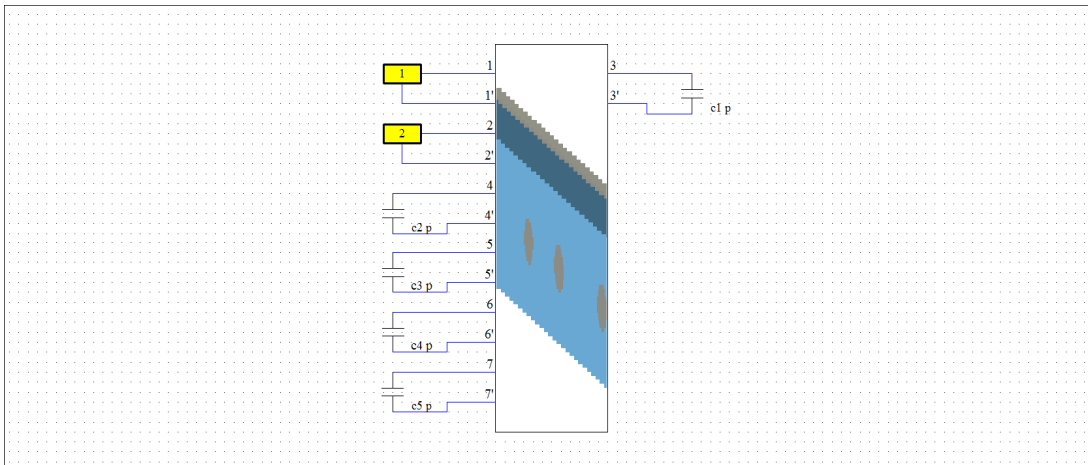

Figure 4.8 The realization of all ports in CST

The group delay values of the resonators are adjusted to the expected ones found via Filpro by following the same procedure given in Chapter 3. All of the resonators except the first one are short circuited. The first group delay is adjusted via tuning the tapping point and the screw of the first resonator. The final value of the first group delay is given in Figure 4.9 where the group delay of the first resonator is depicted as 1.09 ns at 16830 MHz. This value is close enough to proceed with the second group delay verification.
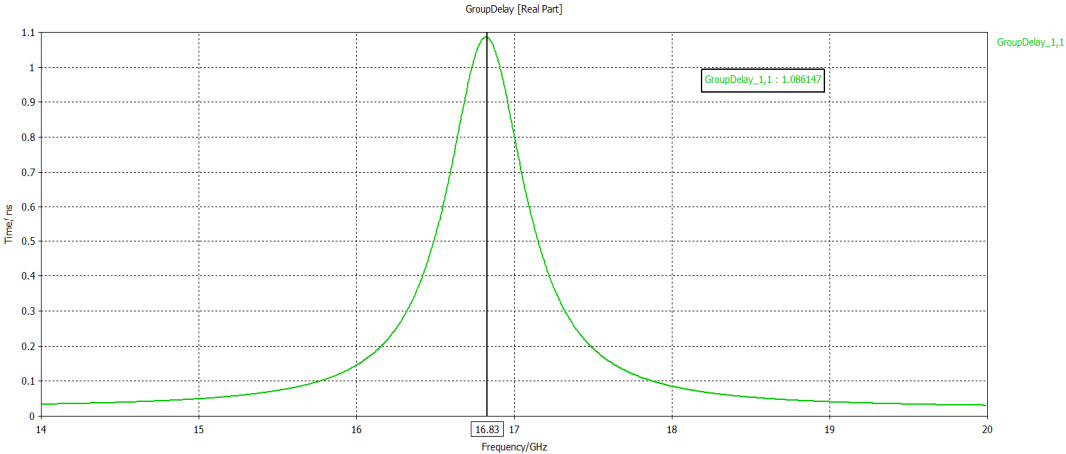

Figure 4.9 First group delay vs. Frequency derived in CST

Next, first and second resonators are restored. After tuning the screws of the first and second resonators, the second group delay is adjusted as illustrated in Figure 4.10 where the pattern is close enough to the one depicted in Figure 4.6.
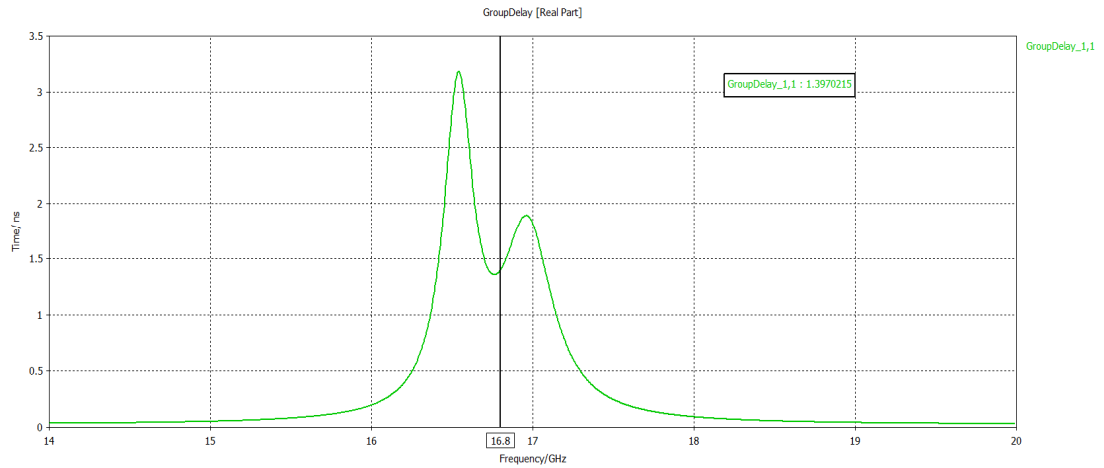
Figure 4.10 Second group delay vs. Frequency derived in CST

Finally, all the resonators are restored and fine tuning of the screws is done to get the filter specifications. After several iterations, the final filter response of the 16600-17000 MHz bandpass filter with one FTZ is plotted in Figure 4.11. The return loss of better than 20dB is achieved as seen in the figure.
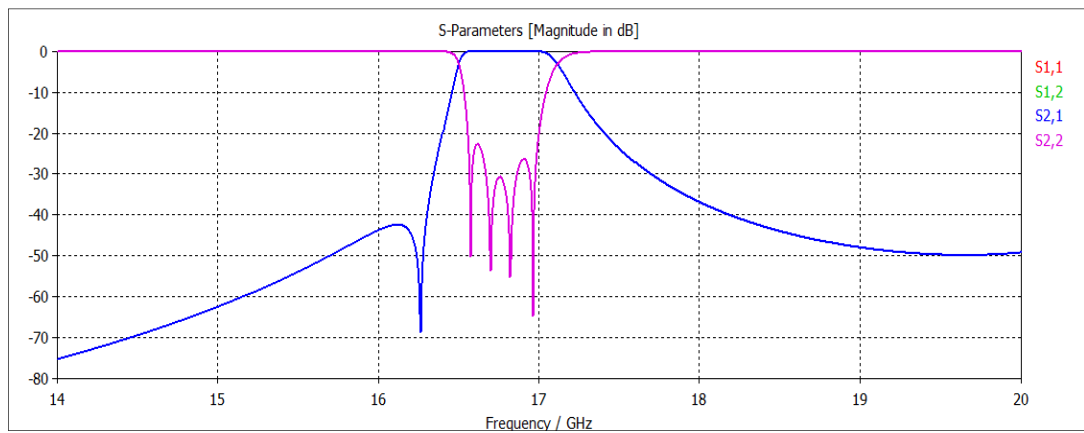

Figure 4.11 4-resonator 1-FTZ filter response calculated via CST

As mentioned before, the external capacitor on Port 7 simulates the FTZ. In order to realize a FTZ, a dielectric block will be used to replace the external capacitor. The material itself will have a capacitive effect and the height of the material will adjust the exact capacitance value that creates FTZ. The material for the block is chosen to be Rogers RO 3003 with the permittivity of ε_r=3. A block of Rogers RO 3003 is placed in between the second and third resonator as illustrated in Figure 4.12.
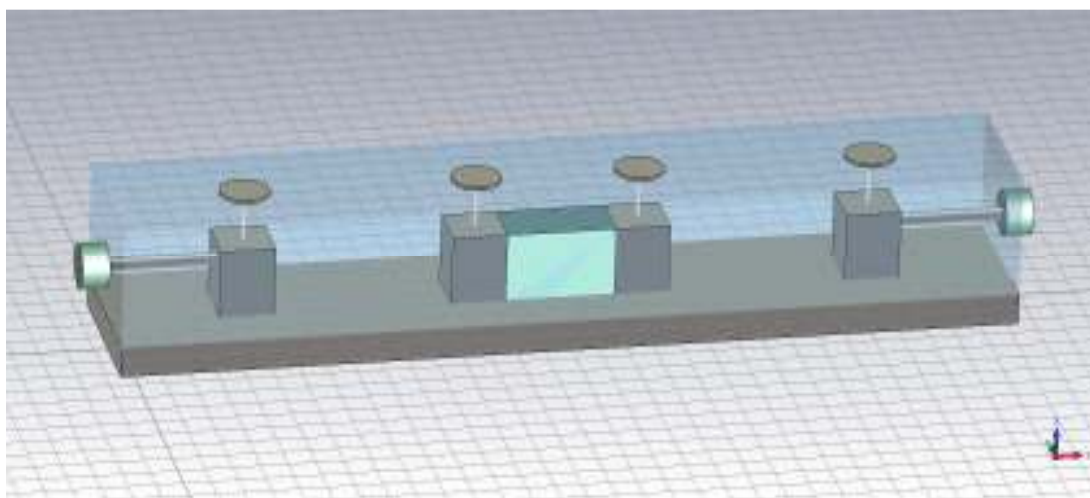

Figure 4.12 The realization of port 7 which corresponds to FTZ in CST

After the insertion of the dielectric block, the response of the filter has been distorted as expected. The variables used to tune the filter before are again tuned. Final filter response including the dielectric material is depicted in Figure 4.13.
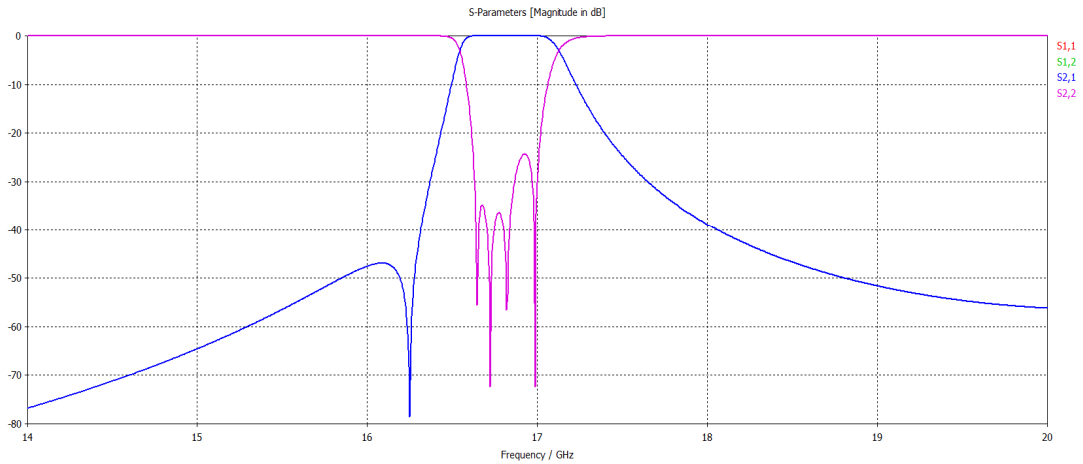
Figure 4.13 4-resonator 1-FTZ final filter response after realization of port 7 (FTZ)

The crucial point regarding to the dielectric block is that the capacitance of the capacitor of port 7 should be tunable to both negative and positive values, which means that the size change of the dielectric material will lead to accurate tuning of the LC resonator representing the FTZ. For the response given in Figure 4.13, the capacitance of port 7 is found to be negative. In order to define a tuning process, a positive capacitance of port 7 should be derived as well. So, the height of the dielectric block is decreased as illustrated in Figure 4.14.
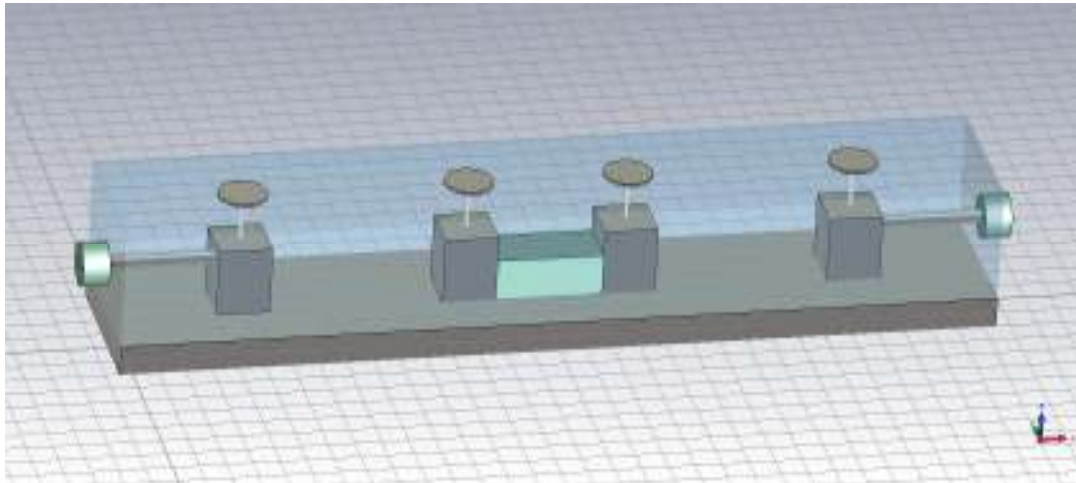
Figure 4.14 The drawing showing how to tune the dielectric block that corresponds to FTZ

The filter is tuned again via changing the positions of the screws, the gaps in between the resonators and the screws; the S-parameters shown in Figure 4.15 are obtained. On the other hand, it is found out that the capacitor value of port 7 has been tuned to a positive value. This result shows that by changing the height of dielectric a successful tuning cycle is achieved for the resonator representing the FTZ.

Figure 4.15 Final filter response including tuning of the FTZ via height of the dielectric material

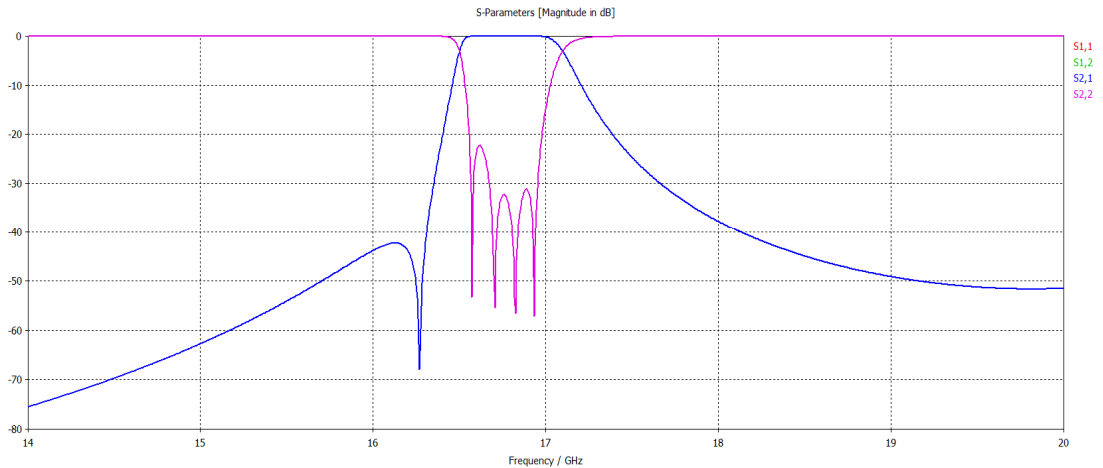As seen from Figure 4.15, The FTZ has been observed at about 16200 MHz, instead of 16000 MHz. Unaccounted EW modes can be the reason of the frequency shift. The final filter length is found to be 33mm. This filter is approximately 15% smaller than the filter designed in Chapter 3, where there are no FTZs.

In the next section, using the same approach the same bandpass filter will be designed with 2 FTZ's located at both upper and lower stopbands achieving better stopband characteristics in both upper and lower bands as well as compact size.

4.2   4-Resonator Filter Design with 2-FTZ

Similar approach given in Section 4.1 will be carried for the bandpass filter with 2-FTZ design. The expected filter specifications are given in Table 4.2.

Table 4.2 4-resonator 2-FTZ filter specifications

By Synthesis	Distributed, BPF, EquiRipple
Ripple (dB)	0.01
Passband Corners (MHz)	16600-17000
Transmission Zeros	1 Nzero, 3 Ninf, 2 FTZ (@16000 MHz and @17500 MHz)
Degree	4
Quarter Wave Frequency (f_q) (MHz)	25200

The derived circuit from Filpro after converting the OC stub components of the OC+SC Stub elements are converted into lumped capacitors is given in Figure 4.16.
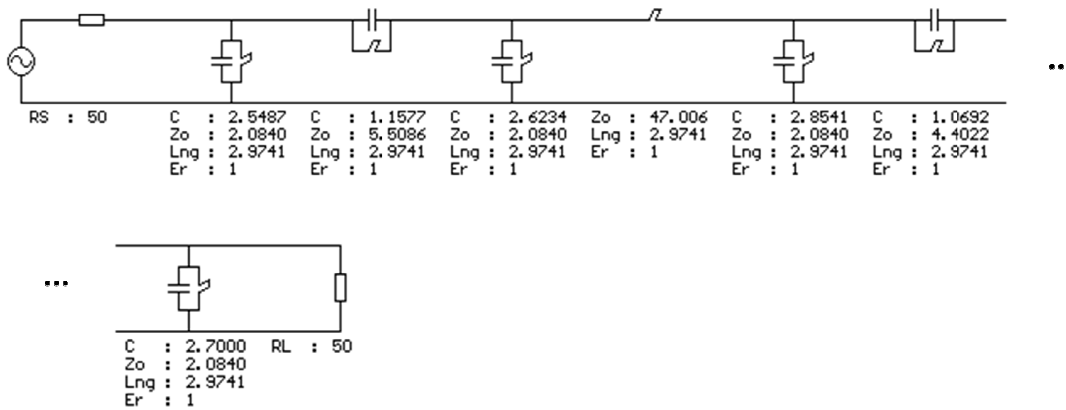

Figure 4.16 4-resonator 2-FTZ bandpass filter design in Filpro

The resultant insertion and return losses derived from Filpro is given in Figure 4.17. Both FTZs are visible in the frequency response. One FTZ is located at about 16

GHz and the other is located at about 17.5GHz. The filter has very good rejection for both upper and lower stopbands.
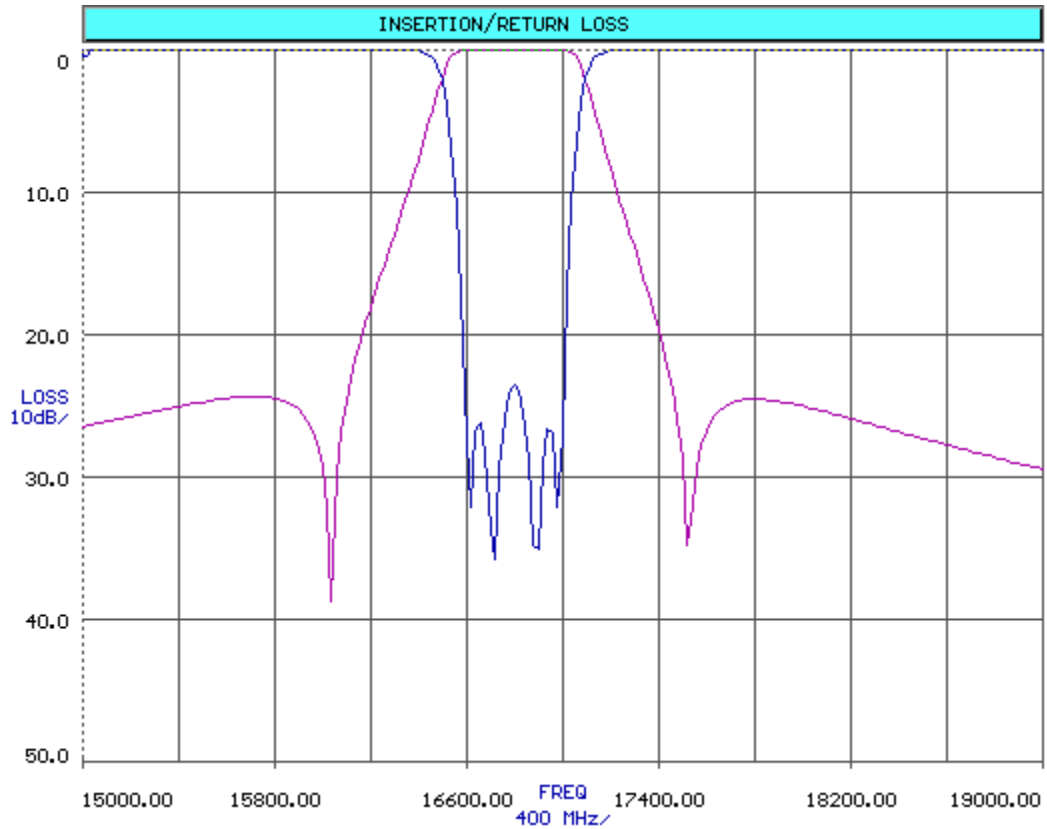
Figure 4.17 4-resonator 2-FTZ filter response calculated via Filpro

By using the group delays found in Filpro, the design is generated in CST. The spacings between the resonators and the ground planes, separation between the adjacent resonators and tapping point are tuned to get the corresponding group delay values of Filpro.

Finally, 2 FTZs are realized via dielectric materials that are placed in between the first and second resonators as well as third and fourth resonators as illustrated in Figure 4.18. The dielectric material considered is the same as before, Rogers RO 3003 with the permittivity of $\varepsilon_r=3$.
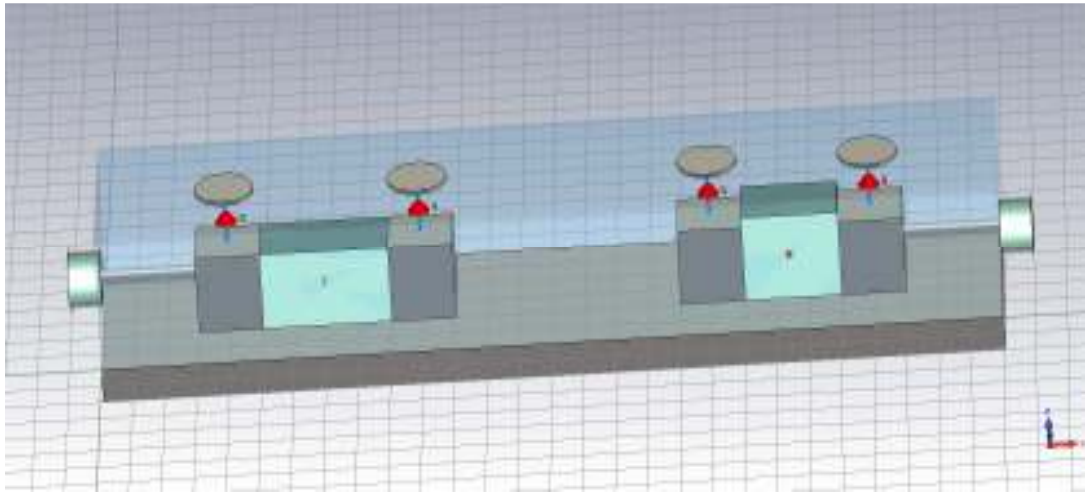
Figure 4.18 4-resonator 2-FTZ filter design via CST

After tuning the screws, i.e., adjusting the capacitances of the ports 3, 4, 5, and 6, the final filter response found is given in Figure 4.19. The capacitance values of port 7 and port 8 regarding to FTZs are calculated to be negative in this case. However those values should also be adjusted to positive value as well in order to provide a converging tuning mechanism after manufacturing the filter.

Figure 4.19 4-resonator 2-FTZ filter response derived via CST

Next, the heights of the dielectric materials are decreased as seen in Figure 4.20 and the filter is tuned again and the response given in Figure 4.21 is derived. The signs of the capacitances for both FTZs are positive, so it is concluded that the filter is realizable.
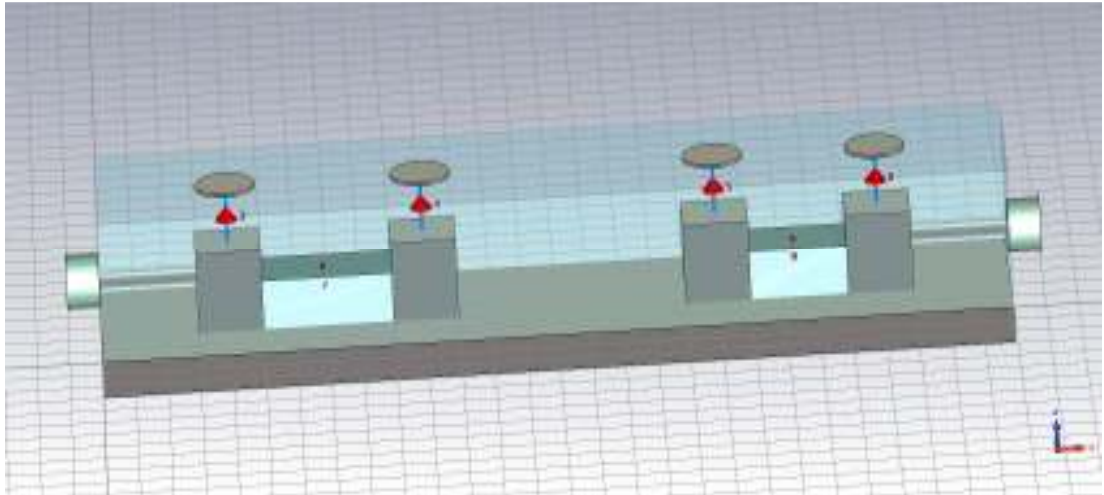
Figure 4.20 4-resonator 2-FTZ filter design via CST showing how to tune the FTZs
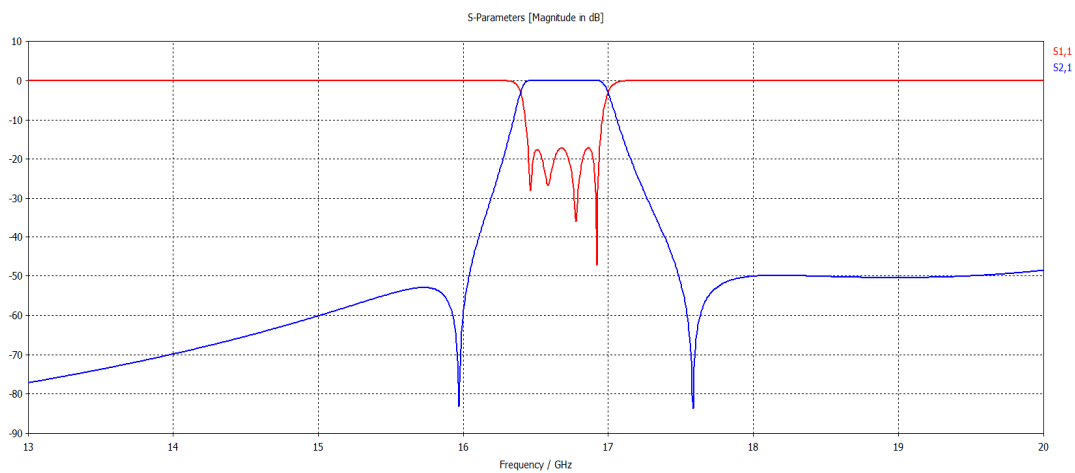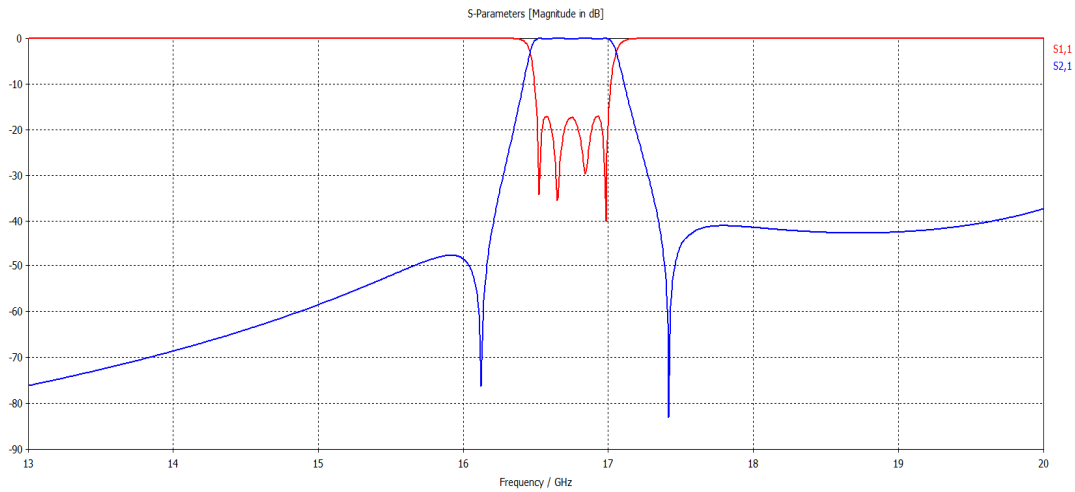
Figure 4.21 4-resonator 2-FTZ filter response derived via CST after tuning the capacitances of FTZs to positive value

When the response is examined, the return loss is well below -18dB in the passband. The insertion loss has a very small passband ripple of about 0.08dB. Both FTZs are located close to the expected frequencies and the rejection of 40dB is achieved at about 17.3GHz at the upper band and 16.25 GHz at the lower band. The wideband response of the filter is depicted in Figure 4.22. There are some spurious signals exist in the frequency range of 20 - 23 GHz. The reason for the corresponding unwanted signals could be the higher order modes of the waves travelling in the waveguide or the fictitious resonance frequencies generated by the waveguide. These issues should be investigated deeply in order to figure out the causes and how to avoid them.
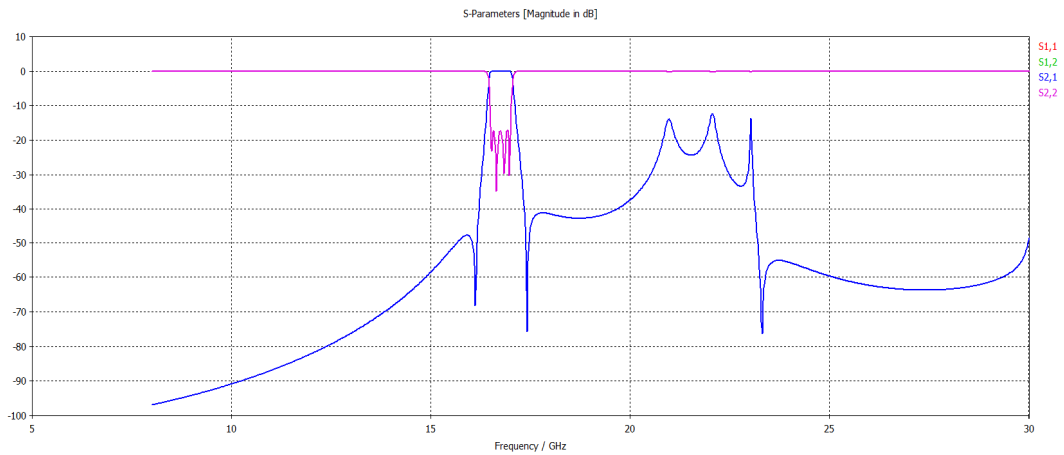
Figure 4.22 Wideband response of the 4-resonator 2-FTZ filter

Final and important comment will be about the sizes of the filters. The EWG combline filters have smaller sizes compared to traditional bandpass or combline filters. The sizes of EWG combline filters even get smaller with the insertion of the FTZ(s).

The bandpass filter given in Chapter 3 has a length of 38.7mm. In the first section of Chapter 4, same filter is designed with 1 FTZ and the length of the filter is derived as 33mm. After 2 FTZs, the length of the filter turned out to be 28mm. From these values, the effect of the FTZ is explicit in terms of size.

CHAPTER 5

CONCLUSION

This thesis has addressed the design of the combline bandpass filters with miniaturized sizes that are more convenient to use in the RF and microwave modules designed with advanced technology. The method used in this thesis for length reduction of the filter, is a novel technique that covers FTZ generation via dielectric block insertion and tuning it by changing its height.

The way for implementation the filter with smaller dimensions used in this thesis is incorporation of combline and evanescent mode waveguide filter structures. Chapter 2 discussed the general theory of both combline and evanescent mode waveguide filters. The key concepts used in design steps are also focused. In order to reduce the length as well as to improve the filter response, FTZ generation in the analysis is detailed.

Chapter 3 described the characterization of a single resonator in terms of characteristic impedance and corresponding quality factor values. Then, an EWG filter is designed. This design is crucial, since finding the approximate separation between the resonators is achieved via EWG design. Using this aforementioned idea to derive the selected waveguide dimensions and separation values between the posts, a 4-resonator EWG combline filter is designed and simulated via CST. This design is carried via group delay method that considers the coupling coefficients and Q values to get the expected group delay values. The group delay values are used for practical and easy design implementation.

Chapter 4 presented two filter designs with the same specifications of Chapter 3 to illustrate FTZ(s) generation in the EWG combline filter design. Both designs lead to length reduction as well as better selectivity and lower stopband. First of all, one FTZ at 16000 MHz is added to the circuit. Higher attenuation is achieved at the lower stopband. FTZ is realized in the 3-D electromagnetic simulator program, CST, with a dielectric block of Rogers RO 3003 (ε_r=3) located in the middle of the filter, between second and third resonators. The capacitance value of the FTZ could be tuned by changing the height of the dielectric block. The length of the filter is decreased by approximately 15% after one FTZ. Following this novel contribution, another design with 2 FTZs is carried out via similar approach. Second FTZ is added to 17500 MHz. FTZs are constructed by adding dielectric blocks in between first and second resonators and third and forth resonators. The selectivity of the filter is increased explicitly in both lower and upper stopbands. The filter length is further decreased by 15% when compared to one FTZ design. Both designs in this chapter are held via group delay approach where simulated group delay plots generated via Filpro.

Consequently, it is shown that, if the length of the filter is a constraint on the design, adding FTZ(s) to the filter is a way of length reduction. Adding FTZ means constituting extra capacitance in between the resonators where FTZ exists. In this thesis, the realization of the FTZ(s) is succeeded by inserting dielectric material Rogers RO 3003. Different dielectric materials according to the expected capacitance values can be considered for different designs.

REFERENCES

[1] K. Packard, "The Origin of Waveguides: A case of Multiple Rediscovery," *IEEE Transactions on Microwave Theory and Techniques,* Vols. MTT-32, pp. 961-969, September 1984.

[2] G. F. Craven and R. F. Skedd, Evanescent Mode Microwave Circuits, Norwood, MA: Artech House, 1987.

[3] R. Levy and S. B. Cohn, "A History of Microwave Filter Research, Design and Development," *IEEE Transactions on Microwave Theory and Techniques,* Vols. MTT-32, pp. 1055-1067, Spetember 1984.

[4] A. Zverev, Handbook of Filter Synthesis, New York: John Wiley & Sons, 1967.

[5] R. Levy, "Theory of Direct-Coupled-Cavity Filters," *IEEE Transcations on Microwave Theory and Techniques,* Vols. MTT-32, pp. 340-348, June 1967.

[6] S. B. Cohn, "Parallel-Coupled Trasmission-line Resonator Filters," *IEEE Transactions on Microwave Theory and Techniques,* pp. 223-231, April 1958.

[7] J. Ishii and H. Ozaki, "Synthesis of a Class of Stripline Filters," *IEEE Transactions on Microwave Theory and Techniques,* Vols. CT-5, pp. 104-109, June 1958.

[8] G. L. Matthaei, "Interdigital band-pass filters," *IEEE Transactions on*

Microwave Theory and Techniques, Vols. MTT-10, pp. 479-491, Novermber 1962.

[9] G. L. Matthaei, "Comb-Line Bandpass Filters of Narrow or Moderate Bandwidth," *Microwave Journal,* vol. 6, no. 9, pp. 82-91, August 1963.

[10] B. F. Nicholson and I.L. Powell, "Equivalence between evanescent-mode and combline filters," *Electronic Letters,* vol. 3, pp. 495-496, November 1967.

[11] R. J. Wenzel, "Synthesis of Comb-line and Capacitively Loaded Interdigital Bandpass Filters of Arbitrary Bandwidth," *IEEE Transactions on Microwave Theory and Techniques,* Vols. MTT-19, no. 8, pp. 678-686, August 1971.

[12] A. Atia and A. Williams, "Measurement of Intercavity Coupling," *IEEE Transactions on Microwave Theory and Techniques,* Vols. MTT-23, pp. 519-522, June 1975.

[13] E. G. Crystal, "Tapped-Line Coupled Transmission Lines with Applications to Interdigital and Combline Filters," *IEEE Transactions on Microwave Theory and Techniques,* Vols. MTT-23, no. 12, pp. 1007-1012, December 1975.

[14] G. R. Hoffman, "Resonated Combline Bandpass Filter," in *European Microwave Conference Proceedings*, 1976.

[15] S. Caspi, J. Adelman, "Design of Combline and Interdigital Filters with Tapped-Line Input," *IEEE Transactions on Microwave Theory and Techniques,* Vols. MTT-36, no. 4, pp. 759-763, January 1979.

[16] J. S. Wong, "Microstrip Tapped Line Filter Design," *IEEE Transactions on*

Microwave Theory and Techniques, Vols. MTT-27, no. 1, pp. 44-50, January 1979.

[17] A. Fukasawa, "Analysis and composition of a new microwave filter configuration with inhomogeneous medium," *IEEE Transactions on Microwave Theory and Techniques,* Vols. MTT-30, no. 9, pp. 1367-1374, September 1982.

[18] M. Sugawara, M. Makimoto and S. Yamashita, "A design method of bandpass filters using dielectric filled coaxial resonators," *IEEE Transactions on Microwave Theory and Techniques,* Vols. MTT-33, pp. 152-157, 1985.

[19] C. Kuang, C. Tzuang and W. T. Lo, "Printed Circuit Realization of a Tapped Combline Bandpass Filter," in *IEEE MTT-S Digest Proceedings*, 1990.

[20] R. Levy, "Simplified analysis of inhomogeneous dielectric block combline filters," *IEEE MTT-S Digest,* pp. 135-138, 1990.

[21] K. Wada, N. Otani, Y. Noguchi and J. Ishii, "Tapped Line Interdigital Bandpass Filters with narrow bandwidth Using Asymmetric Broadside Coupled Coplanar Waveguides," in *EuMC Proceedings*, 1995.

[22] C. Ernst and V. Postoyolka, "Tapped Line Interdigital Filter Equivalent Circuits," in *IEEE MTT-S Digest Proceedings*, Denver, 1997.

[23] R. Levy, H. W. Yao and K. A. Zaki, "Transitional combline/evanescent mode microwave filters," *IEEE Transactions on Microwave Theory and Techniques,* vol. 45, no. 12, pp. 2094-2099, December 1997.

[24] H. W. Yao, K. A. Zaki, A. E. Atia, T. Dolan, "Improvements of spurious

performance of combline filters," *IEEE MTT-S Digest,* pp. 1099-1102, 1997.

[25] J. Ness, "A Unified Approach to the Design, Measurement and Tuning of Coupled Resonator Filters," *IEEE Transactions on Microwave Theory and Techniques,* Vols. MTT-46, no. 4, pp. 343-351, April 1998.

[26] I. Shapir, V. A. Sharir and D. G. Swanson, Jr., "TEM Modeling of Parasitic Bandwidth Expansion in Combline Filters"," *IEEE Transactions on Microwave Theory and Techniques,* vol. 47, no. 9, pp. 1664-1669, September 1999.

[27] R. Levy, R. V. Snyder and G. L. Matthaei, "Design of Microwave Filters," *IEEE Transactions on Microwave Theory and Techniques,* vol. 50, no. 3, pp. 783-793, March 2002.

[28] B. Mohajer-Iravani and M. A. El Sabbagh, "Ultra-wideband and Compact Novel Combline Filters," in *IEEE Int. Symposium on Electromagnetic Compatibility*, Austin, 2009.

[29] S.-J. Park, I. Reines, C. Patel and G. M. Rebeiz, "High-Q RF-MEMS 4-6 GHz Tunable Evanescent-Mode Cavity Filter," *IEEE Transactions on Microwave Theory and Techniques,* vol. 58, no. 2, pp. 381-389, February 2010.

[30] S. Fouladi, F. Huang, W. D. Yan and R. R. Mansour, "High-Q Narrowband Tunable Combline Bandpass Filters Using MEMS Capacitor Banks and Piezomotors," *IEEE Transactions on Microwave Theory and Techniques,* vol. 61, no. 1, pp. 393-402, January 2013.

[31] R. J. Wenzel, "Exact Design of TEM Microwave Networks Using Quarter-

Wave Lines," *IEEE Transactions on Microwave Theory and Techniques,* Vols. MTT-12, pp. 94-111, January 1964.

[32] M. C. Horton and R. J. Wenzel, "General Theory and Design of Optimum Quarter Wave TEM filters," *IEEE Transactions on Microwave Theory and Techniques,* Vols. MTT-13, pp. 316-327, May 1965.

[33] G. L. Matthaei, L. Young, E. M. Jones, Microwave Filters, Impedance Matching Networks and Coupling Structures, New York: Mc Graw Hill, 1964.

[34] P. Martin and J. Ness, "Coupling Bandwidth and Reflected Group Delay Characterization of Microwave Bandpass Filters," *Applied Microwave and Wireless,* pp. 86-98.

[35] K. Schunemann, R. Knochel and G. Begemann, "Components for microwave integrated circuits with evanescent mode resonators," *IEEE Transactions on Microwave Theory and Techniques,* Vols. MTT-25, no. 12, pp. 1026-1031, September 1982.

[36] R. W. Rhea, HF Filter Design and Computer Simulation, Tucker: Noble , 1994.

[37] M. A. R. Gunston, Microwave Transmiison-Line Impedance Data, London: Van Nostrand Reinhold Company, 1972.

[38] G. L. Matthaei, Microwave Filters, Impedance-Matching Networks and Coupling Structures, New Jersey: McGraw-Hill, 1980.